


Summer 2004

A high -order finite difference method for solving bioheat transfer equations in three-dimensional triple -layered skin structure

Haofeng Yu
Louisiana Tech University

Follow this and additional works at: <https://digitalcommons.latech.edu/dissertations>

 Part of the [Biophysics Commons](#), [Mathematics Commons](#), and the [Other Biomedical Engineering and Bioengineering Commons](#)

Recommended Citation

Yu, Haofeng, "" (2004). *Dissertation*. 646.
<https://digitalcommons.latech.edu/dissertations/646>

This Dissertation is brought to you for free and open access by the Graduate School at Louisiana Tech Digital Commons. It has been accepted for inclusion in Doctoral Dissertations by an authorized administrator of Louisiana Tech Digital Commons. For more information, please contact digitalcommons@latech.edu.

A HIGH-ORDER FINITE DIFFERENCE METHOD FOR SOLVING
BIOHEAT TRANSFER EQUATIONS IN THREE-DIMENSIONAL
TRIPLE-LAYERED SKIN STRUCTURE

by

Haofeng Yu, B.S., M.S

A Dissertation Presented in Partial Fulfillment
of the Requirements for the Degree
Doctor of Philosophy

COLLEGE OF ENGINEERING AND SCIENCE
LOUISIANA TECH UNIVERSITY

August 2004

UMI Number: 3135578

INFORMATION TO USERS

The quality of this reproduction is dependent upon the quality of the copy submitted. Broken or indistinct print, colored or poor quality illustrations and photographs, print bleed-through, substandard margins, and improper alignment can adversely affect reproduction.

In the unlikely event that the author did not send a complete manuscript and there are missing pages, these will be noted. Also, if unauthorized copyright material had to be removed, a note will indicate the deletion.

UMI[®]

UMI Microform 3135578

Copyright 2004 by ProQuest Information and Learning Company.

All rights reserved. This microform edition is protected against unauthorized copying under Title 17, United States Code.

ProQuest Information and Learning Company
300 North Zeeb Road
P.O. Box 1346
Ann Arbor, MI 48106-1346

LOUISIANA TECH UNIVERSITY

THE GRADUATE SCHOOL

July 13, 2004

Date

We hereby recommend that the dissertation prepared under our supervision
by Haofeng Yu
entitled A High-Order Finite Difference Method for Solving Bioheat Transfer
Equations in a Three-Dimensional Triple-Layered Skin Structure

be accepted in partial fulfillment of the requirements for the Degree of
Doctor of Philosophy in Computational Analysis and Modeling

Wizhong Shi
Supervisor of Dissertation Research
Richard J. Greedie
Head of Department
CAM
Department

Recommendation concurred in:

Wizhong Shi

Raja Natar

Andrei Pan

Richard J. Greedie

Advisory Committee

Approved:

Bala Panachandran
Director of Graduate Studies

Approved:

Terry McLaughlin
Dean of the Graduate School

Stan Nappa
Dean of the College

ABSTRACT

Investigations on instantaneous skin burns are useful for an accurate assessment of burn-evaluation and for establishing thermal protections for various purposes. Meanwhile, hyperthermia with radiation is important in the treatment of cancer, and it is essential for developers and users of hyperthermia systems to predict, and interpret correctly the biomass thermal and vascular response to heating. In this dissertation, we employ the well-known Pennes' bioheat transfer equation to predict the degree of skin burn and the temperature distribution in hyperthermia cancer treatment.

A fourth-order compact finite difference scheme is developed to solve Pennes' bioheat transfer equation in a three-dimensional single vessel embedded triple-layered skin structure, with two different boundary conditions (constant heating and insulation) on the top surface. To this end, we employ the fourth-order compact finite difference method to discretize the Pennes' bioheat equation, where the second-order derivatives of temperature at boundaries and interfaces are calculated using a combined compact finite difference method incorporating the boundary conditions and interfacial conditions. As such, the solution system becomes a diagonal-dominated tridiagonal linear system.

To demonstrate the applicability of the scheme, we investigate four physical models. Numerical results show that this compact finite difference scheme is unconditionally stable for a one-dimensional uniform-layered skin structure and more

accurate than the Crank-Nicholson scheme. The comparison of the numerical results in the three-dimensional triple-layered skin structures shows that the blood vessel has a significant influence on the thermal response of the biomass. Thus, the outcomes described above provide a reliable, flexible and efficient numerical method for solving Pennes' bioheat model in a comparatively realistic skin structure.

APPROVAL FOR SCHOLARLY DISSEMINATION

The author grants to the Prescott Memorial Library of Louisiana Tech University the right to reproduce, by appropriate methods, upon request, any or all portions of this Dissertation. It is understood that "proper request" consists of the agreement, on the part of the requesting party, that said reproduction is for his personal use and that subsequent reproduction will not occur without written approval of the author of this Dissertation. Further, any portions of the Dissertation used in books, papers, and other works must be appropriately referenced to this Dissertation.

Finally, the author of this Dissertation reserves the right to publish freely, in the literature, at any time, any or all portions of this Dissertation.

Author Haofeng Yu
Date Aug 3rd, 2004

To my parents

Guo-zheng Yu and Xiu-yun Feng

TABLE OF CONTENTS

LIST OF TABLES.x
LIST OF FIGURES.xi
NOMENCLATURExiii
ACKNOWLEDGMENTSxiv
CHAPTER 1 INTRODUCTION1
1.1 General Overview1
1.2 Research Objectives2
1.3 Organization of the Dissertation3
CHAPTER 2 BACKGROUND AND PREVIOUS WORK4
2.1 Bioheat Transfer Models4
2.2 Numerical Methods for Bioheat Transfer Models19
2.2.1 Numerical Methods19
2.2.2 Finite Element Method (FEM)20
2.2.3 Boundary Element Method (BEM)22
2.2.4 Finite Difference Method24
2.3 Compact Finite Difference Scheme25
2.3.1 Background25
2.3.2 General Explicit Schemes25
2.3.3 Boundary Formulation28
2.3.4 Applications29
CHAPTER 3 MATHEMATICAL MODELS AND COMPACT FINITE DIFFERENCE SCHEMES30
3.1 General Governing Equations30
3.1.1 Problem Description30
3.1.2 General Governing Equations30
3.2 One-Dimensional Uniform-Layered Case32
3.2.1 Model Description32
3.2.2 Governing Equations33

3.2.3	Finite Difference Scheme.....	34
3.2.4	Algorithm.	38
3.2.5	Convergence Analysis.....	39
3.3	One-Dimensional Triple-Layered Case.....	43
3.3.1	Model Description.....	43
3.3.2	Governing Equations.....	44
3.3.3	Finite Difference Scheme.....	44
3.4	Three-Dimensional Triple-Layered Case.....	48
3.4.1	Model Description.....	48
3.4.2	Governing Equations.....	49
3.4.3	Finite Difference Scheme.....	49
3.4.4	Algorithm.....	50
3.5	Three-Dimensional Single Vessel Embedded Triple-Layered Case...51	
3.5.1	Model Description.....	51
3.5.2	Governing Equations.....	51
3.5.3	Finite Difference Scheme.....	52
3.5.4	Algorithm.....	52
CHAPTER 4	NUMERICAL EXAMPLES AND RESULTS.....	54
4.1	One-Dimensional Uniform-Layered Case.....	54
4.2	One-Dimensional Triple-Layered Case	56
4.3	Three-Dimensional Triple-Layered Case.....	58
4.4	Three-Dimensional Single Vessel Embedded Triple-Layered Case...72	
CHAPTER 5	CONCLUSIONS AND FUTURE WORK.....	86
APPENDIX A	SOURCE CODE FOR SOLVING PENNES' BIOHEAT TRANSFER EQUATION IN A ONE-DIMENSIONAL UNIFORM-LAYERED SKIN STRUCTURE.....	88
APPENDIX B	SOURCE CODE FOR SOLVING PENNES' BIOHEAT TRANSFER EQUATION IN A ONE-DIMENSIONAL TRIPLE-LAYERED SKIN STRUCTURE.....	92
APPENDIX C	SOURCE CODE FOR SOLVING PENNES' BIOHEAT TRANSFER EQUATION IN A THREE-DIMENSIONAL TRIPLE-LAYERED SKIN STRUCTURE.....	98
APPENDIX D	SOURCE CODE FOR SOLVING PENNES' BIOHEAT TRANSFER EQUATION IN A THREE-DIMENSIONAL SINGLE VESSEL EMBEDDED TRIPLE-LAYERED SKIN STRUCTURE.....	109
APPENDIX E	SOURCE CODE OF A SUBROUTINE FOR EVALUATING TWO ARRAYS.....	121

**APPENDIX F SOURCE CODE OF A SUBROUTINE FOR SOLVING A
TRIDIAGONAL LINEAR SYSTEM.....123**
REFERENCES125

LIST OF TABLES

Table 4.1	Parameters for the uniform layer in the human skin tissue.....	54
Table 4.2	Comparison of the running time with different grid sizes.....	56
Table 4.3	Parameters for the three layers in the human skin structure.....	56
Table 4.4	Parameters of laser power for the three layers in the skin structure.....	59
Table 4.5	Parameters of blood vessel.....	72
Table 4.6	Contrast of running time for three-dimensional cases.....	85

LIST OF FIGURES

Figure 2.1	Schematic diagram for the intermediate tissue of the skin.....	5
Figure 2.2	Gautherie's thermal conductivity model	7
Figure 2.3	Song-Weinbaum-Jiji thermal conductivity model.....	9
Figure 2.4	Illustration of Zhou's model.....	11
Figure 2.5	Schematic geometry of three-layered skin structure.....	14
Figure 2.6	Tissue regions involved in practical hyperthermia treatment.....	16
Figure 2.7	Schematic diagram of a single large blood vessel embedded in a perfused tissue.....	18
Figure 2.8	Non-homogeneous domain blood vessel-tissue.....	19
Figure 2.9	Areas of different tissue types in the prostate cross-section generated by ANSYS.....	22
Figure 2.10	Finite element mesh generated by ANSYS PC/SOLID.....	22
Figure 3.1	Schematic configuration of a three-dimensional triple-layered skin structure and laser power.....	31
Figure 3.2	Schematic configuration of a one-dimensional uniform-layered skin structure.	32
Figure 3.3	One-Dimensional triple-layered skin structure and laser power.	43
Figure 3.4	Laser radiated three-dimensional triple-layered skin structure.....	48
Figure 4.1	Comparison of numerical errors between the second-order Crank-Nicholson scheme and the fourth-order compact finite difference scheme.....	55

Figure 4.2	Transient temperatures under constant heating with a duration of 150 seconds.....	57
Figure 4.3	Transient temperatures distribution under constant heating after 150 seconds.....	58
Figure 4.4	Contour of temperature distribution in the yz-cross section in three-dimensional case with constant heating boundary at various times.....	60-65
Figure 4.5	Contour of temperature distribution in the yz-cross section in three-dimensional case with insulated boundary at various times.....	66-71
Figure 4.6	Contour of temperature distribution in the yz-cross section in three-dimensional single vessel embedded case with constant heating boundary at various times.....	73-78
Figure 4.7	Contour of temperature distribution in the yz-cross section in three-dimensional single vessel embedded case with insulated boundary at various times.....	79-85

NOMENCLATURE

A, B, H, I	matrix
C, C_l	specific heat of skin layer l
K_l	thermal conductivity of skin layer l
ρ_l	density of skin layer l
q	heat flux
W_b^l	blood perfusion rate
θ	elevated tissue temperature
σ	standard deviation of the width of a normally distributed laser beam
α_l	laser absorbtivity of skin layer l
P_o	laser power
Q_r^l	volumetric heat due to spatial heating.
$Reff_l$	laser reflectivity of skin layer l
L	thickness of the tissue
Δt	time increment
t	time
T	temperature
x, y, z	coordinates
$\vec{b}, \vec{d}, \vec{x}, \vec{\theta}$	vector

ACKNOWLEDGMENTS

I would like so much to express my gratitude to my advisor, Dr. Weizhong Dai, a mentor, whom I will follow all my life without any hesitation, and wonderful friend with all the precious characteristics of Chinese people. Under his guidance, I expanded my horizon tremendously in mathematical modeling.

Of the same importance is my appreciation for Dr. Raja Nassar's patience, encouragement, and innate humor. From him, I learn to think "statistically." With a joint confidence level of 99.9%, I say that Dr. Nassar is a nice professor, and he is ready for joking with you right now. My special thanks to Dr. Richard Greechie. He encouraged me to enter the world of mathematics and to appreciate its inner beauty. His philosopher looks and childlike smile are forever sweet memories of my life in Ruston. I would also like to thank Dr. Andri Paun for his help on my dissertation work as an important committee member and for his friendship.

Thanks for my precious friends, Galen and Joshua. Galen showed me the art of teaching mathematics. As for Joshua, if you can detect a little bit of American Southern accent in my slurring, that is from him.

Thanks for my church family at Temple, Ruston, and so-called "Friday Church". I appreciate so much being a member of them.

Last, I would like to thank the Ph.D. CAM program at Louisiana Tech University for providing the financial support to conduct this research.

CHAPTER 1

INTRODUCTION

1.1 General Overview

Skin burns caused by exposure to heat in a flash fire, laser irradiation, or by being in contact with hot substances are the most commonly encountered hazards in daily life and in industry [Moritz 1947][Stoll 1959][Bechnke 1984][Li 1989][Killer 1991][Lecarpentier 1993][Chen 1993][Torvi 1994]. This kind of heating has two common distinctive characteristics. Even though such a heating process is often short (i.e., less than 5 seconds), the heat flux on the surface of skin can be very high (i.e., 83.2 kW/m²) [Torvi 1994]. Investigations on such instantaneous thermal injuries can be useful for an accurate assessment on burn-evaluation and for establishing thermal protections for various purposes, e.g., fire fighter's safe guard.

In recent years, there has been an increasing interest in the research of hyperthermia combined with radiation and cytotoxic drugs to enhance the killing of tumors. Conventional hyperthermia (target temperatures of 42-46°C) [Van Der Zee 1986] [Dewhirst 1984] in conjunction with radiation has demonstrated an increased effectiveness in the treatment of certain types of cancer, such as the treatment of liver metastases.

Now, because hyperthermia with radiation has become important in the treatment of cancer, it has therefore become a very active area of study. There are two overarching issues related to the research in this dissertation. First, when we heat tumor tissue, it is crucial to keep the surrounding normal tissue below the temperature that will produce harm [Larkin 1977] [Pettigrew 1974]. Therefore, an accurate prediction of temperature distribution in human tissue is important. Second, tissue vasculature plays an important role in the temperature responses of biological bodies subjected to laser heating. Consequently, increasing attention has been paid to the effect of a single blood vessel on tissue temperature prediction during laser-induced thermal therapy. Therefore, a model that takes all these factors into account is important. For these purposes, a high-order compact finite difference scheme for solving Pennes' bioheat transfer equation in a three-dimensional single vessel embedded triple-layered skin structure will be developed in this work.

1.2 Research Objectives

The first objective of this dissertation is to develop a fourth-order compact finite difference scheme, following the idea of Lele [Lele 1992], for solving Pennes' bioheat transfer equation.

A series of steps will be taken in order to achieve this objective:

Step 1. Develop a fourth-order compact finite difference scheme for solving Pennes' bioheat transfer equation in a one-dimensional uniform-layered skin structure.

Step 2. Analyze the convergence of the finite difference scheme.

Step 3. Develop a fourth-order compact finite difference scheme for solving Pennes' bioheat transfer equation in a one-dimensional triple-layered skin structure.

Step 4. Extend the fourth-order compact finite difference scheme to solve Pennes' bioheat transfer equation in a three-dimensional triple-layered skin structure composed of epidermis, dermis and subcutaneous tissue.

The second objective of this dissertation is to model the interactions among human tissue, a single blood vessel and external heat sources, e.g., constant heating and laser power. Given a pre-specified heat source, the application of the fourth-order compact finite difference scheme to the model will facilitate prediction of the temperature distribution.

1.3 Organization of the Dissertation

In Chapter 1, a general review of the main idea of our work is given. The two objectives of this dissertation are specified. Chapter 2 provides some background of this active research area. Bioheat transfer equations, numerical methods for them and the compact finite difference schemes will be discussed in this chapter. After this, Chapter 3 details the fourth-order compact finite difference scheme and its applications for Pennes' bioheat transfer equation in four physical models. Then, Chapter 4 gives the numerical results of the calculations of the models presented in Chapter 3. Lastly, in Chapter 5, we give the conclusions of our work and suggest future research work.

CHAPTER 2

BACKGROUND AND PREVIOUS WORK

2.1 Bioheat Transfer Models

Biological tissues are complicated structures. They contain dispersed cells separated by voids. The mechanism of energy and mass transportation is even more complicated; however, knowledge of thermal transport mechanisms in biological tissues is important for the therapeutic medical methods which employ the localized application of heat to perfused biological tissue [Khaled 2003].

A general description of the thermal transport mechanism can be made as follows: blood enters biological tissues through vessels referred to as arteries and perfuses to the tissue cells via blood capillaries as shown in Figure 2.1. Returned blood from the capillaries is accumulated in veins where the blood is pumped back to the heart; energy transport within these tissues is due to thermal conduction, blood perfusion and heat generation (e.g. metabolic heat generation) [Khaled 2003].

Various models have been developed to address the thermal transport mechanism, yet most of them are intertwined, and therefore it is hard to completely distinguish one from the other. Several important models are discussed below to show the development in this area. The bioheat transfer equation developed by Pennes [Pennes 1948] is one of

the earliest models for energy transport in biological tissues (Figure 2.1) and so is taken as the beginning point of the development of these models.

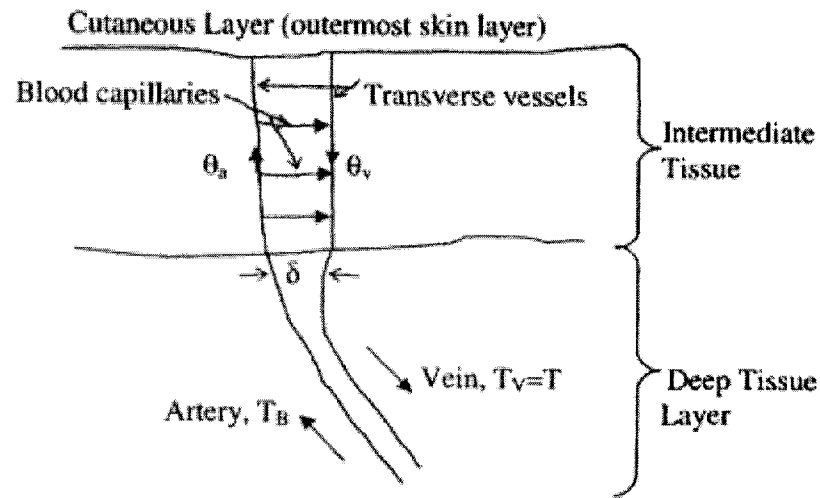


Figure 2.1 Schematic diagram for the intermediate tissue of the skin [Khaled 2003]

Pennes' equation has been most frequently used in biological research works and is found to be quite useful because of its simplicity. The equation that Pennes used is summarized in a simple form as follows:

$$\rho C \frac{\partial T}{\partial t} = K \nabla^2 T - W_b C_b (T_B - T) + Q, \quad (2.1)$$

where t is the time, ρ the tissue density, C the tissue specific heat, C_b the blood specific heat, W_b the blood volumetric perfusion rate, K tissue thermal conductivity and Q the term of heat sources within the tissue. Here, ∇ is a gradient operator [Pennes 1948][Chato 1989][Khaled 2003]. Pennes proposed that heat was transferred not only by conduction but also by blood circulating through the region at the arterial temperature when the region's temperature differs from that of the blood. Pennes considered all the properties appearing for the conduction and thermal storage terms to be for the tissue, while he referred to the blood properties in the blood perfusion term. This term was

modeled to be proportional to the difference between the arterial temperature and the temperature at a given location. Pennes assumed that the arterial blood temperature T_B was uniform throughout the tissue while he considered the vein temperature to be equal to the tissue temperature, denoted by T at the same point. The added term, $W_b C_b (T_B - T)$ takes this blood perfusion into account and it represents a heat sink when positive and a heat source when negative.

In Pennes' bioheat transfer equation, K is a constant, which assumes that the effect of blood flow on tissue heat transfer is equivalent to that of a heat sink or source. This assumption has been questioned by many subsequent researchers. In Gautherie's temperature dependent conductivity model [Gautherie 1969], there is no blood perfusion term $W_b C_b \theta$, and the tissue conductivity K is assumed to be a function of the local tissue temperature $K(T)$. A simple form of Gautherie's model is

$$\rho C \frac{\partial T}{\partial t} = \nabla(K(T)\nabla T) + Q. \quad (2.2)$$

The effect of the increase in conductivity with temperature is a reduction of the temperature gradient as the tissue increases in temperature. A graph of this function can be seen in Figure 2.2.

Following a thermal equilibration length analysis, the Chen-Holmes bioheat transfer model is proposed based on a more realistic vascular anatomy of perfused tissues than that of Pennes' model. Considering the blood-perfused tissue as a continuum by excluding the large vessels which can be treated individually, the model is given as follows [Chen 1980] [Chato 1989]:

$$\rho C \frac{\partial T}{\partial t} = \nabla(K\nabla T) + \rho_b W_b C_b (T_b - T) - \rho_b W_b \bar{u} (T_b - T) + \nabla(K_p \nabla T) + Q \quad (2.3)$$

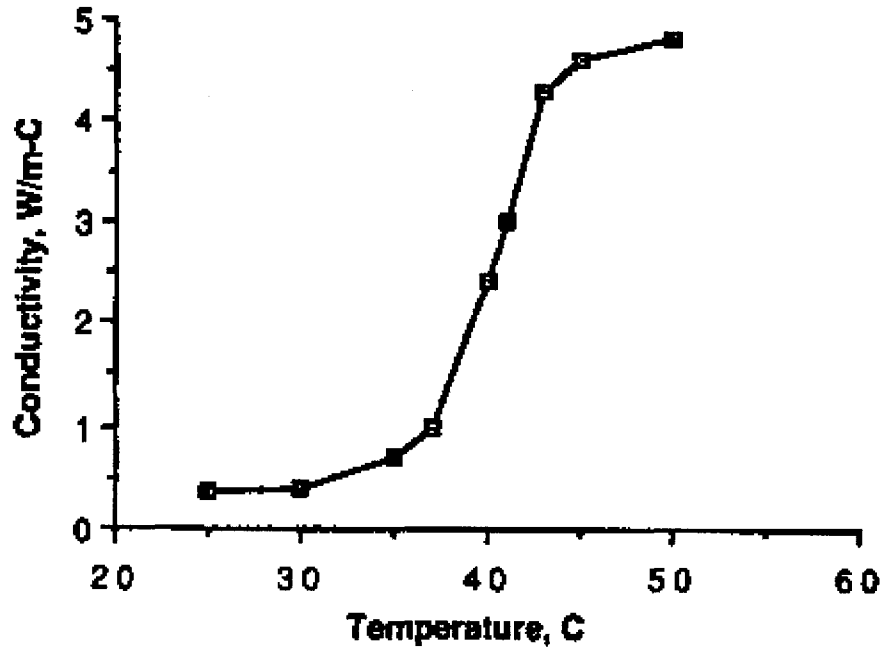


Figure 2.2 Gautherie's thermal conductivity model [Chato 1989]

In this model, the heat transfer mechanism between blood vessels and tissue was examined in detail and separated into three terms. The first term, $\rho_b W_b C_b (T_b - T)$, reflects the actual equilibration of blood temperature. The second term, $\rho_b W_b \bar{u} (T_b - T)$, concerns the convective heat transfer contributed by the net blood flow velocity within the tissue relative to already thermally equilibrated vessels. The third term, $\nabla(K_p \nabla T)$, relates the thermal contribution from the vessels being nearly in equilibrium with the surrounding tissue. The conductivity related to blood perfusion, K_p depends on the local microvasculature and local blood perfusion rate. However, Chen and Holmes, in their model, made no effort to evaluate the actual thermal contribution of each term to the total heat balance [Chato 1989].

Based on anatomical observations in peripheral tissue and on high spatial resolution measurements, Weinbaum et al. [Weinbaum 1984] concluded that the local

blood contribution to tissue heat transfer is mainly associated with an incomplete countercurrent heat exchange mechanism between paired arteries and veins rather than with the capillary perfusion. The following is the bioheat transfer equation of Weinbaum-Jiji for living tissue [Weinbaum 1985][Charney 1990]:

$$\rho C \frac{\partial T}{\partial t} = \nabla K_{eff} \nabla T + Q. \quad (2.4)$$

This model focuses on the vasculature in the subcutaneous region, and it is unique in that it quantifies tissue heat transfer with a single equation independent of any blood temperature. They used the hypothesis that small arteries and veins are parallel and the flow direction is countercurrent resulting in counterbalanced heating and cooling effects. This kind of tissue vascularization causes the isotropic blood perfusion term in Pennes' bioheat transfer equation to be negligible, and it causes the tissue to behave as an anisotropic heat transfer medium. Accordingly, Weinbaum and Jiji modified the thermal conductivity in Pennes' bioheat transfer equation by means of an "effective conductivity" related quadratically to the blood perfusion rate, which is affected by the dimensions and the directions of the vessels. They also showed that isotropic blood perfusion between the countercurrent vessels can have a significant influence on heat transfer in regions where the countercurrent vessels are under $70\mu m$ in diameter [Weinbaum 1985][Chato 1989][Charney 1990][Khaled 2003].

The importance of "effective thermal conductivity" is further revealed by Song et al. [Song 1987][Khaled 2003], in Song-Weinbaum-Jiji model. They propose that the conductivity K be a function of depth, z , and Peclet number (blood flow in the supply artery), Pe , representing the blood flow in the main supply artery, which varies according

to whether the person is at rest or exercising. The graph of this function for different Peclet numbers is shown in Figure 2.3.

They also demonstrated that a tissue which exhibits only a small increase in the thermal conductivity due to countercurrent convection in its vasoconstricted state (the narrowing of the blood vessel) can exhibit more than a fivefold increase in the thermal conductivity in its vasodilated state (during relaxation of the blood vessel) [Khaled 2003].

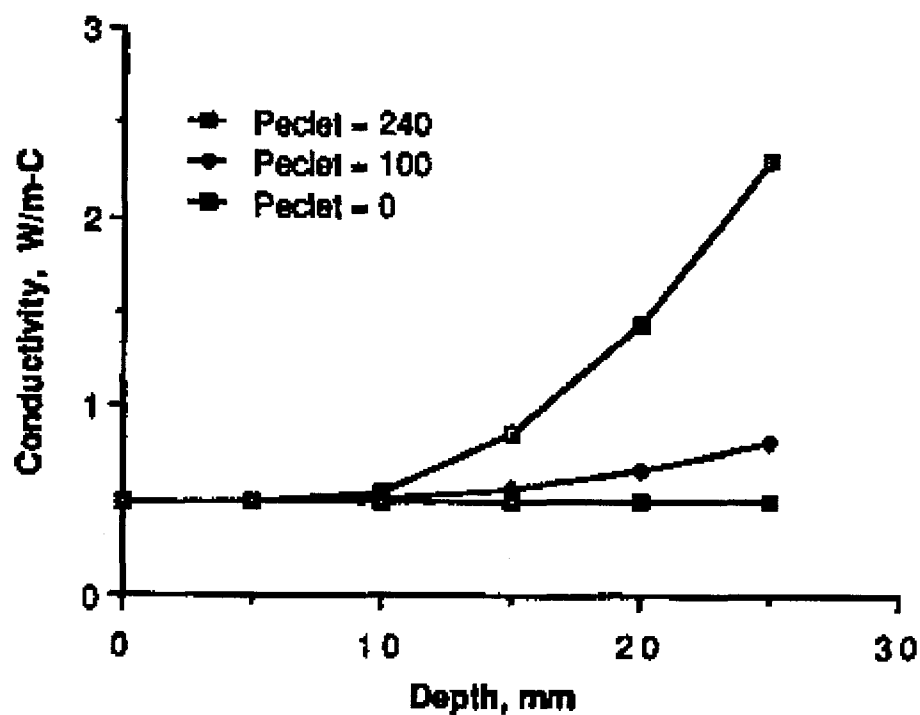


Figure 2.3 Song-Weinbaum-Jiji thermal conductivity model [Chato 1989]

An important example of research work example that used Weinbaum and Jiji's model is the work of Guiot et al. [Guiot 1998]. They employed the Weinbaum and Jiji's model, assuming a linear relation between the effective thermal conductivity and the blood perfusion rate, to determine the increase in the thermal conductivity in a perfused tissue. They reported an 11% increase in the thermal conductivity and their results suggested that, in addition to a "temperature map", a "perfusion map" within the heated

volume should be monitored routinely throughout the hyperthermic sessions since the local value of perfusion can vary substantially within a few centimeters [Khaled 2003].

A numerical comparison of the three bioheat transfer models of Pennes, Gautherie and Song-Weinbaum-Jiji, is given by Chato and Eckburg [Chato 1989], using finite difference techniques. They concluded that Pennes' model yielded the fastest response rates and the lowest steady state temperatures, while the Song-Weinbaum-Jiji model was the slowest with the highest temperatures. "To the best of our knowledge, Gautherie's model is not currently being used very extensively. Pennes' model, however, can be recommended as the first approximation because of its relative simplicity and past success".

Another comparison was made by Xu et al. [Xu 1991]. They compared and contrasted Pennes' model, the Chen-Holmes model and the Weinbaum-Jiji models in a pig kidney cortex. Based on the theoretical analyses performed in his study, it is known that the three models differ in the way they handle the thermal contribution from the flowing blood in living tissue: Pennes' equation has only the blood perfusion-related source term and the Weinbaum-Jiji equation has only the blood perfusion enhanced thermal conduction term, whereas the Chen-Holmes equation has both as well as an additional convection term accounting for the thermal effect from the directional blood flow within the tissue.

There are also other models very different from the classic Penne's bioheat transfer equation. In Barun and Ivanov's work [Barun 2003], a simple model for optical and thermal properties of two-component biological tissues (bloodless basic tissue and blood vessels randomly distributed over it) is proposed as applied to studies of thermal

fields under external illumination. The problem of light thermal action on tissues is reduced to the construction of a model for optical and thermal characteristics of the medium on the base of the tissue structure, and to the solution of radiation and heat transfer equations using the optical and thermal characteristics as inputs to evaluate light and thermal fields.

Another interesting model is provided by Zhou [Zhou 2004]. In this model, Tissue vasculature plays an important role in the temperature responses of biological bodies subject to laser heating. For example, interfaces between a blood vessel and its surrounding tissue may lead to reflection or absorption of the coming laser light. Different from most of the previous efforts, which focus mainly on a collective model, the model by Zhou solves simultaneously the three-dimensional light and heat transport in several typical tissue domains with either a single blood vessel or two countercurrent blood vessels running through, as shown in the Figure 2.4.

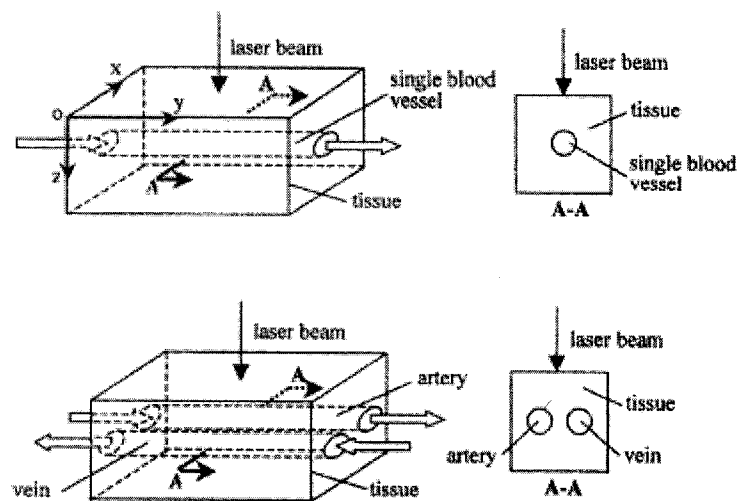


Figure 2.4 Illustration of Zhou's model [Zhou 2004]

Unlike the previous studies, heat transfer coefficients or Nusselt numbers were not used to calculate heat transfer to large blood vessels. Instead, the conjugate heat transfer problem is solved numerically by modeling the heat transfer in tissues and blood regions as a whole. The energy equations used to describe the transient temperature distributions in the blood and tissue domains take the same form:

$$\rho C \frac{\partial T}{\partial t} + \rho C v \frac{\partial T}{\partial y} = K \nabla^2 T + Q, \quad (2.5)$$

where v is the velocity component on the y -axis.

In living tissue, a large blood vessel can carry away a significant amount of the energy deposited from any heat source applied to the tissue, and this carry-away of the energy results in a local cooling of the tumor cells immediately adjacent to the vessel and leads to possible regeneration of the tumor. This reduction of the velocity of the blood before it arrives at the tumor region is often used to reduce the localized cooling of large blood vessels. However, when the velocity of the blood flowing through the vessel is reduced drastically, the buoyancy-driven flow due to density variations may become significant. To account for this problem, Zhou and Liu [Zhou 2004] use three-dimensional Navier-Stokes equations to calculate the flow field. They state that it is reasonable to assume that blood flow behavior can be described by such a continuum model, such as Navier-Stokes equations, because in the multiphase system consisting of plasma and blood cells, the diameter of the main blood cell is of the order of several micrometers, much less than the diameter of the blood vessel [Zhou 2004].

Among these models discussed above, Pennes' model is of a more general nature and, although it has been strongly criticized as a model, it has produced remarkably good

correlations with experimental data. And, therefore, it is the most frequently used model for hyperthermia treatment planning.

Compared with the explosion of activity in studying the hyperbolic heat conduction, investigations on the thermal wave propagation in living tissues were carried out only very recently in the bioheat transfer field. The conduction term in Pennes' bioheat transfer equation is based on Fourier's law, which is

$$q(\vec{r}, t) = -K\nabla T(\vec{r}, t) \quad (2.6)$$

where \vec{r} stands for the position vector. This equation implies an instantaneous thermal energy deposition in medium; i.e., any local temperature disturbance causes an instantaneous perturbation in temperature at each point in medium. Vernotte [Vernotte 1958] and Cattaneo [Cattaneo 1958] formulated a modified unsteady heat conduction equation (the CV equation) as follow:

$$q(\vec{r}, t) + \tau \frac{\partial q(\vec{r}, t)}{\partial t} = -K\nabla T(\vec{r}, t) \quad (2.7)$$

where τ is defined as thermal relaxation time in homogeneous substances, which ranges from 10^{-18} – 10^{-14} s [Kaminski 1990]. Since most of the heating processes are much longer than this time scale, Fourier's law has therefore been successfully applied to heat conduction in these materials [Liu 1999].

Biological systems are comprised of porous capillary bodies and cells that are heterogeneous, multiphasic and surface-dominated systems. In such highly non-homogeneous inner structures, τ can have a meaning which is different from the commonly referred thermal relaxation time. In such a setting, τ is defined as the characteristic time needed for accumulating the thermal energy required for propagative transfer to the nearest element within the nonhomogeneous inner structures [Kaminski

1990]. It reflects energy interaction at the structural level rather than that at the molecular or crystal lattice level as in homogeneous materials; and it may, thus, take a much greater value. The value of τ in biological systems has been predicted to be in the range between 20 and 30 seconds [Liu 1999].

Based on Equation (2.7) for heat flux including the characteristic time τ as well as Pennes' bioheat transfer equation, a general form of the Thermal Wave Model of Bioheat Transfer (TWMBT) in living tissues was initially introduced by Liu et al. [Liu 1995][Liu 1999] as:

$$\begin{aligned} & \nabla \cdot [K \nabla T(r, t)] + [W_b C_b (T_b - T)] + Q_m + Q_r + \tau (-W_b C_b \frac{\partial T}{\partial t} + \frac{\partial Q_m}{\partial t} + \frac{\partial Q_r}{\partial t}) \\ & = \rho C [\tau (\frac{\partial^2 T}{\partial t^2} + \frac{\partial T(r, t)}{\partial t})], \end{aligned} \quad (2.8)$$

where Q_m and Q_r are volumetric heat due to metabolism and spatial heating, respectively; T_b is the artery temperature, and T is the tissue temperature.

The one-dimensional TWMBT in a finite medium, as shown in Figure 2.5, was solved by Liu [Liu 1999] using separation of variables.

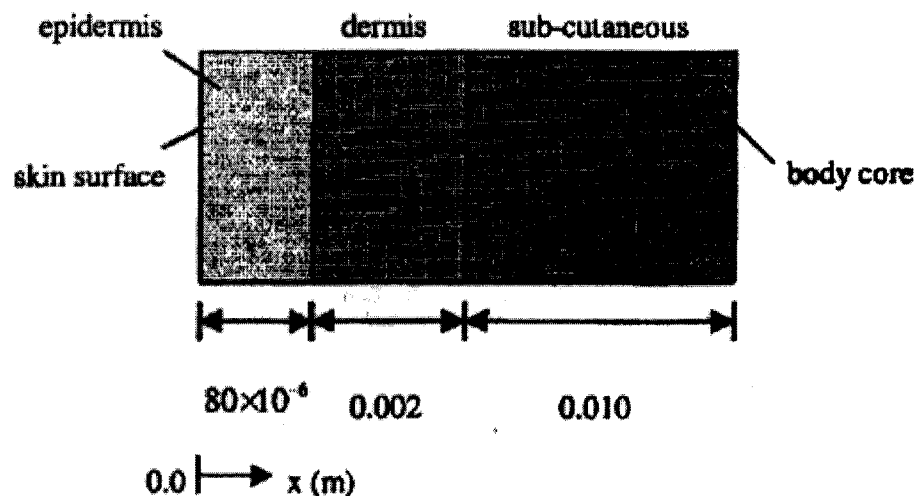


Figure 2.5 Schematic geometry of three-layered skin structure [Liu 1999]

Moreover, the analytical solution showed distinctive wave behaviors of bioheat transfer in skin subjected to instantaneous heating. The finite difference method was used to simulate and study practical problems involved in burn injuries in which skin was stratified as three layers with various thermal physical properties. Deviations between the TWMBT and the traditional Pennes' equation imply that, for high flux heating with extremely short duration (i.e., flash fire), the TWMBT, which accounts for finite thermal wave propagation, may provide realistic predictions on burn evaluation. A general heat flux criterion has been established to determine when the thermal wave propagation dominates the principal heat transfer process and the model can be used for tissue temperature prediction.

Liu furthered his study in a survey on the mechanisms of the wave-like behaviors of heat transfer in living tissue [Liu 2000a]. In his work, the mechanism of the wave-like behavior of heat transfer in living tissues was studied through introducing a new concept of multi-mode energy coupling. With this study, a phenomenological thermal wave model of bioheat transfer was obtained, and a new conceptual equation was proposed to correlate the heat flux with the temperature gradient. Thus the intriguingly high magnitude of the characteristic time in living tissues was better understood, and a simple temperature criterion was established to determine when the thermal wave propagation dominates the principal heat transfer process.

One important application of the models described above is hyperthermia treatment planning. Hyperthermia with radiation is a form of cancer therapy in which the objective is to heat the diseased tissue to some therapeutic temperature. As laser-induced hyperthermia becomes a more important method for the treatment of tumors, more

attention has been paid to the research of bioheat transfer in a living biomass under microwave hyperthermia [Vanderby 1988][Clegg 1989][Mandal 1989][Martin 1989][Roemer 1989][Roemer 1991][Xu 1993][Chatterjee 1994][Kolios 1995][Kolios 1998][Habash 1999][Mans 2003]. During the hyperthermia treatment, temperature distribution has to be precisely controlled to achieve the temperature to kill the tumor yet leave the surrounding tissue unharmed. This effect would be an easier task if the therapy temperature distribution could be predicted before the treatment. An example of the tissue regions involved in practical hyperthermia treatment is shown in Figure 2.6.

Clegg and Roemer performed hyperthermia sessions on a normal canine thigh to test the ability of a state and parameter estimation method to accurately predict the complete three-dimensional temperature distribution. To determine if thermal prescription has been achieved, invasive thermometry is used by inserting a large number of thermocouples into the thigh. A small subset of the measures were used as input in the Pennes' bioheat transfer equation to predict the parameter of perfusion, and thus reconstructed the three-dimensional model [Clegg 1989].

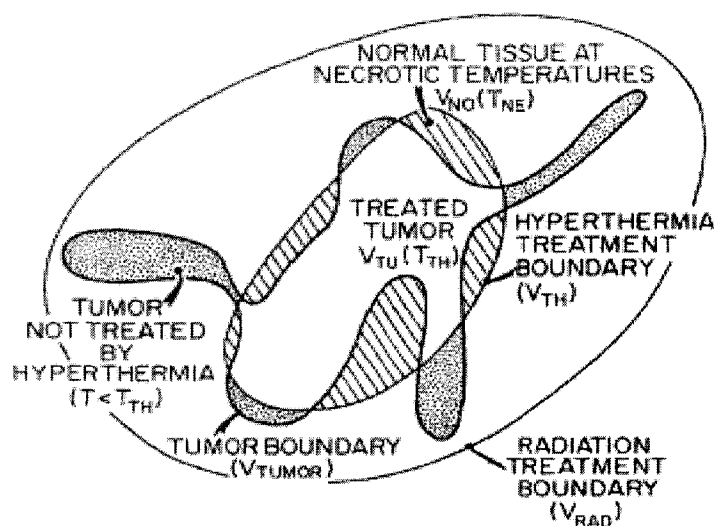


Figure 2.6 Tissue regions involved in practical hyperthermia treatment [Roemer 1991]

An example of recent research work using Pennes' equation is that of Zhu and Diao [Zhu 2001]. They used Pennes' equation to simulate the steady state temperature distribution within the brain after head injury. They determined where to place temperature sensors for infants and adults beneath the brain tissue in order to monitor the volumetric and average brain tissue temperature. Another example is the work of Deng and Liu [Deng 2001]. Using Pennes' bioheat transfer equation, they analytically studied the effect of pulsative blood perfusion on the tissue temperature.

Zhen and Dai incorporated an inverse problem into the three-dimensional Pennes' model [Zhen 2003]. They calculate the required laser power to obtain a pre-specified temperature at a pre-specified location of the skin after a pre-specified laser exposure time.

Zhang and Dai developed a numerical model for optimizing laser power irradiating on a three-dimensional triple-layered skin structure [Zhang 2004]. The method determines the required laser intensity in order to obtain pre-specified temperature at the given locations of the skin after pre-specified laser exposure time.

One of the major advantages of Pennes' bioheat transfer equation is that it is a field equation, which can be readily solved for distributions of temperature in space and time. However, one of the inherent deficiencies of Pennes' bioheat transfer equation arises from this major advantage. Pennes' bioheat transfer equation has the inherent limitation that it cannot simulate the effects of large, widely spaced thermally significant blood vessels; such situations are usually described by another equation [Huang 1994].

Such vessels are distributed throughout the body, and can locally and significantly perturb the temperature field [Chen 1980][Rawnsley 1994][Khaled 2003]. Thus, several

efforts have been made to add blood vessels to the simulations of in vivo temperatures. Several investigations [Mooibroek 1985][Crezee 1990][Chen 1993][Lagendijk 1982] present the numerical simulation results of the influence of either one or a pair of large blood vessels during hyperthermia.

Analytical and numerical studies can also be found in the literature for the heat transfer of tissues containing large blood vessels [Chato 1980][Crezee 1990][Chen 1993][Cai 1995][Cai 1998]. These studies are restricted to simple geometries. Chato studied a cylindrical non-perfused, unheated tissue with a single vessel traversing through. Huang extended and complemented Chato's working by developing the analytical solution for predicting the average axially varying temperature of the blood and the temperatures in its surrounding tissue for a single vessel traversing a perfused, heated tissue as shown in Figure 2.7 [Huang 1994].

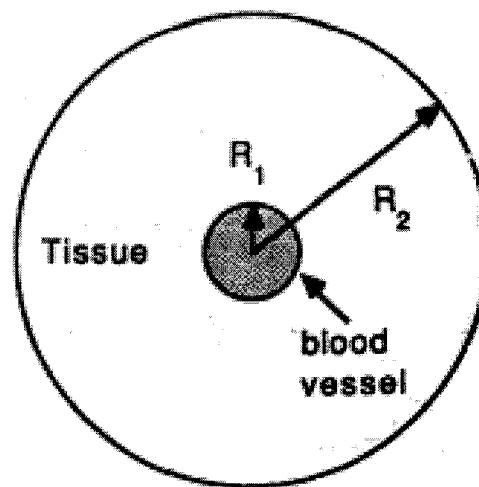


Figure 2.7 Schematic diagram of a single large blood vessel embedded in a perfused tissue [Huang 1994]

Several investigators [Charney 1988][Charney 1989][Roemer 1990][Williams 1990][Baish 1990][Huang 1994] try to model the heat transfer in tissue with blood vessels by combining Pennes' bioheat transfer equation for the tissue and the energy

equation for the vessels. Majchrzak and Mochnacki considered the thermal processes proceeding within a perfused tissue in the presence of a vessel, as shown in Figure 2.8.

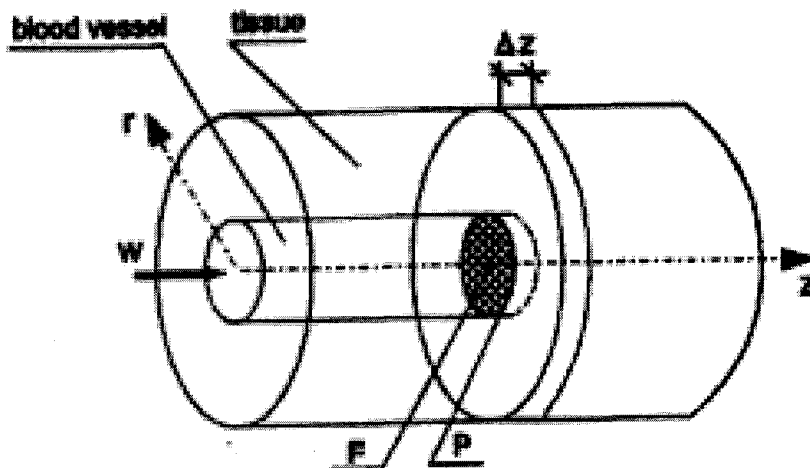


Figure 2.8 Non-homogeneous domain blood vessel-tissue [Majchrzak 1999]

Pennes' bioheat transfer equation determines the steady state temperature field in the tissue sub-domain, while the ordinary differential equation resulting from the energy balance describes the change of blood temperature along the vessel. The problem is solved using the combined numerical algorithm, in particular the boundary element method (for the tissue sub-domain) and the finite difference method (for the blood vessel sub-domain). Only steady state is considered. The Coupling of two equations results from the boundary condition given on the blood vessel wall [Majchrzak 1999].

2.2 Numerical Methods for Bioheat Models

2.2.1 Numerical Methods

The complexity of the mathematical modeling of the heat transfer process within a human tissue is enormous. But the analytical solution for most of the varieties of models discussed above are limited to a simple homogeneous geometry. It is very hard to obtain an analytical solution for a more complicated structure. The difficulties arise from

the fact that the skin is extremely heterogeneous [Chan 1992]. In this work, a complicated three-dimensional single vessel embedded triple-layered skin structure is considered and we might be able to solve it only by using numerical methods.

A review of the numerical solutions of the bioheat transfer equation can be found in Strohbehn and Roemer's work [Strohbehn 1984].

One of the numerical techniques is the method of moments, which enables us to determine the heat patterns in a body with arbitrary distribution of conductivity [Iskander 1982].

Another interesting method is the Cellular Neural Network (CNN) method. Niu and his colleagues applied CNN method to solve Pennes' bioheat transfer equation [Niu 2001]. Numerical solutions were obtained for a two-dimensional steady-state temperature field from ultrasound heat sources. The cellular neural networks' key features of asynchronous parallel processing, continuous-time dynamics and local interaction enable real-time temperature field estimation for clinical hyperthermia.

Among all the numerical methods used to solve the bioheat transfer equation for the thermal response of the human body under a flash fire or hyperthermia treatment, the most frequently used have been the finite difference method and finite element method. The former has gained more popularity than the latter.

2.2.2 Finite Element Method (FEM)

The disadvantage of the finite difference method is in that, in order to model the tissue inhomogeneities and the complex contours of the human body, one has to use very small grid sizes and even unequally spaced grids. But for FEM, it may be possible to obtain models which accurately represent the tissue inhomogeneity of the human body,

by using triangular elements in two-dimensional case and tetrahedral elements in three-dimensional case [Chatterjee 1994].

To study the thermal response of skin subjected to a flash fire, Trovi developed a variable property, multiple layer finite element model developed to predict skin temperatures and times to second and third degree burns in a triple-layered structure under simulated flash fire condition. The finite element matrix equation was derived using Galerkin's weighted residual method from the one-dimensional Pennes' bioheat transfer equation for blood-perfused skin. Five cubic Hermitian temperature interpolation polynomial elements were used, one for the epidermis, and two each for the dermis and subcutaneous region. The model is reported to be more accurate in making temperature and burn predictions than the constant single layer closed form solution for heat flux [Torvi 1994].

Chatterjee developed a three-dimensional finite element model of the prostate region of the human body which is generated using the automatic mesh generation capabilities of the software package ANSYS. The tissue types included are skin, fat, muscle, bone, intestine, nerve, prostate and tumor tissue. Variation of blood flow rates due to the increasing temperatures during hyperthermia is included. This might be the first time that a commercially available software package has been used to predict the detailed temperature profiles in the human body undergoing hyperthermia treatment for cancer. Figure 2.9 shows the various areas generated by ANSYS with different tissue types, and the corresponding mesh using triangular elements is shown in Figure 2.10 [Chatterjee 1994].

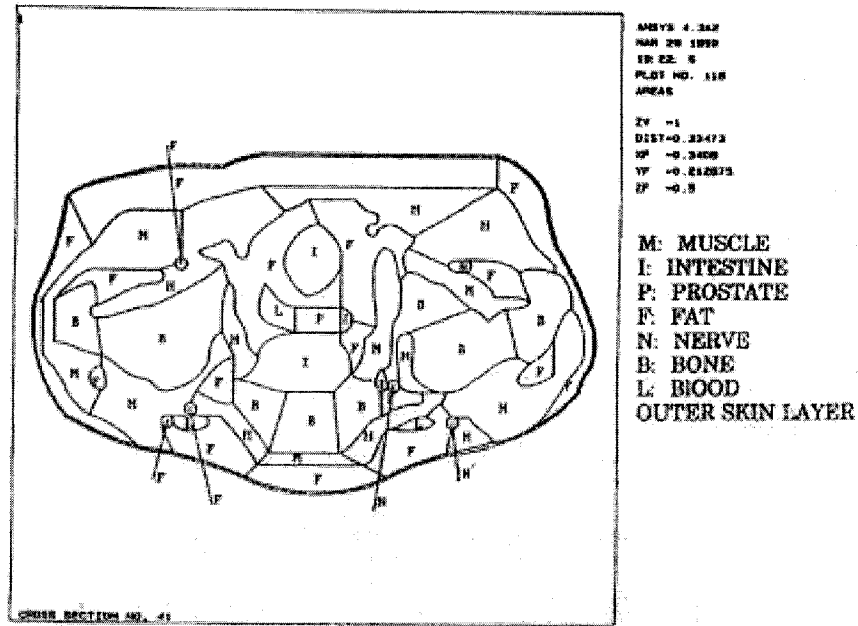


Figure 2.9 Areas of different tissue types in the prostate cross-section generated by ANSYS [Chatterjee 1994]

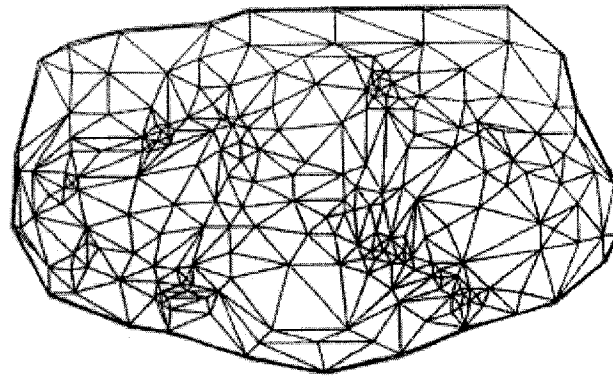


Figure 2.10 Finite element mesh generated by ANSYS PC/SOLID [Chatterjee 1994]

2.2.3 Boundary Element Method (BEM)

The Boundary element method is another powerful general purpose method. It is far more tolerant of aspect ratio degradation than the FEM and can yield secondary variables as accurately as the primary ones. The discretization of the boundary can be tailored to any irregular shape, thus it is capable of handling complex geometries [Chan 1992].

Mukherjee [Mukherjee 1984] and Chan [Chan 1992] compared the efficiency and accuracy of the BEM and the FEM for the Laplace equation. They found that the BEM results are more accurate than the FEM, implying that for the same desired level of accuracy, the BEM requires a coarser mesh than the FEM. They also found that the BEM accuracy, with a fixed boundary mesh, does not change appreciably with the number of internal sampling points, but the FEM accuracy is very sensitive to the internal mesh.

In Chan's work [Chan 1992], the BEM was formulated for transient and steady state, in both two-dimensional and three-dimensional problems. The two-dimensional steady-state BEM formulation was first verified by comparison with the analytical solution; then it was applied to model the heat transfer within a tissue adjacent to a blood vessel. An analytical expression of the one-dimensional model for the heat transfer within the blood vessel is incorporated into BEM. The resulting equation governs the conjugate heat transfer of a tissue adjacent to a blood vessel. Excellent agreement with the analytical solution was obtained in both of the two cases.

Traditional BEM has severe restrictions for solving TWMBT. First, the fundamental solution to the TWMBT is very difficult to derive; therefore, the boundary integral equation cannot be easily obtained. Second, the non-homogeneous terms accounting for effects, such as distributed heating Q , were included in the formulation by means of domain integrals, which weaken its "boundary only" character. Liu and Lu proposed a dual reciprocity boundary element method to avoid the above restrictions [Liu 1997][Liu 2000b].

In Lu's work [Lu 1998], the reciprocity boundary element method was extended to simulate the thermal wave propagation in biological tissues. A deep insight into

thermal wave behaviors, like reflection, decay, phase jumping, superposition and resolution, in a two-dimensional zone under certain boundary conditions is obtained.

2.2.4 Finite Difference Method

Although the advantages of the FEM and the BEM are in the flexibility in handling complicated geometries, the finite difference method is much simpler to use in the geometries of regular shape. Also, the accuracy of various FEM is usually of second order or even first order; yet with delicate derivation, higher-order accuracy can be achieved, comparatively easily, through the finite difference method.

Chato and Eckburg gave a comparison of Pennes' bioheat transfer model, Gautherie's model, and the Song-Weinbaum-Jiji model using finite difference techniques [Chato 1989]. Young and Boehm developed a numerical analysis for calculating the temperature fields of a percutaneous transluminal microwave angioplasty system using Specific Absorption Rates (SAR) data generated by finite difference time domain computations [Young 1993]. In Liu's work [Liu 1999], a numerical computation code based on finite difference scheme was developed to solve TWMBT. Because the epidermis, dermis and subcutaneous tissue have different physiological and thermal properties, temperature transients were computed within each layer and continuities of temperature and heat flux were applied to the boundaries of adjacent layers.

At Louisiana Tech University, a research group has focused on solving bioheat transfer problems, using the finite difference method [Dai 2003a][Dai 2003b][Dai 2004]. Zhen and Dai [Zhen 2003] incorporate a finite difference scheme and a laser power optimization algorithm using the least square method to solve an inverse problem in a three-dimensional rectangle triple-layered Pennes' model. Zhang and Dai [Zhang 2004]

did this in a three-dimensional cylindrical triple-layered skin structure. Each of these solutions has only a second-order accuracy, making it expensive to calculate a complicated geometry. In the next section, a compact finite difference scheme will be discussed. The technique of this compact scheme will lead to a fourth-order finite difference scheme in the present work.

2.3 Compact Finite Difference Scheme

2.3.1 Background

The idea of a compact finite difference scheme in this dissertation is mainly from [Lele 1992]. Lele's work can be summarized in the rest of Section 2.3.

Many physical phenomena have a range of space and time scales, turbulent fluid flows being a common example. Direct numerical simulations of these processes require all the relevant scales to be properly represented in the numerical model. These requirements have led to the development of spectral methods [Gottlieb 1977].

Some examples of the direct simulation of turbulent flows by spectral methods may be found in [Rogallo 1984] and [kim 1987]. Now the use of spectral methods is, however, limited to flows in simple domains and simple boundary conditions. These difficulties may be overcome by employing alternative numerical representations. And this is the motivation of the compact finite difference scheme. Rai and Moin [Rai 1989], present simulations of a turbulent channel flow using a high-order, upwind-biased finite difference scheme.

2.3.2 General Explicit Schemes

Given the values of a function on a set of nodes the finite difference approximation to the derivative of the function is expressed as a linear combination of the

given function values. For simplicity, we consider a uniformly spaced mesh where the nodes are indexed by i . The independent variable at each node i is $x_i = h(i-1)$ for $1 \leq i \leq N$, and the function values at the nodes $f_i = f(x_i)$ are given. The finite difference approximation f'_i to the first derivative $(df/dx)(x_i)$ at node i depends on the function values at nodes near i . For second and fourth-order central differences, the approximation, f'_i depends on the sets (f_{i-1}, f_{i+1}) and $(f_{i-2}, f_{i-1}, f_{i+1}, f_{i+2})$, respectively. In the spectral methods, however, the value of f'_i depends on all the nodal values. The Pade or compact finite difference schemes [Kreiss 1972] mimic this global dependence. The schemes presented here are generalizations of the Pade scheme. These generalizations are derived by writing approximations of the form:

$$\beta f'_{i-2} + \alpha f'_{i-2} + f'_{i-2} + \alpha f'_{i-2} + \beta f'_{i-2} = c \frac{f_{i+3} - f_{i-3}}{6h} + b \frac{f_{i+2} - f_{i-2}}{4h} + a \frac{f_{i+1} - f_{i-1}}{2h}. \quad (2.9)$$

The relations between the coefficients a , b , c and α, β are derived by matching the Taylor series coefficients of various orders. The first unmatched coefficient determines the formal truncation error of the approximation (2.9). These constraints are:

$$a + b + c = 1 + 2\alpha + 2\beta \quad (\text{Second order}) \quad (2.10)$$

$$a + 2^2 b + 3^2 c = 2 \frac{3!}{2!} (\alpha + 2^2 \beta) \quad (\text{Fourth order}) \quad (2.11)$$

Similarly, the derivation of compact approximations for the second derivative proceeds analogously to that of the first order derivative. This relations is of the form

$$\beta f''_{i-2} + \alpha f''_{i-2} + f''_{i-2} + \alpha f''_{i-2} + \beta f''_{i-2} = c \frac{f_{i+3} - 2f_i + f_{i-3}}{9h^2} + b \frac{f_{i+2} - 2f_i + f_{i-2}}{4h^2} + a \frac{f_{i+1} - 2f_i + f_{i-1}}{h^2}, \quad (2.12)$$

where f''_i is the second derivative at the node i . Once again, the relations between the

coefficients a , b , c and α, β are derived by matching the Taylor series coefficients of various orders. These constraints are:

$$a + b + c = 1 + 2\alpha + 2\beta, \quad (\text{Second order}) \quad (2.13)$$

$$a + 2^2 b + 3^2 c = \frac{4!}{2!}(\alpha + 2^2 \beta), \quad (\text{Fourth order}) \quad (2.14)$$

which appear very similar to the constraints of the first derivative approximations but different in their right hand sides. By choosing $\beta = 0$ and $c = 0$, a one-parameter family of fourth-order schemes is generated. This family has

$$\beta = 0, \quad c = 0, \quad a = \frac{4}{3}(1 - \alpha), \quad b = \frac{1 - 10\alpha}{3}. \quad (2.15)$$

It may be noted that as $\alpha \rightarrow 0$ this family coincides with the well-known fourth-order central difference scheme. For $\alpha = \frac{1}{10}$, the classical Pade scheme is recovered.

If the dependent variables are periodic in x , then the system of relations, Equations (2.9) and (2.12), can be solved as a linear system of equations for the unknown derivative values. This linear system is a cyclic pentadiagonal (tridiagonal) when β is nonzero (zero, respectively). The general non-periodic case requires additional relations appropriate for the near boundary nodes. The resulting linear system is amenable to efficient numerical solution. Equations (2.9) and (2.12), along with a mathematically defined mapping between a non-uniform physical mesh and a uniform computational mesh, provide derivatives on a non-uniform mesh. It is also possible to derive relations, analogous to Equations (2.9) and (2.12), for a non-uniform mesh directly (e.g., relations corresponding to the traditional Pade scheme were derived in [Goedheer 1985]).

2.3.3 Boundary Formulation

The general non-periodic case requires additional relations appropriate for the near boundary nodes. Many applications involve computations in domains with non-periodic boundaries. This section introduces approximations for the first and second derivatives for the near boundary nodes.

The first derivative at the boundary $i = 1$ may be obtained from a relation of the form coupled to the Equation (2.9) written for the interior nodes as follows:

$$f_1' + \alpha f_2' = \frac{1}{h} (af_1 + bf_2 + cf_3 + df_4). \quad (2.16)$$

Requiring Equation (2.16) to be at least second-order accurate constrains the coefficients to

$$a = -\frac{3 + \alpha + 2d}{2}, \quad b = 2 + 3d, \quad c = -\frac{1 - \alpha + 6d}{2}. \quad (2.17)$$

Similarly, the relations appropriate for near boundary nodes between the nodal values of a function and its second derivative may be derived by Taylor series expansions. The compact scheme analogous to Equation (2.16) is given by

$$f_1'' + \alpha f_2'' = \frac{1}{h^2} (af_1 + bf_2 + cf_3 + df_4 + ef_5). \quad (2.18)$$

Requiring Equation (2.18) to be at least second-order accurate constrains the coefficients to

$$a = \alpha + 2 + e, \quad b = -(2\alpha + 5 + 4e), \quad c = \alpha + 4 + 6e, \quad d = -(1 + 4e). \quad (2.19)$$

2.3.4 Applications

The different schemes described above provide an improved resolution of the short-length scales. Furthermore, the schemes have a pure central difference form (except near the boundaries); specifically, they have no built-in artificial dissipation. It is, therefore, necessary that the applications to which they are applied be such that there is a well-defined cutoff for the shortest scales. In other words, the shortest scales should be determined physically and not numerically, and this rules out applications to problems with discontinuities (in variables and their derivatives). This is not to say that the present method is inapplicable to inviscid problems. It is, however, restricted to problems with smooth solutions.

The spectral-like nature of the finite difference schemes also makes it necessary to use accurate boundary conditions. Boundary conditions, which may seem suitable with low-order schemes (and with built-in dissipation), may not perform well with the schemes described here. These were used in [Lele 1989] and [Sandham 1989] in applications to compressible mixing layers. A full discussion of the different boundary conditions, comparisons with other methods commonly used with low-order schemes, and application to reacting and non-reacting flows are presented in [Poinsot 1989]. Applications to three-dimensional incompressible mixing layers and wakes (along with spectral methods in two directions) are described by Buell [Buell 1989].

CHAPTER 3

MATHEMATICAL MODELS AND COMPACT FINITE

DIFFERENCE SCHEMES

3.1 General Governing Equations

3.1.1 Problem Description

To study the thermal behavior in the human skin, we consider a three-dimensional single vessel embedded triple-layered skin structure composed of epidermis, dermis and subcutaneous tissue. A physical description of heat flow in Pennes' bioheat transfer model can be schematically expressed as in Figure 3.1. Here, a single blood vessel goes through the subcutaneous layer, and two different heat sources are considered: First, constant heating is applied to the top surface. Second, a laser beam focuses on top of the skin and penetrates into the inner structure.

3.1.2 General Governing Equations

The governing equation that describes the thermal behavior of the three-dimensional structure based on Pennes' bioheat transfer equation [Pennes 1948] is described as follows:

$$\rho_l C_l \frac{\partial \theta_l}{\partial t} = K_l \left(\frac{\partial^2 \theta_l}{\partial x^2} + \frac{\partial^2 \theta_l}{\partial y^2} + \frac{\partial^2 \theta_l}{\partial z^2} \right) - W_b^l C_b^l \theta_l + Q_l, \quad l = 1, 2, 3. \quad (3.1)$$

where θ_1 is the elevated tissue temperature above surrounding temperature due to heating or laser radiation, while ρ_1 , C_1 and k_1 denote density, specific heat, and thermal conductivity of tissue, respectively. C_b^l is the specific heat of blood, W_b^l is the blood perfusion rate and Q_r^l the volumetric heat due to spatial heating.

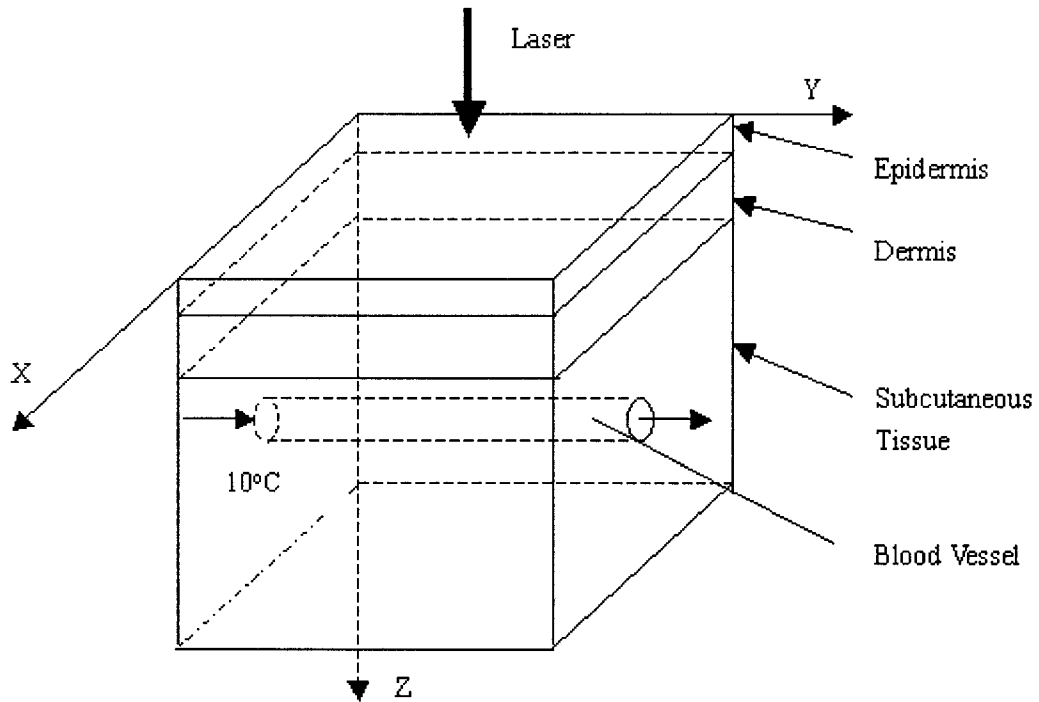


Figure 3.1 Schematic configuration of a three-dimensional triple-layered skin structure and laser power

The boundary condition of the top surface is Dirichlet, when constant heating is applied, specifically,

$$\theta_1 = \text{constant}, \quad z = 0. \quad (3.2)$$

The boundary condition of the top surface is Neumann, when laser radiation is applied, specifically,

$$\frac{\partial \theta_1}{\partial z} = 0, \quad z = 0. \quad (3.3)$$

In the three-dimensional triple-layered skin structure, perfect contact (continuous temperature and equality of flux-in and flux-out) is assumed. The boundary conditions for the interfaces and the bottom surface are listed as follows:

$$\theta_1 = \theta_2, \quad k_1 \frac{\partial \theta_1}{\partial z} = k_2 \frac{\partial \theta_2}{\partial z}, \quad z = L_1, \quad (3.4)$$

$$\theta_2 = \theta_3, \quad k_2 \frac{\partial \theta_2}{\partial z} = k_3 \frac{\partial \theta_3}{\partial z}, \quad z = L_1 + L_2, \quad (3.5)$$

$$\frac{\partial \theta_3}{\partial z} = 0, \quad z = L_1 + L_2 + L_3. \quad (3.6)$$

On the lateral walls we have

$$\nabla \theta = 0. \quad (3.7)$$

The initial conditions are

$$\theta_l = 0, \quad t = 0, \quad l = 1, 2, 3. \quad (3.8)$$

3.2 One-Dimensional Uniform-Layered Case

3.2.1 Model Description

For the sake of simplicity, we begin with a one-dimensional uniform skin structure to demonstrate the fourth-order compact finite difference scheme. A physical description of heat flow in Pennes' bioheat transfer model for this one-dimensional skin structure can be schematically expressed as in Figure. 3.2. This skin is composed of a uniform layer. The numbers in the Figure 3.2 represent the order of discretized grids.

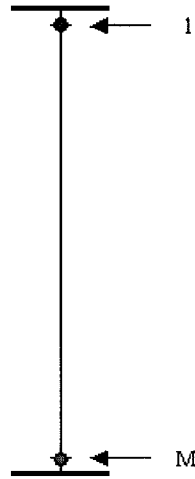


Figure 3.2 Schematic configuration of a one-dimensional uniform-layered skin structure

3.2.2 Governing Equations

The general governing Equation (3.1) is simplified to describe the thermal behavior of uniform-layered skin structures as follows:

$$\rho C \frac{\partial \theta}{\partial t} = K \frac{\partial^2 \theta}{\partial x^2} - W_b C_b \theta + Q. \quad (3.9)$$

Compared with the general governing equation, the terms corresponding to the y and z Axes, the contribution of the perfusion of the single blood vessel, and the heat source Q are eliminated. Constant heating is applied, which suggests that the boundary condition at the top surface is Dirichlet, as Equation (3.2). The boundary condition at the bottom surface is

$$\frac{\partial \theta}{\partial z} = 0, \quad z = L. \quad (3.10)$$

The initial condition is

$$\theta = 0, \quad t = 0. \quad (3.11)$$

3.2.3 Finite Difference Scheme

Let θ_j^t be the numerical approximation of $\theta(j\Delta x, t\Delta t)$, where Δx and Δt are the spatial and temporal mesh sizes, respectively. Here, j is chosen to be $0 \leq j \leq M + 1$, where $(M + 1)\Delta x = L$.

Using the compact finite difference method [Lele 1992], we develop a fourth-order compact finite difference scheme for solving the above initial and boundary value problem in the following.

Discretize Equation (3.9) with finite different method and we have

$$\rho C \frac{\theta_j^{t+1} - \theta_j^t}{\Delta t} = \frac{K}{2} (\theta_{xx}^{t+1} + \theta_{xx}^t)_j - W_b C_b \frac{\theta_j^{t+1} + \theta_j^t}{2}, \quad 1 \leq j \leq M, \quad (3.12)$$

where, for non-interface layer, θ_{xx}^{t+1} and θ_{xx}^t satisfy

$$\frac{1}{10} (\theta_{xx}^t)_{j-1} + (\theta_{xx}^t)_j + \frac{1}{10} (\theta_{xx}^t)_{j+1} = \frac{6}{5\Delta x^2} (\theta_{j-1}^t - 2\theta_j^t + \theta_{j+1}^t), \quad 2 \leq j \leq M - 1 \quad (3.13)$$

and

$$\frac{1}{10} (\theta_{xx}^{t+1})_{j-1} + (\theta_{xx}^{t+1})_j + \frac{1}{10} (\theta_{xx}^{t+1})_{j+1} = \frac{6}{5\Delta x^2} (\theta_{j-1}^{t+1} - 2\theta_j^{t+1} + \theta_{j+1}^{t+1}), \quad 2 \leq j \leq M - 1. \quad (3.14)$$

The derivation of Equations (3.13) and (3.14) is shown as follows:

A generalization of this relation will take the form of

$$b(\theta_{xx})_{j-1} + a(\theta_{xx})_j + c(\theta_{xx})_{j+1} = \frac{1}{\Delta x^2} (d\theta_{j-1} + e\theta_j + f\theta_{j+1}). \quad (3.15)$$

Using the Taylor series at location j , we have

$$(\theta_{xx})_{j-1} = (\theta_{xx})_j - \Delta x (\theta_{xxx})_j + \frac{\Delta x^2}{2!} (\theta_{xxxx})_j + O(\Delta x^3), \quad (3.16)$$

$$(\theta_{xx})_{j+1} = (\theta_{xx})_j + \Delta x (\theta_{xxx})_j + \frac{\Delta x^2}{2!} (\theta_{xxxx})_j + O(\Delta x^3), \quad (3.17)$$

$$\theta_{j-1} = (\theta)_j - \Delta x(\theta_x)_j + \frac{\Delta x^2}{2!}(\theta_{xx})_j - \frac{\Delta x^3}{3!}(\theta_{xxx})_j + \frac{\Delta x^4}{4!}(\theta_{xxxx})_j + O(\Delta x^5), \quad (3.18)$$

$$\theta_{j+1} = (\theta)_j + \Delta x(\theta_x)_j + \frac{\Delta x^2}{2!}(\theta_{xx})_j + \frac{\Delta x^3}{3!}(\theta_{xxx})_j + \frac{\Delta x^4}{4!}(\theta_{xxxx})_j + O(\Delta x^5), \quad (3.19)$$

The relation between the coefficients a, b, c, d, e and f are derived by matching the Taylor series coefficients of various orders,

$$\text{balancing of the 0}^{\text{th}} \text{ order derivative, } (\theta)_j, \text{ will give } d + e + f = 0; \quad (3.20)$$

$$\text{balancing of the 1}^{\text{st}} \text{ order derivative, } (\theta_x)_j, \text{ will give } -d + f = 0; \quad (3.21)$$

$$\text{balancing of the 2}^{\text{nd}} \text{ order derivative, } (\theta_{xx})_j, \text{ will give } b + a + c = \frac{1}{2!}d + \frac{1}{2!}f; \quad (3.22)$$

$$\text{balancing of the 3}^{\text{rd}} \text{ order derivative, } (\theta_{xxx})_j, \text{ will give } -b + c = -\frac{1}{3!}d + \frac{1}{3!}f. \quad (3.23)$$

Let coefficient a be free and $b = \frac{1}{10}a$ in Equation (3.15). Solve the group of equations

$$(3.20-3.23) \text{ and we have } b = \frac{1}{10}a, \quad c = \frac{1}{10}a, \quad d = \frac{6}{5}a, \quad e = -\frac{12}{5}a, \quad f = \frac{6}{5}a. \text{ If we let } a$$

$= 1$, we will have Equations (3.13) and (3.14).

When a constant heating boundary is applied, specifically, θ_0 is given, $(\theta_{xx})_1$ is calculated by a second order approximation

$$(\theta_{xx})_1 = \frac{1}{\Delta x^2}(\theta_0 - 2\theta_1 + \theta_2). \quad (3.24)$$

when an insulated boundary is applied, specifically, $(\theta_x)_0 = 0$, $(\theta_{xx})_1$ is determined by the following equation

$$\frac{b}{\Delta x}(\theta_x)_0 + a(\theta_{xx})_1 + c(\theta_{xx})_2 = \frac{1}{\Delta x^2}(e\theta_2 + f\theta_1), \quad (3.25)$$

where a, b, c, e and f are constants. The relation between the coefficients a, b, c, e and f are derived again by matching the Taylor series coefficients of various orders,

$$\text{balancing of the } 0^{\text{th}} \text{ order derivative, } \theta_0, \text{ will give } e + f = 0; \quad (3.26)$$

$$\text{balancing of the } 1^{\text{st}} \text{ order derivative, } (\theta_x)_0, \text{ will give } b = 2e + f; \quad (3.27)$$

$$\text{balancing of the } 2^{\text{nd}} \text{ order derivative, } (\theta_{xx})_0, \text{ will give } a + c = \frac{2^2}{2!}e + \frac{1^2}{2!}f; \quad (3.28)$$

$$\text{balancing of the } 3^{\text{th}} \text{ order derivative, } (\theta_{xxx})_0, \text{ will give } 2b + a = \frac{2^3}{3!}e + \frac{1^3}{3!}f. \quad (3.29)$$

Matching the coefficients, we obtain $a = \frac{11}{6}e, b = -e, c = -\frac{1}{3}e$ and $f = -e$ in order to

have a fourth order approximation. Let $e = 1$, then Equation (3.25) becomes

$$\frac{11}{6}(\theta_{xx})_1 - \frac{1}{3}(\theta_{xx})_2 = \frac{1}{\Delta x}(\theta_x)_0 + \frac{(\theta_2 - \theta_1)}{\Delta x^2}. \quad (3.30)$$

$(\theta_{xx})_M$ is determined by the following equation:

$$b(\theta_{xx})_{M-1} + a(\theta_{xx})_M + \frac{c}{\Delta x}(\theta_x)_{M+1} = \frac{1}{\Delta x^2}(e\theta_{M-1} + f\theta_M), \quad (3.31)$$

where a, b, c, e and f are constants.

The relation between the coefficients a, b, c, e and f are derived again by matching the Taylor series coefficients of various orders,

$$\text{balancing of the } 0^{\text{th}} \text{ order derivative, } \theta_{M+1}, \text{ will give } e + f = 0; \quad (3.32)$$

$$\text{balancing of the } 1^{\text{st}} \text{ order derivative, } (\theta_x)_{M+1}, \text{ will give } c = -2e - f; \quad (3.33)$$

$$\text{balancing of the } 2^{\text{nd}} \text{ order derivative, } (\theta_{xx})_{M+1}, \text{ will give } b + a = \frac{2^2}{2!}e + \frac{1^2}{2!}f; \quad (3.34)$$

$$\text{balancing of the } 3^{\text{th}} \text{ order derivative, } (\theta_{xxx})_{M+1}, \text{ will give } -2b - a = -\frac{2^3}{3!}e - \frac{1^3}{3!}f. \quad (3.35)$$

Matching the coefficients, we obtain $a = \frac{11}{6}e$, $c = -e$, $b = -\frac{1}{3}e$ and $f = -e$ in order to

have a fourth order approximation. Let $e = 1$, then Equation (3.31) becomes

$$-\frac{1}{3}(\theta_{xx})_{M-1} + \frac{11}{6}(\theta_{xx})_M = \frac{1}{\Delta x}(\theta_x)_{M+1} + \frac{(\theta_{M-1} - \theta_M)}{\Delta x^2}. \quad (3.36)$$

Equations (3.24), (3.13) or (3.14) and (3.36) will form a tridiagonal system that can be transformed into

$$\frac{1}{10}A\bar{\theta}_{xx} = -\frac{1}{5\Delta x^2}B\bar{\theta} + f(\theta_0), \quad (3.37)$$

where

$$A = \begin{pmatrix} 10 & & & & \\ 1 & 10 & 1 & & \\ & \dots & \dots & \dots & \\ & & 1 & 10 & 1 \\ & & & -4 & 22 \end{pmatrix}$$

and

$$B = \begin{pmatrix} 10 & -5 & & & \\ -6 & 12 & -6 & & \\ & \dots & \dots & \dots & \\ & & -6 & 12 & -6 \\ & & & -6 & 6 \end{pmatrix}$$

Therefore we have

$$\bar{\theta}_{xx} = -\frac{2}{\Delta x^2}A^{-1}B\bar{\theta} + f(\theta_0) \quad (3.38)$$

Similarly, Equations (3.30), (3.13) or (3.14) and (3.36) will form a tridiagonal system that can be transformed into

$$\frac{1}{10}C\bar{\theta}_{xx} = -\frac{1}{5\Delta x^2}D\bar{\theta}, \quad (3.39)$$

where

$$C = \begin{pmatrix} 22 & -4 & & & \\ 1 & 10 & 1 & & \\ & \dots & \dots & \dots & \\ & & 1 & 10 & 1 \\ & & & -4 & 22 \end{pmatrix}$$

and

$$D = \begin{pmatrix} 6 & -6 & & & \\ -6 & 12 & -6 & & \\ & \dots & \dots & \dots & \\ & & -6 & 12 & -6 \\ & & & -6 & 6 \end{pmatrix}$$

Therefore we have

$$\bar{\theta}_{xx} = -\frac{2}{\Delta x^2} C^{-1} D \bar{\theta} \quad (3.40)$$

Solving the two tridiagonal linear systems, Equations (3.38) and (3.40), will give solution for $\bar{\theta}_{xx}$, which can be used to solve Pennes' bioheat transfer equation through iteration.

3.2.4 Algorithm

To solve the discretized form of the one-dimensional Pennes' bioheat transfer equation, Equation (3.10), the following steps will be taken:

Step 1. Apply θ_j^t , at time $t = 0, 1, 2, \dots$, to the right hand side of the tridiagonal system, Equation (3.38) or (3.40) to calculate $(\theta_j^t)_{xx}$.

Step 2. Apply $(\theta_j^{t+1})^n$, at time $t = t+1$ and $n = 0, 1, 2, \dots$, to the right hand side of the tridiagonal system to calculate $(\theta_j^{t+1})_{xx}^n$. When $n = 0$, let $(\theta_j^{t+1})^n$ be equal to $(\theta_j^t)^n$.

Step 3. Substitute $(\theta_j^t)_{,xx}$ and $(\theta_j^{t+1})_{,xx}^n$ back to Equation (3.12) to get $(\theta_j^{t+1})^{n+1}$. Let $(\theta_j^{t+1})^n$ be equal to the newest obtained $(\theta_j^{t+1})^{n+1}$.

Step 4. Repeat step 2-3 until $\text{MAX} \left| (\theta_j^{t+1})^{n+1} - (\theta_j^{t+1})^n \right| < \varepsilon$.

Step 5. Increment time level by 1, and then repeat step 1-4 until the criteria for time is satisfied.

3.2.5 Convergence Analysis

Convergence analysis of a finite difference scheme is important in that its property of convergence will decide the flexibility in choosing the spatial and temporal grid sizes. We begin with investigating the convergence of the compact finite difference scheme for a uniform-layered skin structure with a constant heating boundary condition.

Theorem 1: The compact finite difference we developed above is unconditionally stable for Pennes' bioheat transfer equation in a uniform-layered skin structure with constant heating boundary condition.

Proof: Substituting Equation (3.38) back to Equation (3.12), we have

$$\rho C \frac{\bar{\theta}^{n+1} - \bar{\theta}^n}{\Delta t} = \frac{-2K}{2\Delta x^2} (A^{-1}B\bar{\theta}^{n+1} + A^{-1}B\bar{\theta}^n)_j - W_b C_b \frac{\bar{\theta}^{n+1} + \bar{\theta}^n}{2} + c, \quad (3.41)$$

where c is some constant. Multiply both sides by Δt , we have

$$2\rho C(\bar{\theta}^{n+1} - \bar{\theta}^n) = -K\gamma(A^{-1}B\bar{\theta}^{n+1} + A^{-1}B\bar{\theta}^n)_j - W_b C_b(\bar{\theta}^{n+1} + \bar{\theta}^n)\Delta t + c, \quad (3.42)$$

where $\gamma = \frac{2\Delta t}{\Delta x^2}$

Solve for $\bar{\theta}^{n+1}$, we obtain

$$(2\rho C I + \Delta t W_b C_b I + K\gamma A^{-1}B)\bar{\theta}^{n+1} = (2\rho C I - \Delta t W_b C_b I - K\gamma A^{-1}B)\bar{\theta}^n + c \quad (3.43)$$

and then

$$\bar{\theta}^{n+1} = (2\rho cI + \Delta t W_b C_b I + K\gamma A^{-1}B)^{-1} (2\rho cI - \Delta t W_b C_b I - K\gamma A^{-1}B) \bar{\theta}^n + c = H\bar{\theta}^n + c. \quad (3.44)$$

We have the following lemma, which we state without proof.

Lemma 1 [Burden 2001]: for any $X^{(0)} \in R^n$, the sequence $\{X^{(k)}\}_{k=0}^{\infty}$ defined by $X^{(k)} = TX^{(k-1)} + C$, for each $k \geq 1$, converges to the unique solution if and only if the spectral radius $\rho(T)$ satisfies $\rho(T) < 1$.

We will show that $\rho(H) < 1$ holds. Let λ be an eigenvalue of $A^{-1}B$ and \bar{x} its corresponding eigenvector.

$$\lambda \bar{x} = A^{-1}B\bar{x} \Rightarrow \lambda A\bar{x} = B\bar{x} \Rightarrow \lambda \bar{x}^T A\bar{x} = \bar{x}^T B\bar{x}. \quad (3.45)$$

Observe that

$$\bar{x}^T A\bar{x} = (x_1 \quad x_2 \quad \dots \quad x_n) \begin{pmatrix} 10 & & & & \\ & 1 & 10 & 1 & \\ & & \dots & \dots & \dots \\ & & & 1 & 10 & 1 \\ & & & & -4 & 22 \end{pmatrix} \begin{pmatrix} x_1 \\ x_2 \\ \vdots \\ x_n \end{pmatrix} \quad (3.46)$$

$$= 10x_1^2 + x_1x_2 + 10x_2^2 + x_2x_3 + 10x_3^2 + x_3x_4 + \dots + x_{m-2}x_{m-1}$$

$$+ 10x_{m-1}^2 - 4x_{m-1}x_m + x_{m-1}x_m + 22x_m^2$$

$$\geq 10x_1^2 - \frac{1}{2}(x_1^2 + x_2^2) + 10x_2^2 - (x_2^2 + x_3^2) + 10x_3^2 - (x_3^2 + x_4^2) + \dots + (x_{m-2}^2$$

$$+ x_{m-1}^2) + 10x_{m-1}^2 - \frac{3}{2}(x_{m-1}^2 + x_m^2) + 22x_m^2$$

$$= \frac{19}{2}x_1^2 + \frac{17}{2}x_2^2 + 8x_3^2 + \dots + 8x_{m-2}^2 + \frac{15}{2}x_{m-1}^2 + \frac{41}{2}x_m^2$$

$$\geq 0$$

and

$$\begin{aligned}
\bar{x}^T B \bar{x} &= (x_1 \ x_2 \ \dots \ x_n) \begin{pmatrix} 10 & -5 & & & \\ -6 & 12 & -6 & & \\ & \dots & \dots & \dots & \\ & & -6 & 12 & -6 \\ & & & -6 & 6 \end{pmatrix} \begin{pmatrix} x_1 \\ x_2 \\ \vdots \\ x_n \end{pmatrix} \quad (3.47) \\
&= 10x_1^2 - 5x_1x_2 - 6x_1x_2 + 12x_2^2 - 6x_2x_3 - 6x_2x_3 + 12x_3^2 - 6x_3x_4 - \dots - 6x_{m-2}x_{m-1} \\
&\quad + 12x_{m-1}^2 - 6x_{m-1}x_m - 6x_{m-1}x_m + 6x_m^2 \\
&\geq 10x_1^2 - \frac{5}{2}(x_1^2 + x_2^2) - 3(x_1^2 + x_2^2) + 12x_2^2 - 3(x_2^2 + x_3^2) - 3(x_2^2 + x_3^2) + 12x_3^2 - \\
&\quad 3(x_3^2 + x_4^2) - \dots - 3(x_{m-2}^2 + x_{m-1}^2) + 12x_{m-1}^2 - 3(x_{m-1}^2 + x_m^2) - 3(x_{m-1}^2 + x_m^2) + 6x_m^2 \\
&= \frac{9}{2}x_1^2 + \frac{1}{2}x_2^2 \\
&\geq 0.
\end{aligned}$$

Thus, we can conclude that $\lambda \geq 0$. Because ρ, c, W_b, C_b are all positive, we have

$2\rho cI + \Delta t W_b C_b I > 0$, so

$$\left| (2\rho cI - \Delta t W_b C_b I - K\gamma\lambda(A^{-1}B)) \right| < \left| (2\rho cI + \Delta t W_b C_b I + K\gamma\lambda(A^{-1}B)) \right|, \quad (3.48)$$

therefore, we conclude that

$$|\lambda(H)| = \left| (2\rho cI + \Delta t W_b C_b I + K\gamma A^{-1}B)^{-1} (2\rho cI - \Delta t W_b C_b I - K\gamma A^{-1}B) \right| < 1 \quad (3.49)$$

Thus, by Lemma 1, we have proved Theorem 1.

Now, we investigate the convergence of the compact finite difference scheme for a uniform-layered skin structure with insulated boundary condition.

Theorem 2: The compact finite difference we developed above is unconditionally stable for Pennes' bioheat transfer equation in a uniform-layered skin structure with insulated boundary condition.

Proof: Similarly, Substitute Equation (3.40) back to Equation (3.12), then we have

$$\bar{\theta}^{n+1} = (2\rho cI + \Delta t W_b C_b I + K\gamma C^{-1}D)^{-1} (2\rho cI - \Delta t W_b C_b I - K\gamma C^{-1}D) \bar{\theta}^n = H \bar{\theta}^n. \quad (3.50)$$

We will show that $\rho(H) < 1$ holds. Let λ be an eigenvalue of $C^{-1}D$ and \bar{x} its corresponding eigenvector.

$$\lambda \bar{x} = C^{-1}D\bar{x} \Rightarrow \lambda C\bar{x} = D\bar{x} \Rightarrow \lambda \bar{x}^T C\bar{x} = \bar{x}^T D\bar{x}. \quad (3.51)$$

$$\bar{x}^T C\bar{x} = (x_1 \quad x_2 \quad \dots \quad x_n) \begin{pmatrix} 22 & -4 & & & \\ 1 & 10 & 1 & & \\ & \dots & \dots & \dots & \\ & & 1 & 10 & 1 \\ & & & -4 & 22 \end{pmatrix} \begin{pmatrix} x_1 \\ x_2 \\ \vdots \\ x_n \end{pmatrix} \quad (3.52)$$

$$\begin{aligned} &= 22x_1^2 - 4x_1x_2 + x_1x_2 + 10x_2^2 + 2x_2x_3 + 10x_3^2 + 2x_3x_4 + \dots + 2x_{m-2}x_{m-1} \\ &\quad + 10x_{m-1}^2 - 4x_{m-1}x_m + x_{m-1}x_m + 22x_m^2 \\ &\geq 22x_1^2 - \frac{3}{2}(x_1^2 + x_2^2) + 10x_2^2 - (x_2^2 + x_3^2) + 10x_3^2 - (x_3^2 + x_4^2) + \dots + (x_{m-2}^2 \\ &\quad + x_{m-1}^2) + 10x_{m-1}^2 - \frac{3}{2}(x_{m-1}^2 + x_m^2) + 22x_m^2 \\ &= \frac{41}{2}x_1^2 + \frac{15}{2}x_2^2 + 8x_3^2 + \dots + 8x_{m-2}^2 + \frac{15}{2}x_{m-1}^2 + \frac{41}{2}x_m^2 \\ &\geq 0 \end{aligned}$$

and

$$\bar{x}^T D \bar{x} = (x_1 \quad x_2 \quad \dots \quad x_n) \begin{pmatrix} 6 & -6 & & & \\ -6 & 12 & -6 & & \\ & \dots & \dots & \dots & \\ & & -6 & 12 & -6 \\ & & & -6 & 6 \end{pmatrix} \begin{pmatrix} x_1 \\ x_2 \\ \vdots \\ x_n \end{pmatrix} \quad (3.53)$$

$$\begin{aligned} &= 6x_1^2 - 6x_1x_2 - 6x_1x_2 + 12x_2^2 - 6x_2x_3 - 6x_2x_3 + 12x_3^2 - 6x_3x_4 - \dots - 6x_{m-2}x_{m-1} \\ &\quad + 12x_{m-1}^2 - 6x_{m-1}x_m - 6x_{m-1}x_m + 6x_m^2 \\ &\geq 6x_1^2 - 3(x_1^2 + x_2^2) - 3(x_1^2 + x_2^2) + 12x_2^2 - 3(x_2^2 + x_3^2) - 3(x_2^2 + x_3^2) + 12x_3^2 - \\ &\quad 3(x_3^2 + x_4^2) - \dots - 3(x_{m-2}^2 + x_{m-1}^2) + 12x_{m-1}^2 - 3(x_{m-1}^2 + x_m^2) - 3(x_{m-1}^2 + x_m^2) + 6x_m^2 \\ &\geq 0. \end{aligned}$$

Thus, we can conclude that $\lambda > 0$. Again, $2\rho cI + \Delta t W_b C_b I > 0$, so

$$\left| (2\rho cI - \Delta t W_b C_b I - K\gamma\lambda(C^{-1}D)) \right| < \left| (2\rho cI + \Delta t W_b C_b I + K\gamma\lambda(C^{-1}D)) \right|, \quad (3.54)$$

therefore, we conclude that

$$|\lambda(H)| = \left| (2\rho cI + \Delta t W_b C_b I + K\gamma C^{-1}D)^{-1} (2\rho cI - \Delta t W_b C_b I - K\gamma C^{-1}D) \right| < 1. \quad (3.55)$$

Thus, by Lemma 1, we have proved Theorem 2.

3.3 One-Dimensional Triple-Layered Case

3.3.1 Model Description

In this section we extend the finite difference scheme from the one-dimensional uniform layered case to a triple-layered case. The physical description of heat flow in Pennes' bioheat transfer model for this case can be schematically expressed as in Figure 3.3.

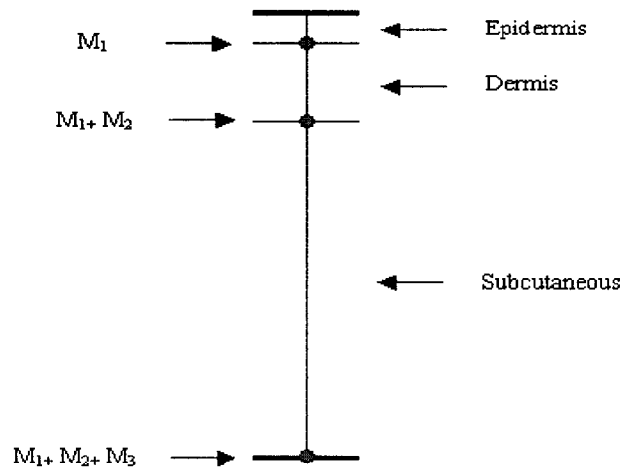


Figure 3.3 One-dimensional triple-layered skin structure and laser power

3.3.2 Governing Equations

To describe the thermal behavior of a one-dimensional triple-layered skin structures, the general governing Equation (3.1) is simplified as follows:

$$\rho_l C_l \frac{\partial \theta_l}{\partial t} = K_l \frac{\partial^2 \theta_l}{\partial x^2} - W_b^l C_b^l \theta_l + Q_l, \quad l = 1, 2, 3. \quad (3.56)$$

Compared with the general governing equation, the terms regarding to y and z Axes, the contribution of the perfusion of the single blood vessel and the heat source Q are eliminated. The boundary and initial conditions are the same as Equations (3.2-3.7).

3.3.3 Finite Difference Scheme

Let θ_j^l be the numerical approximation of $\theta(j\Delta z, t\Delta t)$, where Δz and Δt are the spatial and temporal mesh sizes, respectively. Here, j is chosen such that $0 \leq j \leq M_l$, where $M_l \Delta z = L_l$ and $l=1, 2, 3$.

The compact finite difference scheme for Pennes' bioheat transfer equation in a one-dimensional triple-layered skin structure is different from the previous scheme in

Section 3.2 only in that the relation of row vector $\bar{\theta}_{xx}$ and $\bar{\theta}$ at the interfaces in the tridiagonal system Equations (3.38) and (3.40).

Now, we will show the derivation of such relation in a general case. Assume there is an interface with subscript I which connects two layers of different thermal properties. Two superscripts, *up* and *down*, represent the upper and lower layer relative to the interface. Using the compact finite difference methods [Lele 1994], $(\theta_{xx})_I$ is determined by two equations:

$$\frac{c^{up}}{\Delta x} (\theta_x)_I^{down} + a^{up} (\theta_{xx})_{I-1} + b^{up} (\theta_{xx})_I^{up} = d^{up} \theta_I + e^{up} \theta_{I-1} \quad (3.57)$$

and

$$\frac{c^{down}}{\Delta x} (\theta_x)_I^{down} + a^{down} (\theta_{xx})_{I+1} + b^{down} (\theta_{xx})_I^{down} = d^{down} \theta_I + e^{down} \theta_{I+1}, \quad (3.58)$$

where $c^{up}, a^{up}, b^{up}, d^{up}, e^{up}, c^{down}, a^{down}, b^{down}, d^{down}, e^{down}$ are coefficients.

Using the Taylor series at location I , we have

$$(\theta_{xx})_{I-1} = (\theta_{xx})_I - \Delta x (\theta_{xxx})_I + \frac{\Delta x^2}{2!} (\theta_{xxxx})_I + O(\Delta x^3), \quad (3.59)$$

$$(\theta_{xx})_{I+1} = (\theta_{xx})_I + \Delta x (\theta_{xxx})_I + \frac{\Delta x^2}{2!} (\theta_{xxxx})_I + O(\Delta x^3), \quad (3.60)$$

$$\theta_{I-1} = \theta_I - \Delta x (\theta_x)_I + \frac{\Delta x^2}{2!} (\theta_{xx})_I - \frac{\Delta x^3}{3!} (\theta_{xxx})_I + \frac{\Delta x^4}{4!} (\theta_{xxxx})_I + O(\Delta x^5), \quad (3.61)$$

$$\theta_{I+1} = \theta_I + \Delta x (\theta_x)_I + \frac{\Delta x^2}{2!} (\theta_{xx})_I + \frac{\Delta x^3}{3!} (\theta_{xxx})_I + \frac{\Delta x^4}{4!} (\theta_{xxxx})_I + O(\Delta x^5). \quad (3.62)$$

The relation between the coefficients $c^{up}, a^{up}, b^{up}, d^{up}, e^{up}, c^{down}, a^{down}, b^{down}, d^{down}, e^{down}$ are derived by matching the Taylor series coefficients of various orders. In Equation (3.57),

$$\text{balancing of the } 0^{\text{th}} \text{ order derivative, } \theta_I, \text{ will give } d^{up} + e^{up} = 0; \quad (3.63)$$

$$\text{balancing of the } 1^{\text{st}} \text{ order derivative, } (\theta_x)_I \text{ will give } \frac{c^{up}}{\Delta x} = -\frac{e^{up}}{\Delta x}; \quad (3.64)$$

$$\text{balancing of the } 2^{\text{nd}} \text{ order derivative, } (\theta_{xx})_I \text{ will give } b^{up} + a^{up} = \frac{1}{2!} e^{up}; \quad (3.65)$$

$$\text{balancing of the } 3^{\text{th}} \text{ order derivative, } (\theta_{xxx})_I \text{ will give } -a^{up} = -\frac{1}{3!} e^{up}. \quad (3.66)$$

Let c^{up} be the free coefficient and $c^{up} = 6c$ in Equation (3.57). Solve the group of Equations (3.63-3.66) yields $a^{up} = -1c$, $b^{up} = -2c$, $d^{up} = 6c$, $e^{up} = -6c$. In Equation (3.58),

$$\text{balancing of the } 0^{\text{th}} \text{ order derivative, } \theta_I, \text{ will give } d^{down} + e^{down} = 0; \quad (3.67)$$

$$\text{balancing of the } 1^{\text{st}} \text{ order derivative, } (\theta_x)_I, \text{ will give } \frac{c^{down}}{\Delta x} = \frac{e^{down}}{\Delta x}; \quad (3.68)$$

$$\text{balancing of the } 2^{\text{nd}} \text{ order derivative, } (\theta_{xx})_I, \text{ will give } b^{down} + a^{down} = \frac{1}{2!} e^{down}; \quad (3.69)$$

$$\text{balancing of the } 3^{\text{th}} \text{ order derivative, } (\theta_{xxx})_I, \text{ will give } a^{down} = \frac{1}{3!} e^{down}. \quad (3.70)$$

Let c^{down} be the free coefficient and $c^{down} = 6c$ in Equation (3.58). Solve the group of Equation (3.67-3.70) will give us $a^{down} = 1c$, $b^{down} = 2c$, $d^{down} = -6c$, $e^{down} = 6c$.

By the assumption of perfect contact,

$$K^{up} \cdot (\theta_x)_I^{up} = K^{down} \cdot (\theta_x)_I^{down}. \quad (3.71)$$

Multiplying Equation (3.57) by K^{up} and Equation (3.58) by K^{down} , and subtracting one from the other will give

$$\begin{aligned}
& K^{up} a^{up} (\theta_{xx})_{I-1}^{up} + [b^{up} K^{up} (\theta_{xx})_I^{up} - b^{down} K^{down} (\theta_{xx})_I^{down}] - a^{down} K^{down} (\theta_{xx})_I^{up} \\
& = K^{up} (d^{up} \theta_I + e^{up} \theta_{I-1}) - K^{down} (d^{down} \theta_I + e^{down} \theta_{I+1}). \tag{3.72}
\end{aligned}$$

Notice that $(\theta_{xx})_I^{down}$ and $(\theta_{xx})_I^{up}$ are second order derivatives in two different layers. So, the left hand side of Equation (3.72) has four unknowns. In order to fit Equation (3.72) into tridiagonal system, Equation (3.38) or (3.40), we will eliminate $(\theta_{xx})_I^{down}$ in the following.

By Pennes' bioheat transfer equation, Equation (3.56), we have

$$\rho^{up} C^{up} (\theta_t)_I^{up} = K^{up} (\theta_{xx})_I^{up} - W_b^{up} C_b^{up} \theta_I \tag{3.73}$$

and

$$\rho^{down} C^{down} (\theta_t)_I^{down} = K^{down} (\theta_{xx})_I^{down} - W_b^{down} C_b^{down} \theta_I \tag{3.74}$$

for the interface I . By the assumption of perfect contact, we have

$$(\theta_t)_I^{up} = (\theta_t)_I^{down}. \tag{3.75}$$

Multiplying Equation (3.73) by $\rho^{down} C^{down}$ and Equation (3.74) by $\rho^{up} C^{up}$, and subtracting one from the other will give

$$(\theta_{xx})_I^{down} = \frac{k^{up} \rho^{down} C^{down}}{k^{down} \rho^{up} C^{up}} (\theta_{xx})_I^{up} + \left(\frac{W_b^{down} C_b^{down} \rho^{up} C^{up} - W_b^{up} C_b^{up} \rho^{down} C^{down}}{k^{down} \rho^{up} C^{up}} \right) \theta_I. \tag{3.76}$$

Substitute Equation (3.76) back into Equation (3.72) will give

$$\begin{aligned}
& K^{up} a^{up} (\theta_{xx})_{I-1}^{up} + [b^{up} K^{up} - b^{down} K^{down} \frac{k^{up} \rho^{down} C^{down}}{k^{down} \rho^{up} C^{up}}] (\theta_{xx})_I^{up} - a^{down} K^{down} (\theta_{xx})_I^{up} \\
& = K^{up} (d^{up} \theta_I + e^{up} \theta_{I-1}) - K^{down} (d^{down} \theta_I + e^{down} \theta_{I+1}) + \\
& b^{down} K^{down} \left(\frac{W_b^{down} C_b^{down} \rho^{up} C^{up} - W_b^{up} C_b^{up} \rho^{down} C^{down}}{k^{down} \rho^{up} C^{up}} \right) \theta_I \tag{3.77}
\end{aligned}$$

Equations (3.24), (3.13) or (3.14), (3.36) and (3.77) form a tridiagonal system for a one-dimensional triple-layered skin structure with constant heating boundary condition. Equations (3.30), (3.13) or (3.14), (3.36) and (3.77) form a tridiagonal system for a one-dimensional triple-layered skin structure with insulated boundary condition. The algorithm for the one-dimensional triple-layered case is the same as described in Section 3.2.4.

3.4 Three-Dimensional Triple-layered Case

3.4.1 Model Description

In this section, we extend the previous finite difference scheme to a three-dimensional triple-layered case. A physical description of heat flow in Pennes' bioheat model for this case can be schematically expressed as in Figure 3.4.

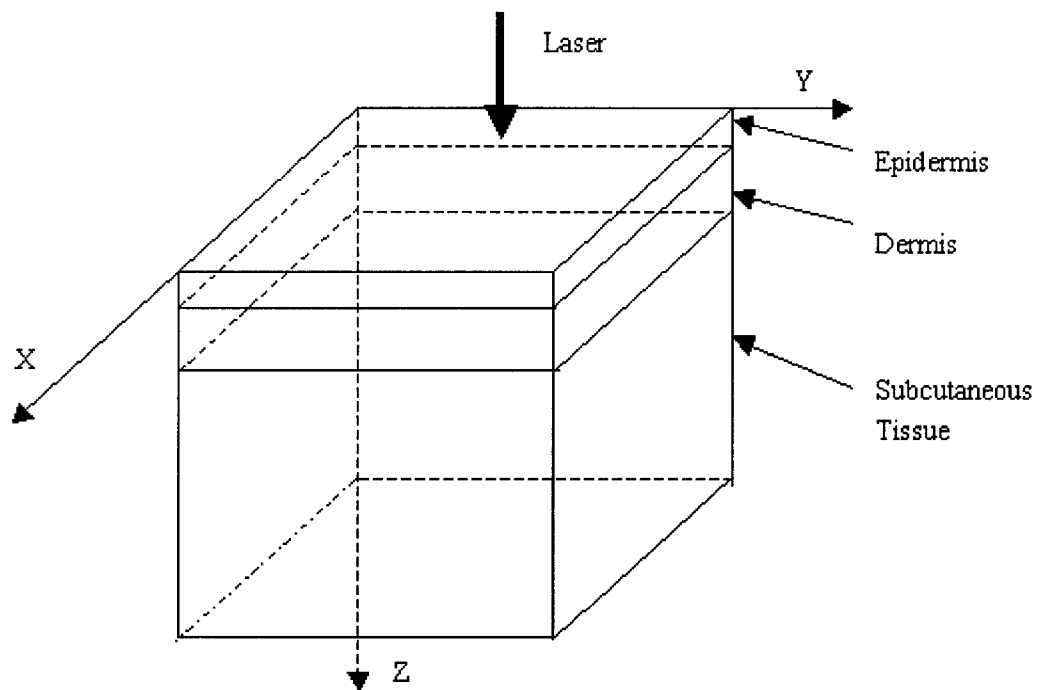


Figure 3.4 Laser radiated three-dimensional triple-layered skin structure

3.4.2 Governing Equations

To describe the thermal behavior of three-dimensional triple-layered skin structure, the general governing Equation (3.1) is simplified as follows:

$$\rho_l C_l \frac{\partial \theta_l}{\partial t} = K_l \left(\frac{\partial^2 \theta_l}{\partial x^2} + \frac{\partial^2 \theta_l}{\partial y^2} + \frac{\partial^2 \theta_l}{\partial z^2} \right) - W_b^l C_b^l \theta_l + Q_l, \quad l = 1, 2, 3 \quad (3.78)$$

The boundary and initial conditions are the same as Equations (3.2-3.7).

Heat sources Q_l^l are introduced in this section (when constant heating boundary condition is applied, this term is 0). We assume that the laser power is continuous and spatial with a normal distribution. The heat source Q_l^l can be described as follows [Han 1994][Zhen 2003]:

$$Q_1 = \alpha_1 e^{-\alpha_1 z} \frac{1}{2\pi\sigma^2} e^{-\frac{(x^2+y^2)}{2\sigma^2}} P(1 - \text{Reff}_1), \quad (3.79)$$

$$Q_2 = \alpha_2 e^{-\alpha_1 \delta_1} e^{-\alpha_2 z} \frac{1}{2\pi\sigma^2} e^{-\frac{(x^2+y^2)}{2\sigma^2}} P(1 - \text{Reff}_2), \quad (3.80)$$

$$Q_3 = \alpha_3 e^{-\alpha_3 z} e^{-\alpha_1 \delta_1} e^{-\alpha_2 \delta_2} \frac{1}{2\pi\sigma^2} e^{-\frac{(x^2+y^2)}{2\sigma^2}} P(1 - \text{Reff}_3), \quad (3.81)$$

where $\alpha_1, \alpha_2, \alpha_3$ are laser absorbtivity of the three layers, $\text{Reff}_1, \text{Reff}_2, \text{Reff}_3$ are laser reflectivity of the three layers of the skin, σ is the standard deviation of the width of a normally distributed laser beam, and $\delta_1, \delta_2, \delta_3$ are the depths of the three layers of the skin.

3.4.3 Finite Difference Scheme

Let $(\theta_l)_{ijk}^t$ be the numerical approximation of $(\theta_l)(i\Delta x, j\Delta y, k\Delta z, t\Delta t)$, where $\Delta x, \Delta y, \Delta z$ and Δt are the spatial and temporal mesh sizes, respectively. Here i, j, k are

chosen to be $0 \leq i \leq N^x + 1, 0 \leq j \leq N^y + 1, 0 \leq k \leq N^z$, so that $N_l^z \Delta z = L_l, l=1,2,3$. Also, we let $(Q_l)_{ijk}$ be the numerical approximation of $(Q_l)(i\Delta x, j\Delta y, k\Delta z)$.

Equation (3.78) can be discretized as

$$\rho_l C_l \frac{\theta_{ijk}^{t+1} - \theta_{ijk}^t}{\Delta t} = \frac{K}{2} (\theta_{xx}^{t+1} + \theta_{xx}^t + \theta_{yy}^{t+1} + \theta_{yy}^t + \theta_{zz}^{t+1} + \theta_{zz}^t)_{ijk} - W_b C_b \frac{\theta_{ijk}^{t+1} + \theta_{ijk}^t}{2} + (Q_l)_{ijk} \quad (3.82)$$

The bioheat transfer in the directions of the three Axes, x, y, z , are assumed to be independent. The bioheat transfer along x and y Axes are considered to be in a uniform-layered skin structure. Therefore it is considered similar as the one-dimensional uniform-layered case in Section 3.2. The bioheat transfer along z Axis is similar to the one-dimensional triple-layered case in Section 3.3.

3.4.4 Algorithm

To solve the discretized form of Pennes' bioheat transfer equation in a one-dimensional triple-layered skin structure, Equation (3.82), the following steps will be taken:

Step 1. Calculate $(Q_l)_{ijk}$.

Step 2. Apply θ_{ijk}^t , at time $t = 0, 1, 2, \dots$, to the right hand side of the tridiagonal system to calculate $(\theta_{ijk}^t)_{xx}, (\theta_{ijk}^t)_{yy}$ and $(\theta_{ijk}^t)_{zz}$.

Step 3. Apply $(\theta_{ijk}^{t+1})^n$, at time $t = t+1$ and $n = 0, 1, 2, \dots$, to the right hand side of the tridiagonal system to calculate $(\theta_{ijk}^{t+1})_{xx}^{n+1}, (\theta_{ijk}^{t+1})_{yy}^{n+1}$ and $(\theta_{ijk}^{t+1})_{zz}^{n+1}$. When $n = 0$, let $(\theta_{ijk}^{t+1})^n$ be equal to $(\theta_{ijk}^t)^n$.

Step 4. Substitute $(\theta'_{ijk})_{xx}$, $(\theta'_{ijk})_{yy}$, $(\theta'_{ijk})_{zz}$, $(\theta^{t+1})_{ijk,xx}^{n+1}$, $(\theta^{t+1})_{ijk,yy}^{n+1}$, $(\theta^{t+1})_{ijk,zz}^{n+1}$ and $(Q_l)_{ijk}$ back to Equation (3.73) to obtain $(\theta^{t+1})_{ijk}^{n+1}$. Let $(\theta^{t+1})_{ijk}^n$ equal to the newest obtained $(\theta^{t+1})_{ijk}^{n+1}$.

Step 5. Repeat step 3-4 until $\text{MAX} \left| (\theta^{t+1})_{ijk}^{n+1} - (\theta^{t+1})_{ijk}^n \right| < \varepsilon$.

Step 6. Increment time level by 1, and then repeat step 2-5 until the criteria for time is satisfied.

3.5 Three-Dimensional Single Vessel Embedded Triple-Layered Case

3.5.1 Problem Description

In this section, the last component, a single blood vessel is added into the subcutaneous tissue to complete our three-dimensional single vessel embedded triple-layered model. A physical description of heat flow in Pennes' bioheat transfer model, in a three-dimensional single vessel embedded triple-layered skin structure, can be schematically expressed as in Figure 3.1 (page 31).

3.5.2 Governing Equations

The governing equations that describe the thermal behavior of triple-layered skin structures are described as follows:

$$\rho_l C_l \frac{\partial \theta_l}{\partial t} = K_l \left(\frac{\partial^2 \theta_l}{\partial x^2} + \frac{\partial^2 \theta_l}{\partial y^2} + \frac{\partial^2 \theta_l}{\partial z^2} \right) - W_b^l C_b^l \theta_l + W_b^l C_b^l \theta_b + Q_l, \quad l = 1, 2, 3. \quad (3.83)$$

The temperature of blood corresponding to co-ordinate z is assumed to be uniform. The constraints of energy balance will lead to the following Ordinary Differential Equation (ODE) [Majchrzak 1999]

$$C_B \nu F \frac{d(\theta_b)}{dy} - \alpha P (\theta_p - \theta_b) = 0, \quad (3.84)$$

where $C_B, \nu, F, \alpha, P, \theta_p, \theta_b$ are specific heat of blood, velocity of blood, vessel lateral section, heat transfer coefficient between and tissue, vessel periphery and vessel wall temperature. We assume $\theta_b = \theta_{b0}$ at the entry.

3.5.3 Finite Difference Scheme

Equation (3.83) can be discretized as

$$\begin{aligned} \rho_l C_l \frac{\theta_{ijk}^{t+1} - \theta_{ijk}^t}{\Delta t} = & \frac{K}{2} (\theta_{xx}^{t+1} + \theta_{xx}^t + \theta_{yy}^{t+1} + \theta_{yy}^t + \theta_{zz}^{t+1} + \theta_{zz}^t)_{ijk} \\ & - W_b^l C_b^l \frac{\theta_{ijk}^{t+1} + \theta_{ijk}^t}{2} + W_b^l C_b^l (\theta_b^t)_j + (Q_l)_{ijk}. \end{aligned} \quad (3.85)$$

The tissue part is the same with that in Section 3.4. For the vessel part, we let $(\theta_b)_j^t$ be the numerical approximation of $\theta_b(j\Delta y, t\Delta t)$, where $0 \leq j \leq N^y + 1$. θ_p is approximated by taking the average of temperature, θ , around the vessel. The ODE (3.84) is solved using second-order Runge-Kutta method.

3.5.4 Algorithm

To solve the discretized form of three-dimensional Pennes' bioheat transfer equation in a three-dimensional single vessel embedded triple-layered skin structure, Equation (3.85), the following steps will be taken:

Step 1. Calculate $(Q_l)_{ijk}$.

Step 2. Apply θ_{ijk}^t , at time $t = 0, 1, 2, \dots$, to the right hand side of the tridiagonal system to calculate $(\theta_{ijk}^t)_{xx}$, $(\theta_{ijk}^t)_{yy}$ and $(\theta_{ijk}^t)_{zz}$.

Step 3. Apply $(\theta_{ijk}^{t+1})^n$, at time $t = t+1$ and $n = 0, 1, 2, \dots$, to the right hand side of the tridiagonal system to calculate $(\theta_{ijk}^{t+1})_{xx}^{n+1}$, $(\theta_{ijk}^{t+1})_{yy}^{n+1}$ and $(\theta_{ijk}^{t+1})_{zz}^{n+1}$. When $n = 0$, let $(\theta_j^{t+1})^n$ be equal to $(\theta_j^t)^n$.

Step 4. Solve the ODE using second order Runge-Kutta method to get $(\theta_b)_j^n$.

Step 5. Substitute $(\theta_b)_j^n$, $(\theta_{ijk}^t)_{xx}$, $(\theta_{ijk}^t)_{yy}$, $(\theta_{ijk}^t)_{zz}$, $(\theta_{ijk}^{t+1})_{xx}^{n+1}$, $(\theta_{ijk}^{t+1})_{yy}^{n+1}$, $(\theta_{ijk}^{t+1})_{zz}^{n+1}$ and $(Q_t)_{ijk}$ back to Equation (3.85) to obtain $(\theta_{ijk}^{t+1})^{n+1}$. Let $(\theta_{ijk}^{t+1})^n$ equal to the newest obtained $(\theta_{ijk}^{t+1})^{n+1}$.

Step 6. Repeat step 3-5 until $\text{MAX} \left| (\theta_{ijk}^{t+1})^{n+1} - (\theta_{ijk}^{t+1})^n \right| < \varepsilon$.

Step 7. Increment time level by 1, and then repeat step 2-6 until the criteria for time is satisfied.

CHAPTER 4

NUMERICAL EXAMPLES AND RESULTS

4.1 One-Dimensional Uniform-Layered Case

To test the accuracy of the compact finite difference scheme presented in Section 3.2, we consider a uniform tissue with depth of 1mm. The material parameters used are listed in Table 4.1.

Table 4.1 Parameters for the uniform layer in the human skin tissue [Liu 1999]

Parameters	Value
C_b	4.2 J/g·°C
C	4.2 J/g·°C
W_b	0.0000005 g/mm ³ ·s
K	0.0002 W/mm·°C
ρ	0.001 g/mm ³
θ_0	12°C

It can be shown that the analytical solution of the above problem is [Liu 1999]

$$\theta(x,t) = \frac{Q_r}{W_b C_b} + \frac{(\theta_0 - \frac{Q_r}{W_b C_b}) \operatorname{ch}[\sqrt{\frac{W_b C_b}{K}}(x-L)]}{\operatorname{ch}(\sqrt{\frac{W_b C_b}{K}}L)} + \sum_{n=1}^{\infty} A_n \exp\{-\alpha[\frac{(2n-1)^2}{4L^2}\pi^2 + \frac{W_b C_b}{K}]t\} \cdot \sin \frac{(n-\frac{1}{2})\pi}{L}x, \quad (4.1)$$

where

$$\alpha = \frac{K}{\rho C}, \quad A_n = -\frac{(2n-1)\theta_0\pi}{\frac{W_b C_b}{K} L^2 + \left(\frac{2n-1}{2}\pi\right)^2}$$

We apply both the fourth-order compact finite difference scheme and second-order Crank-Nicholson scheme to the skin structure. The time increment was chosen to be 0.001 second and the grid size, Δx , to be 0.2, 0.1 and 0.05mm, respectively. The numerical solutions when $0 \leq t \leq 150$ seconds were compared with the analytical solution, as shown in Figure 4.1.

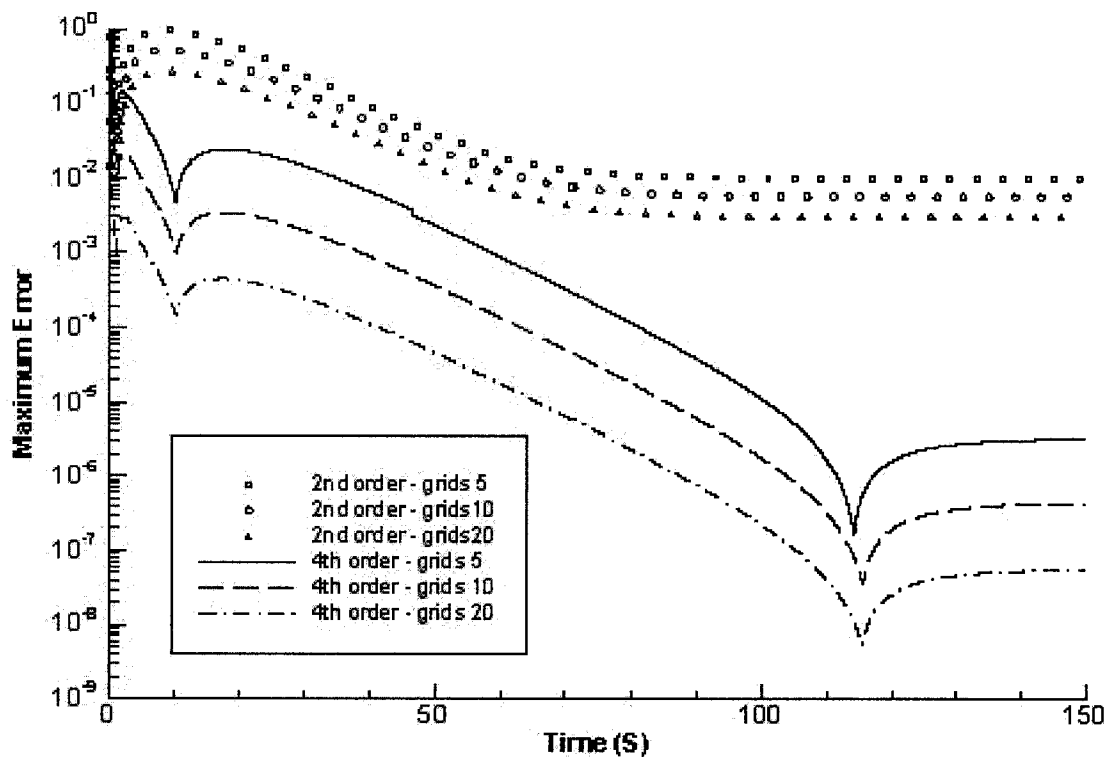


Figure 4.1 Comparison of numerical errors between the second-order Crank-Nicholson scheme and the fourth-order compact finite difference scheme

It can be seen from Figure 4.1 that the compact finite difference scheme that we develop is much more accurate than the Crank-Nicholson scheme. Furthermore, the CPU time in a Sun Workstation for these two schemes with different grid sizes is listed in Table 4.2. One can see that the speeds for both schemes are not much different.

Table 4.2 Comparison of the running time with different grid sizes

Grid Size (mm)	Crank-Nicholson scheme (Second)	Fourth-order compact scheme (Second)
0.2	840.00	792.83
0.1	1776	1559
0.05	3907	3590

4.2 One-Dimensional Triple-Layered Case

We also consider a one-dimensional triple-layered skin structure with depth of 12.08mm. Let $\theta_0 = 12^\circ\text{C}$. The dimension and thermal properties are listed in the Table 4.3.

Table 4.3 Parameters for the three layers in the human skin structure

Layer Paramete	Epidermis	Dermis	Subcutaneous tissue
Thickness (mm)	0.08	2.0	10.0
ρ_l (g/mm ³)	0.0012	0.0012	0.001
C (J/g .°C)	3.6	3.4	3.06
C _b (J/g .°C)	4.2	4.2	4.2
K (W/mm .°C)	0.00026	0.00052	0.00021
W _b (g/mm ³ .s)	0	0.0000005	0.0000005

The time increment is chosen to be 0.001 second and the grid size $\Delta x = 0.02\text{mm}$. The numerical solutions for four locations of different depth, within the time domain [0,150] seconds are shown in Figure 4.2.

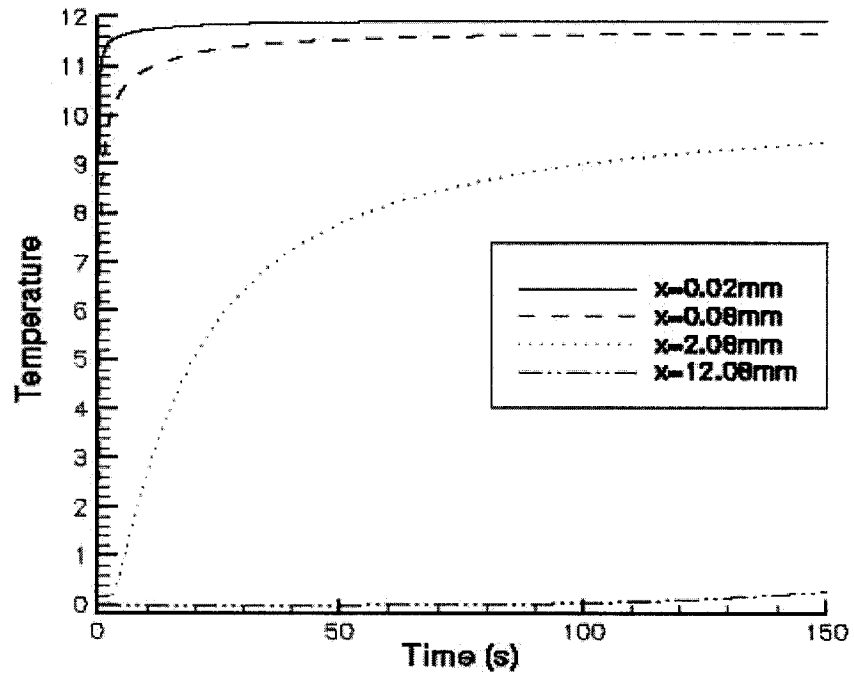


Figure 4.2 Transient temperatures under constant heating with duration of 150 seconds

Totally, 94.98 seconds of CPU time is needed in a Sun Workstation. The numerical solution along the depth after 150 seconds are shown in Figure 4.3. The different thermal properties of different layers account for the sudden change in the curve.

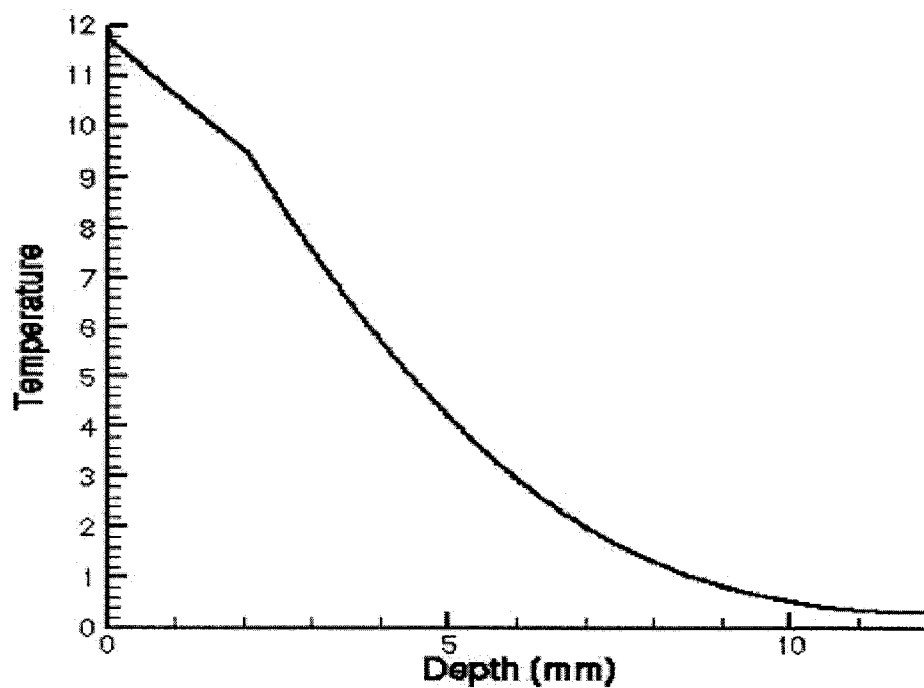


Figure 4.3 Transient temperatures distribution under constant heating after 150 seconds

4.3 Three-Dimensional Triple-Layered Case

We consider a three-dimensional triple-layered skin structure with geometry of $10\text{mm} \times 10\text{mm} \times 12.08\text{mm}$ in width, length and depth. The other dimensions and thermal properties are listed in the Table 4.3. When boundary condition of constant heating is applied for the top surface, θ_0 is set to 12°C . When insulation boundary condition is applied at the top surface, the laser power is introduced. Assume the laser power is continuous and spatial with a normal distribution as described in Equations (3.79-3.81) Parameters of the laser power are shown in Table 4.4.

Table 4.4 Parameters of laser power for the three layers in the skin structure [Han 1994]

$\alpha_1 = 0.1$	<i>Laser absorbtivity of first layer</i>
$\alpha_2 = 0.08$	<i>Laser absorbtivity of 2nd layer</i>
$\alpha_3 = 0.04$	<i>Laser absorbtivity of 3rd layer</i>
$Reff_1 = 0.93$	<i>Laser reflectivity of first layer</i>
$Reff_2 = 0.93$	<i>Laser reflectivity of 2nd layer</i>
$Reff_3 = 0.93$	<i>Laser reflectivity of 3rd layer</i>
$\sigma = 1mm$	<i>Standard deviation of Laser beam width</i>

In Figure 4.4, we show the contours of temperature distribution in the yz-cross section in the three-dimensional triple-layered case with constant heating at the top surface.

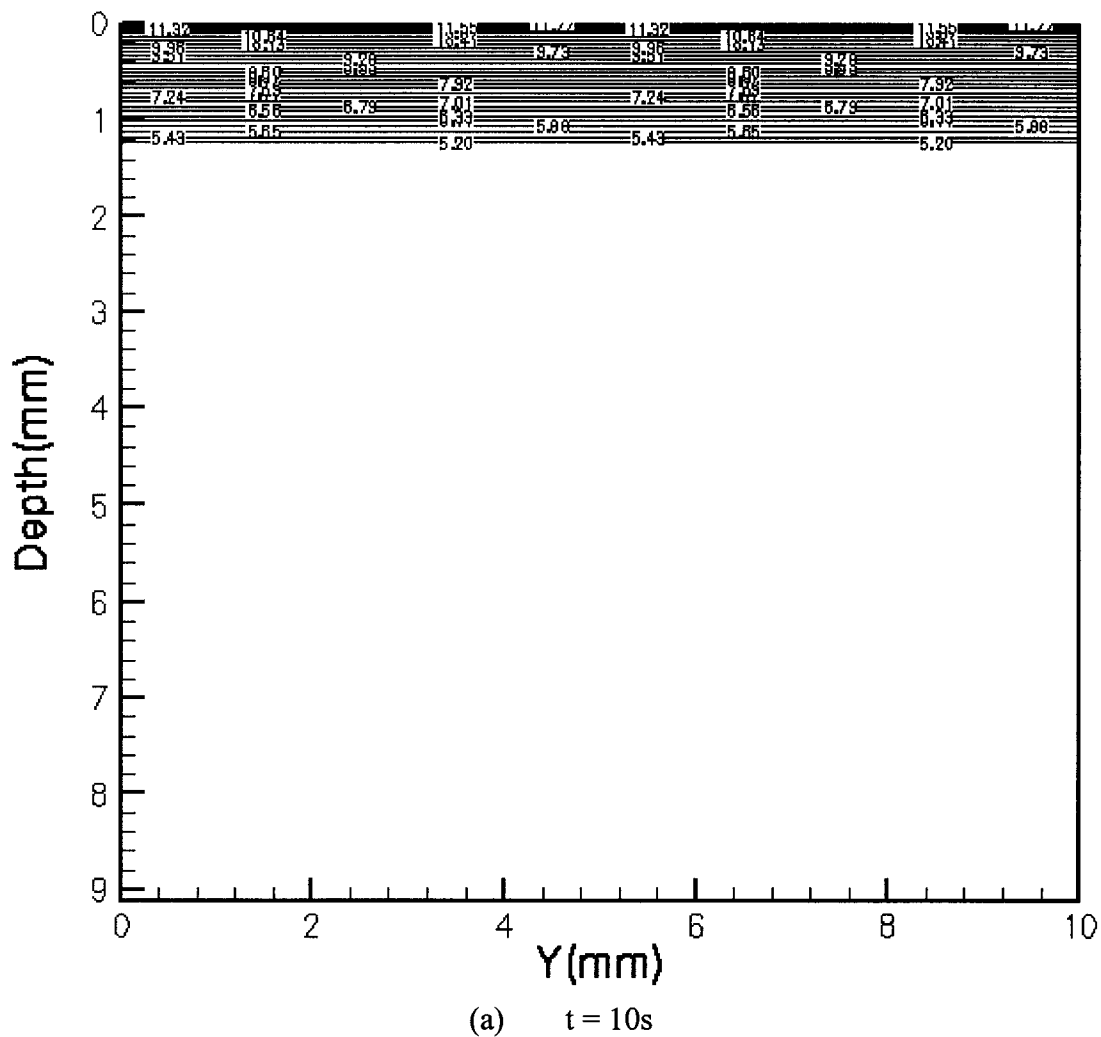
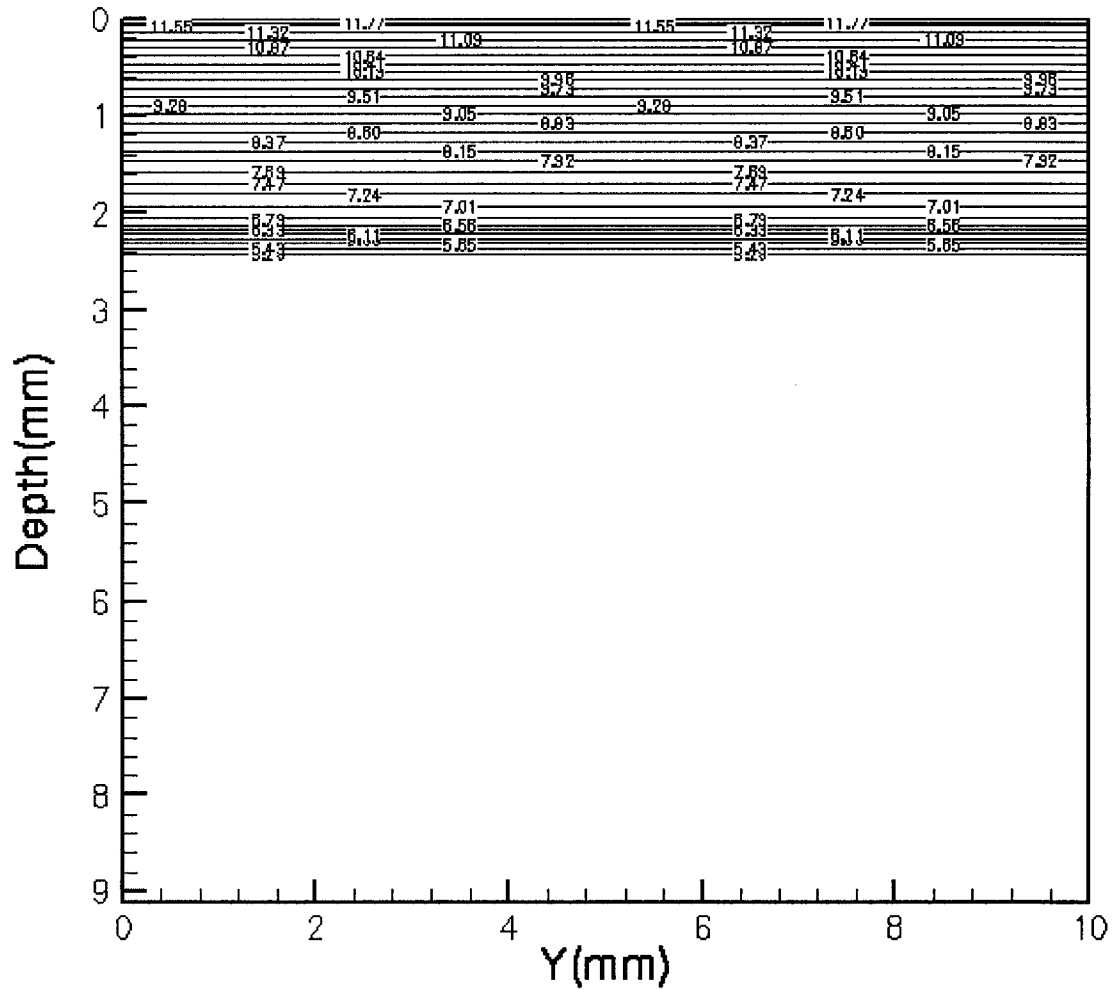
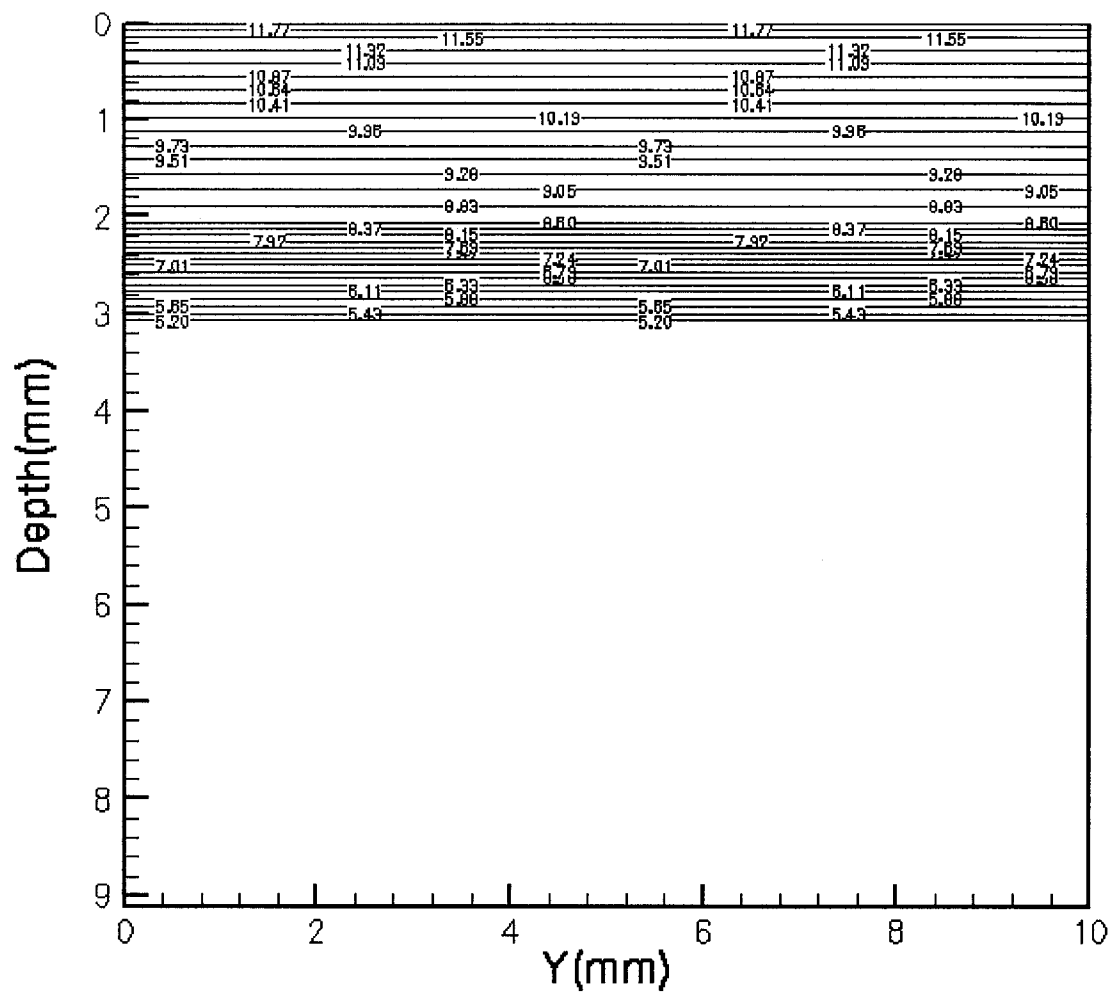


Figure 4.4 Contour of temperature distribution in the yz-cross section in three-dimensional case with constant heating boundary at various times



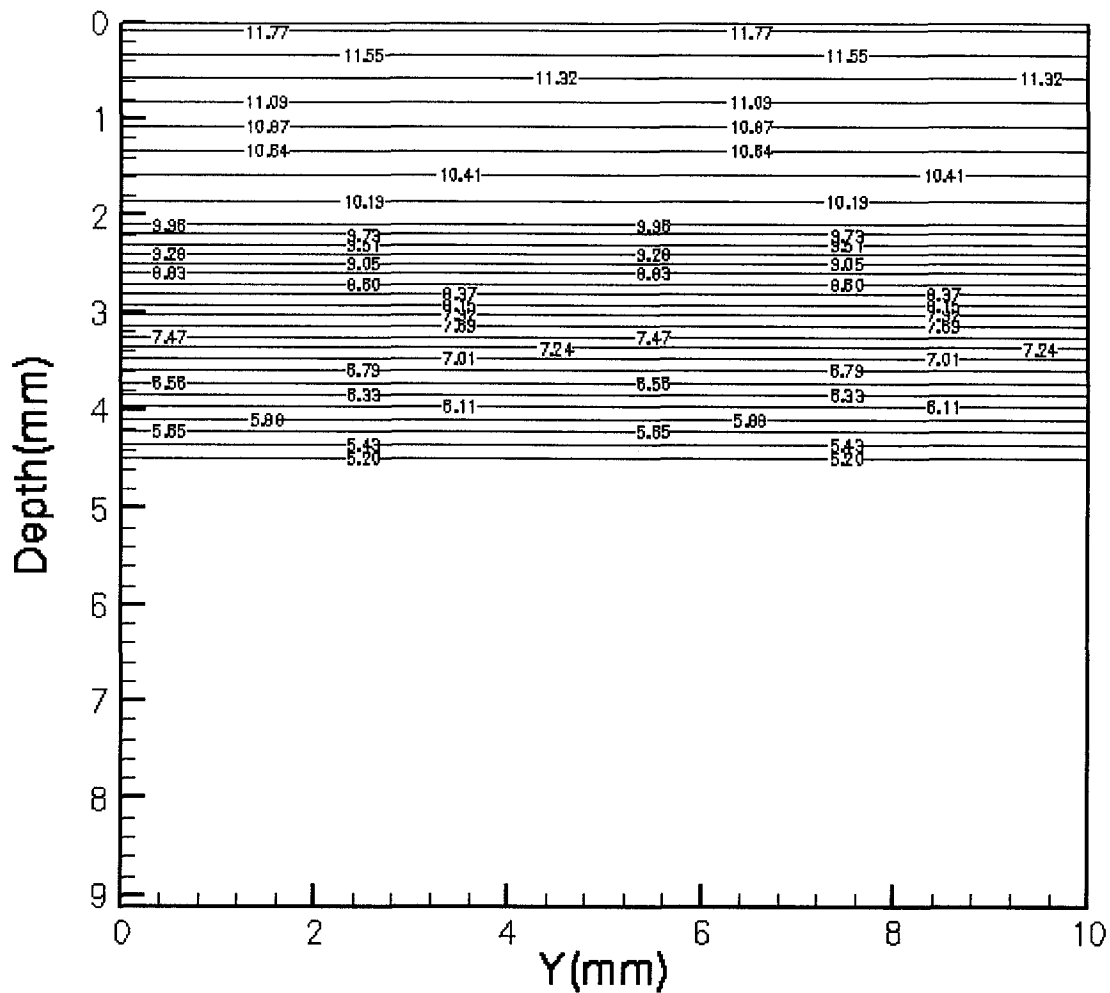
(b) $t = 30$ seconds

Figure 4.4 (continued)



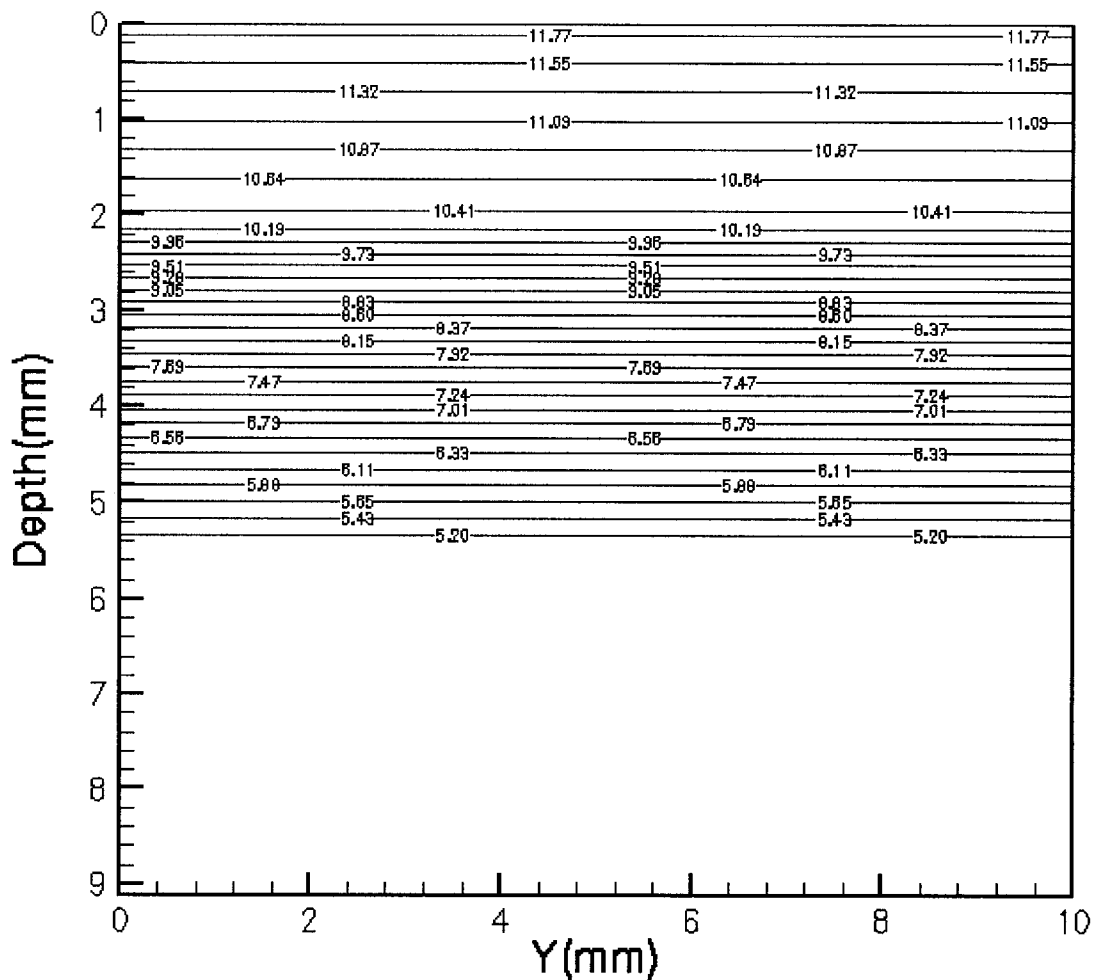
(c) $t = 60$ seconds

Figure 4.4 (continued)



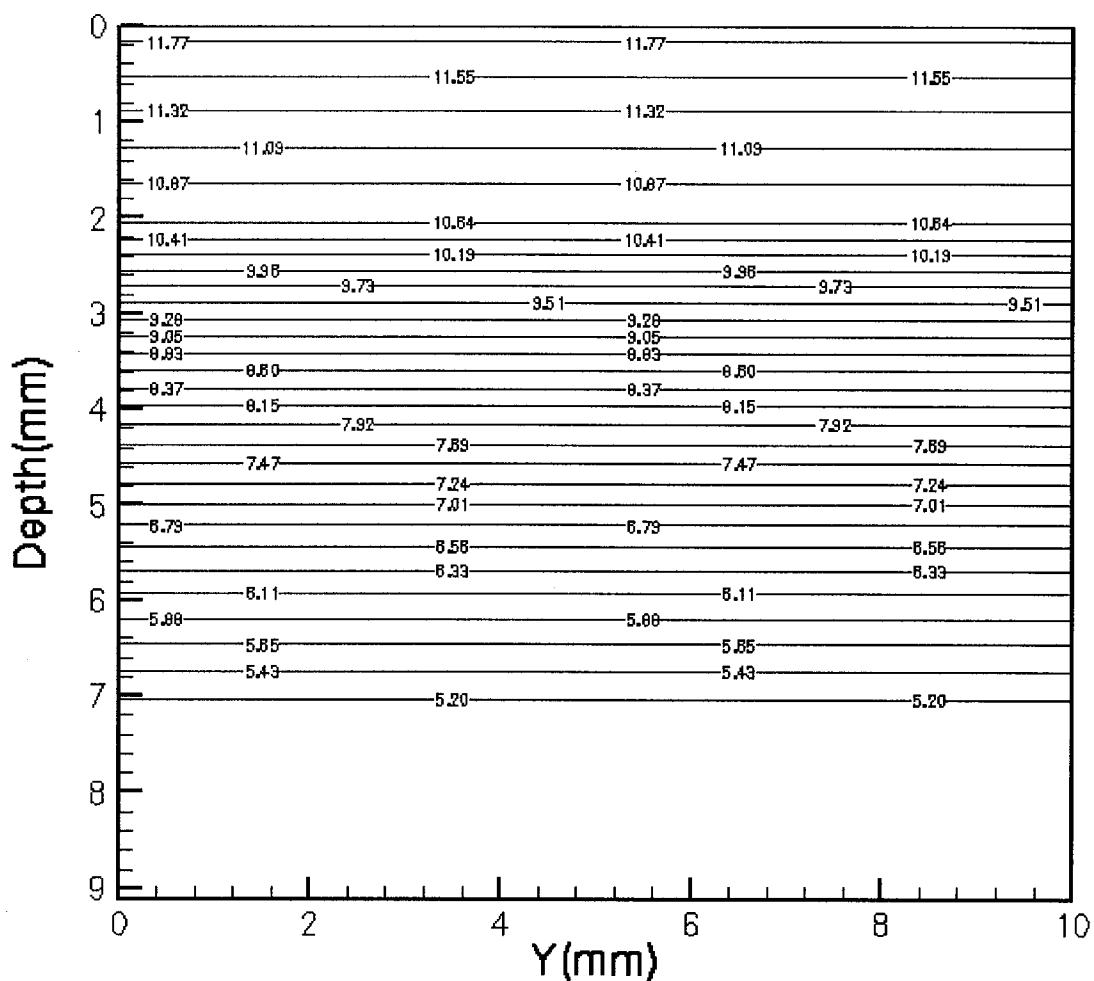
(d) $t = 3$ minutes

Figure 4.4 (continued)



(e) $t = 5$ minutes

Figure 4.4 (continued)



(f) $t = 10$ minutes

Figure 4.4 (continued)

As shown in Figure 4.4, heat transfers, smoothly and uniformly, down from the top surface, which maintains a temperature of 12°C .

Now, in Figure 4.5, we show the contours of temperature distribution in the yz-cross section in the three-dimensional triple-layered case with insulated boundary under laser radiation.

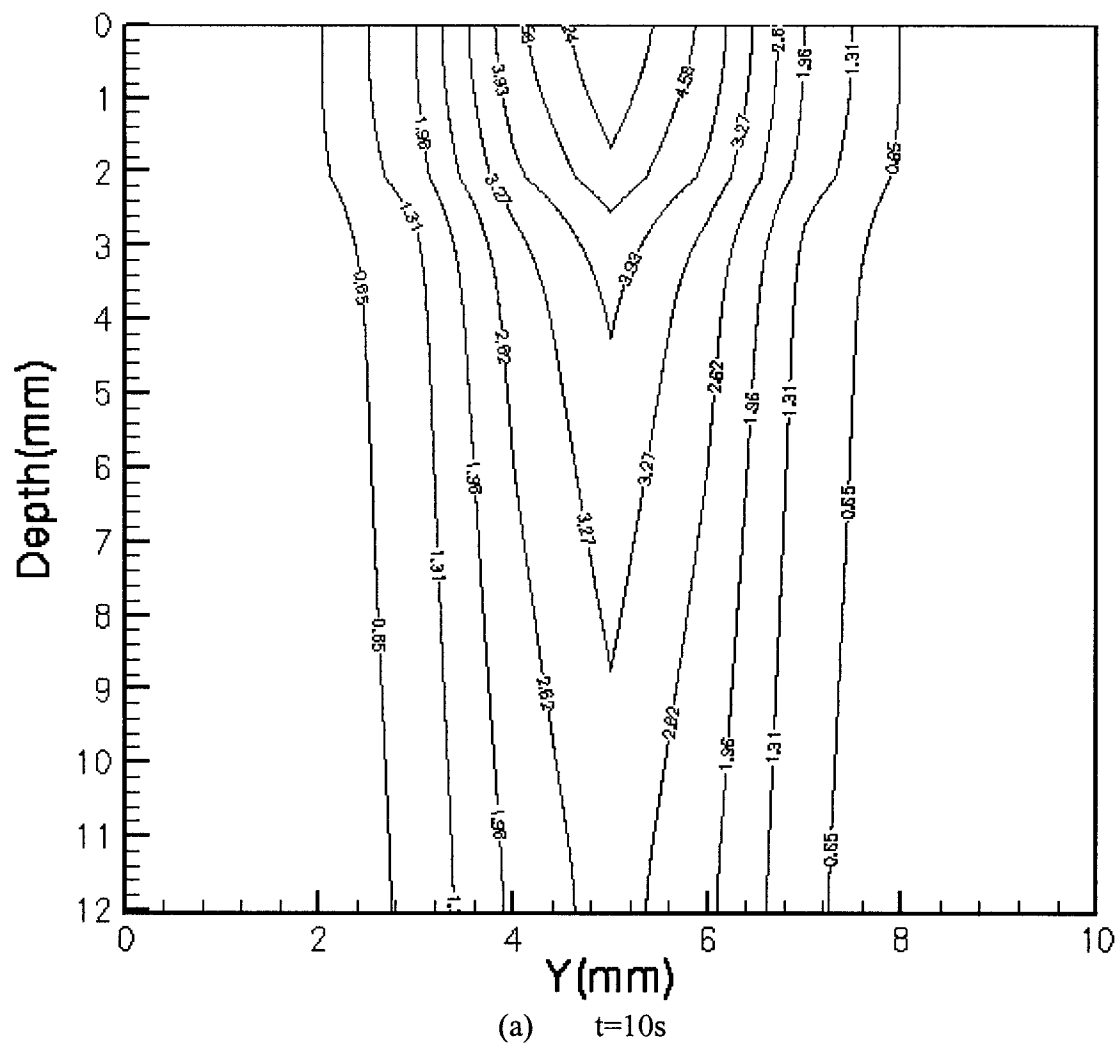
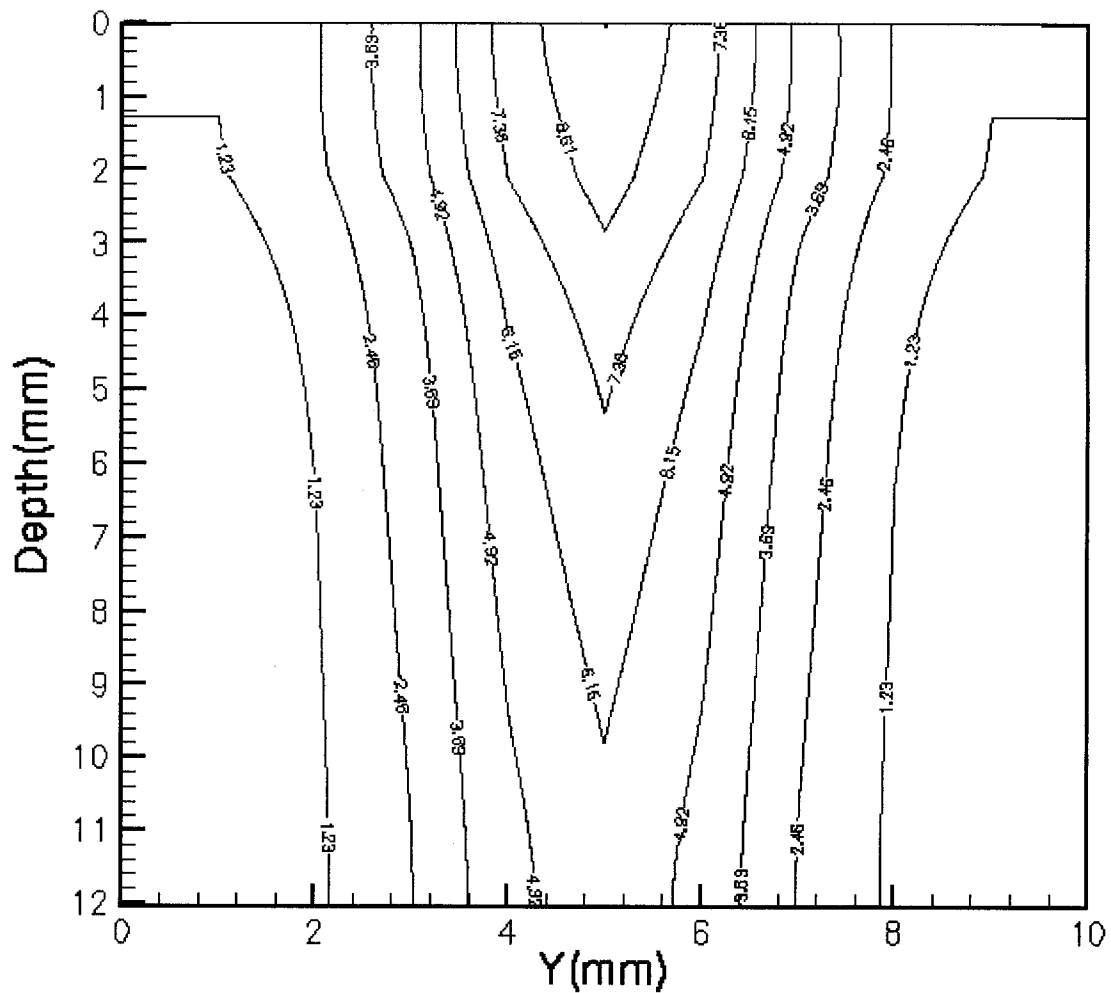
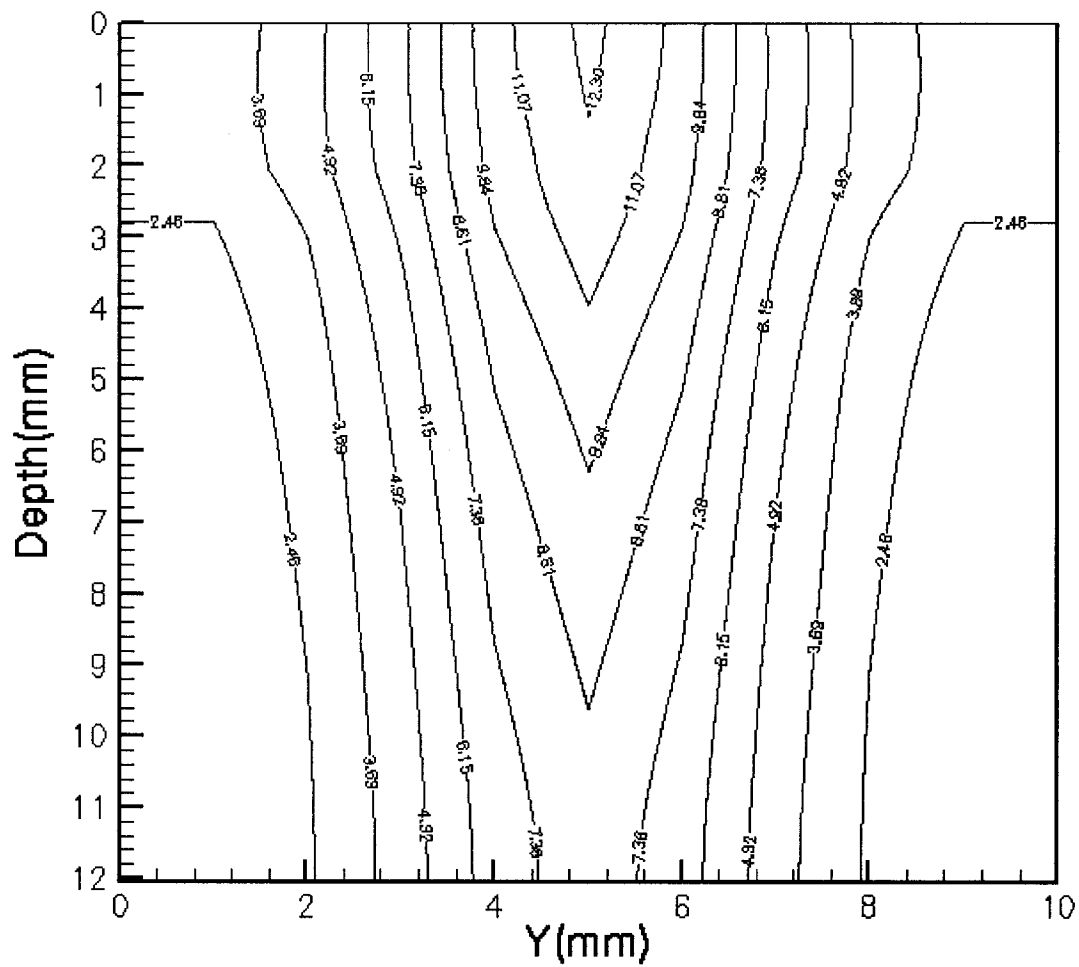


Figure 4.5 Contour of temperature distribution in the yz-cross section in three-dimensional case with insulated boundary at various times



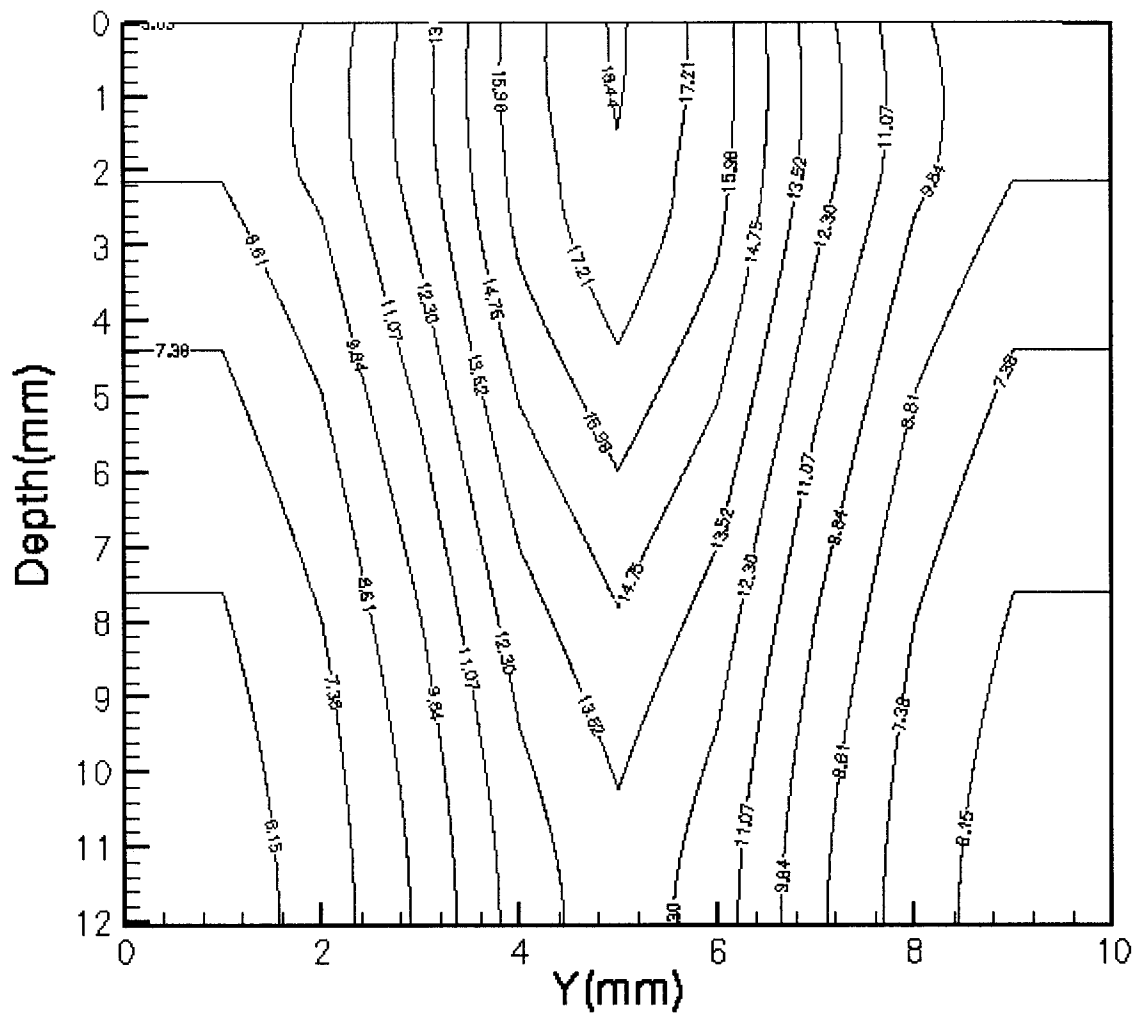
(b) $t = 30$ seconds

Figure 4.5 (continued)



(c) $t = 60$ seconds

Figure 4.5 (continued)



(d) $t = 3$ minutes

Figure 4.5 (continued)

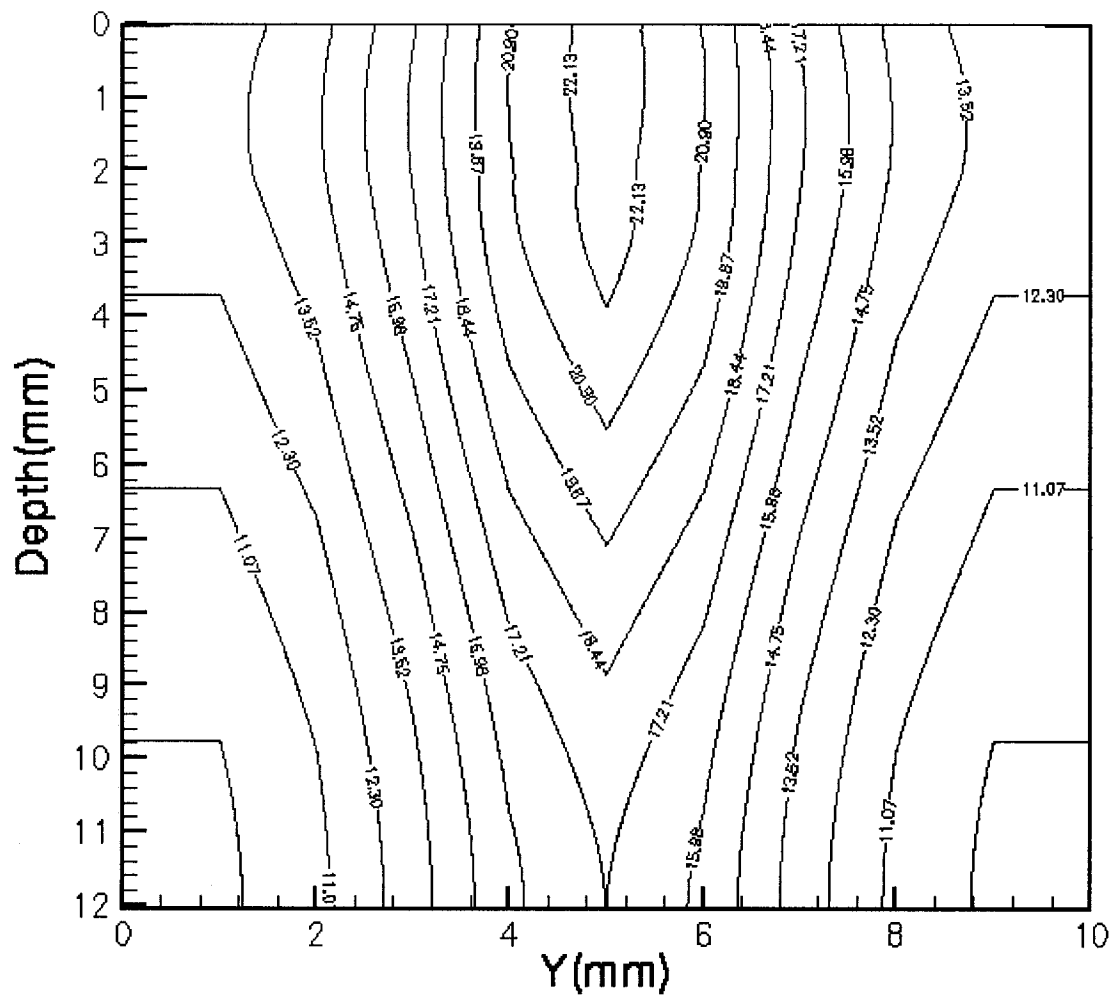
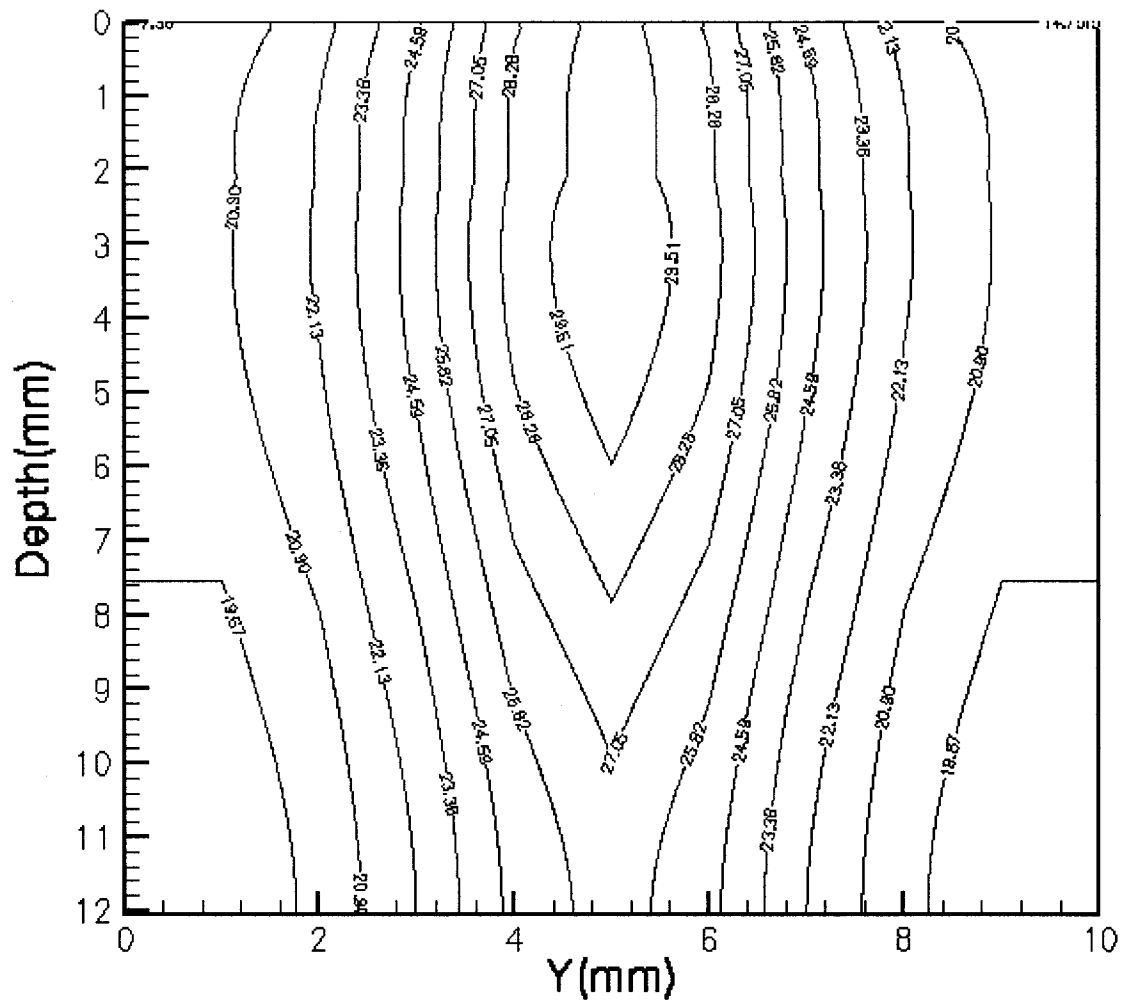
(e) $t = 5$ minutes

Figure 4.5 (continued)



(f) $t = 10$ minutes

Figure 4.5 (continued)

As shown in Figure 4.5, heat generated by laser power smoothly and uniformly spreads out from the center and down from the upper tissue because of the higher temperature in the upper tissue.

4.4 Three-Dimensional Single Vessel Embedded Triple-Layered Case

This case is different from that described in Section 4.3 only in that a single vessel parallel to the y Axis with radius of 0.01mm goes through the subcutaneous tissue. The center of vessel locates at $X = 4.99\text{mm}$ and $Z = 6.09\text{mm}$. The thermal properties of blood vessel are listed in Table 4.5.

Table 4.5 Parameters of blood vessel [Majhrzak 1999]

Parameters	Value
α	$2000W / m^2 K$
C_b	$4.134 \times 10^6 J / m^3 K$
v	0.08m/s

In Figure 4.6, we show the contours of temperature distribution in the yz -cross section in the three-dimensional single vessel embedded triple-layered case with constant heating at the top surface.

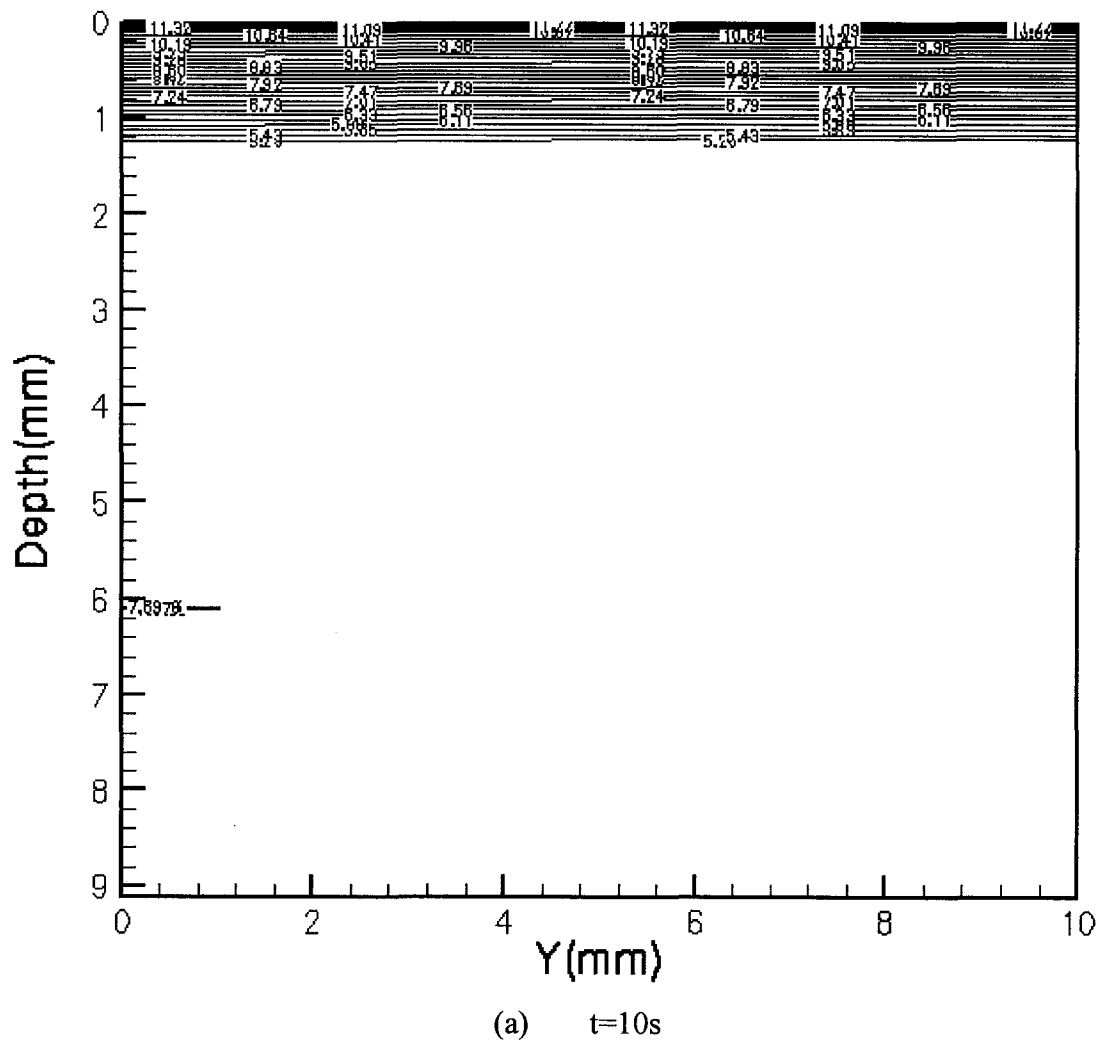
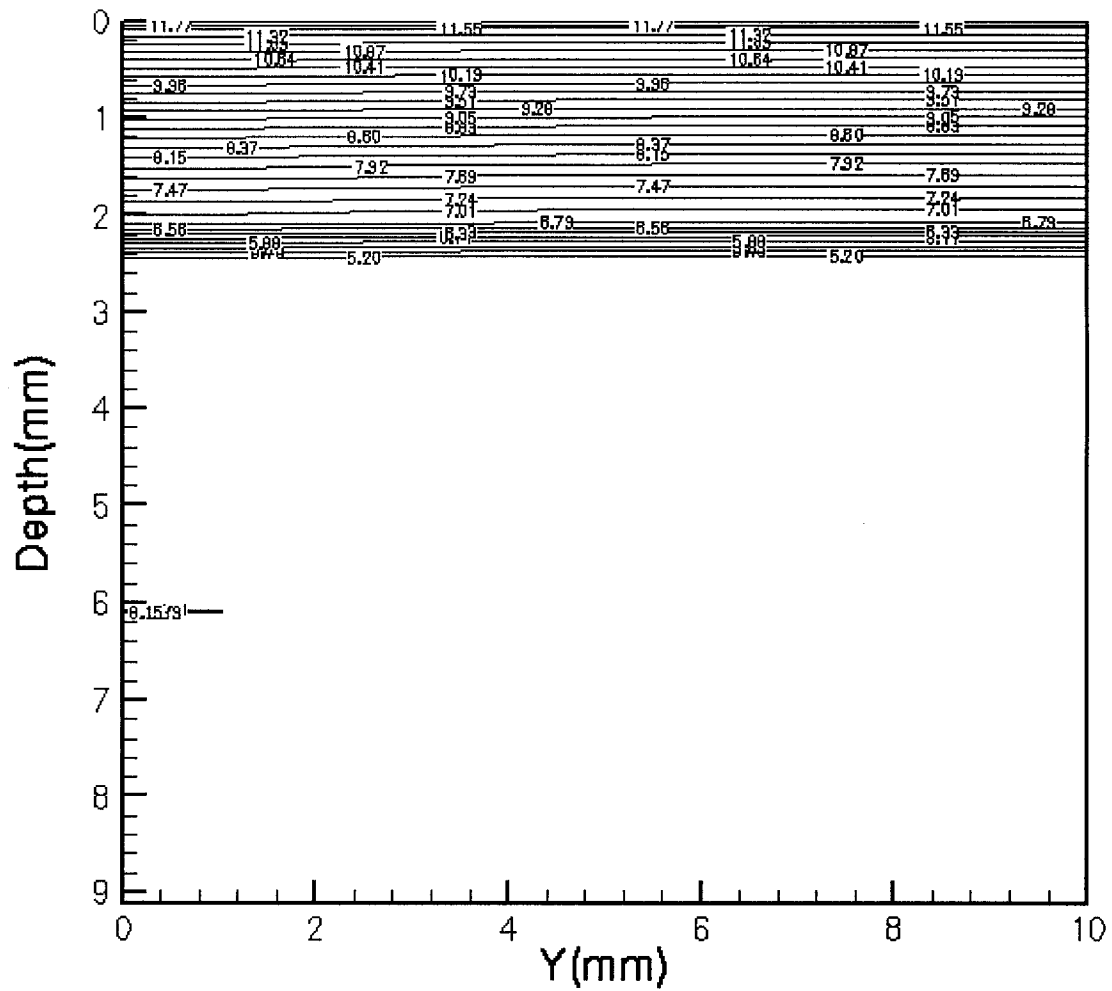
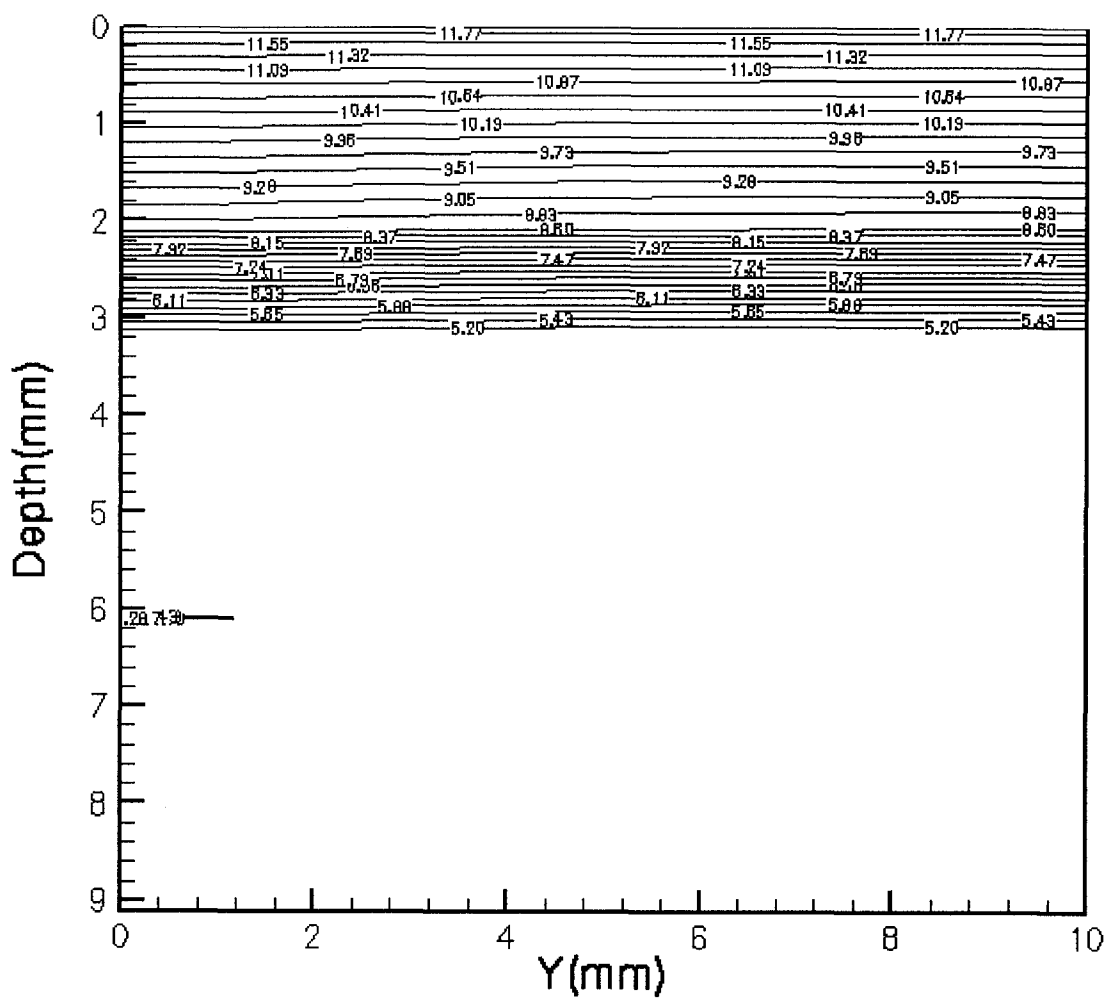


Figure 4.6 Contour of temperature distribution in the yz-cross section in three-dimensional single vessel embedded case with constant heating boundary at various times



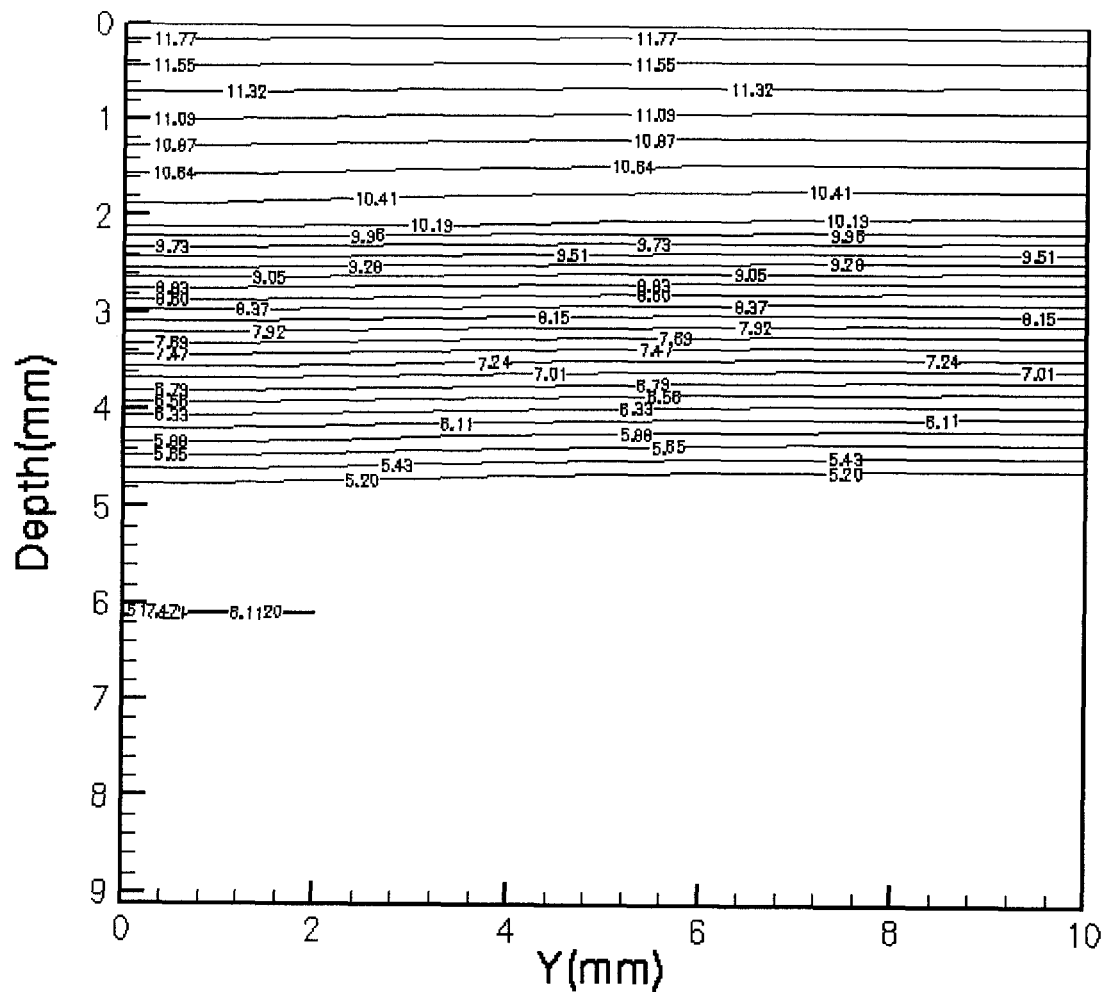
(b) $t = 30$ seconds

Figure 4.6 (continued)



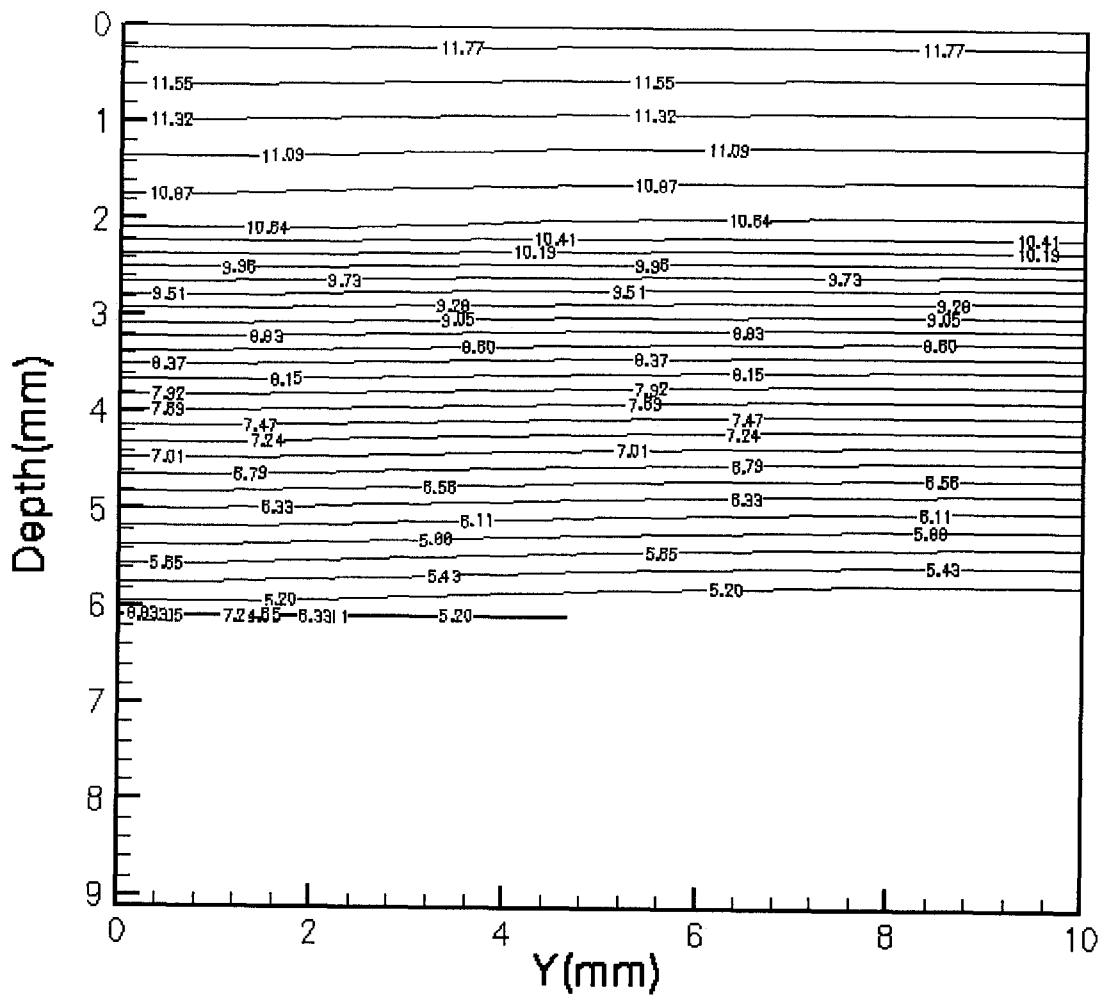
(c) $t = 60$ seconds

Figure 4.6 (continued)



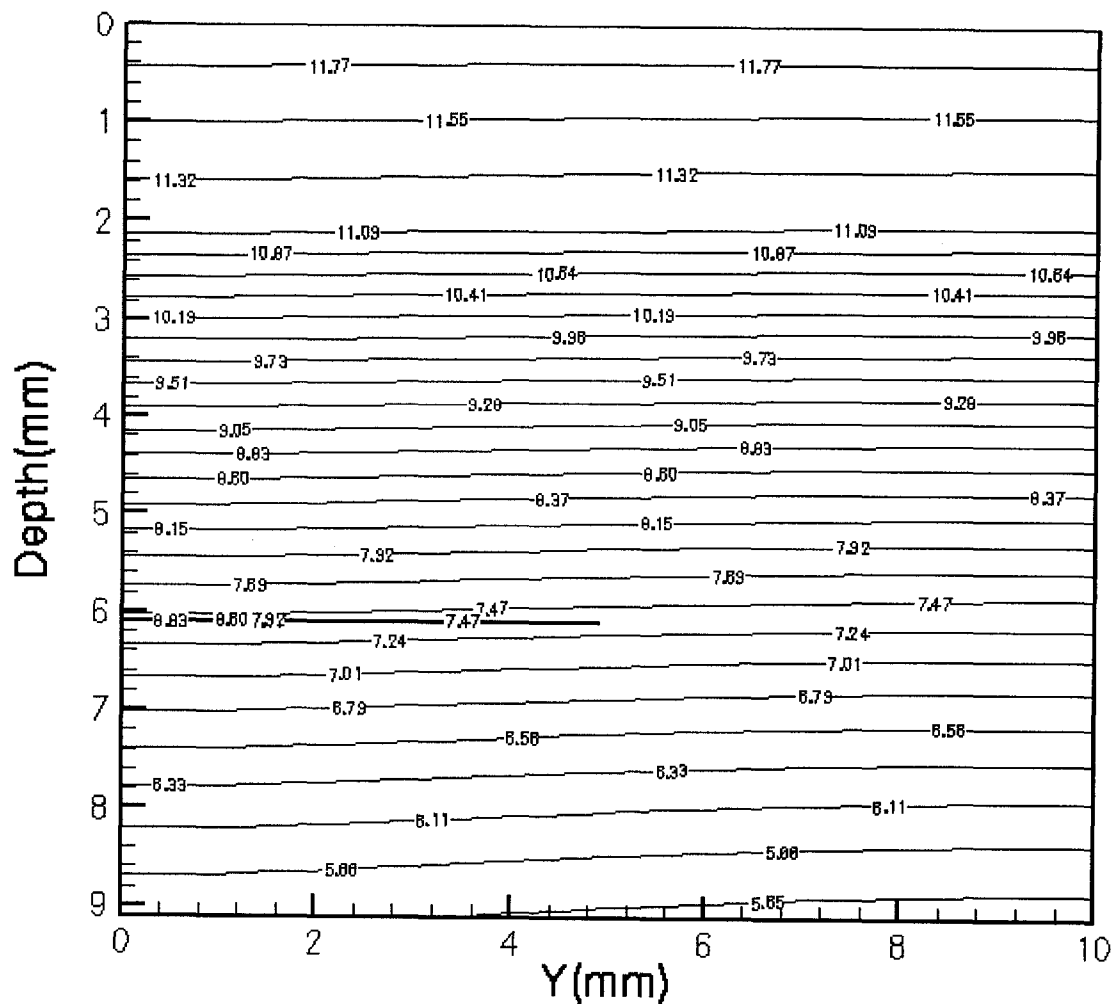
(d) t = 3 minutes

Figure 4.6 (continued)



(e) t = 5 minutes

Figure 4.6 (continued)



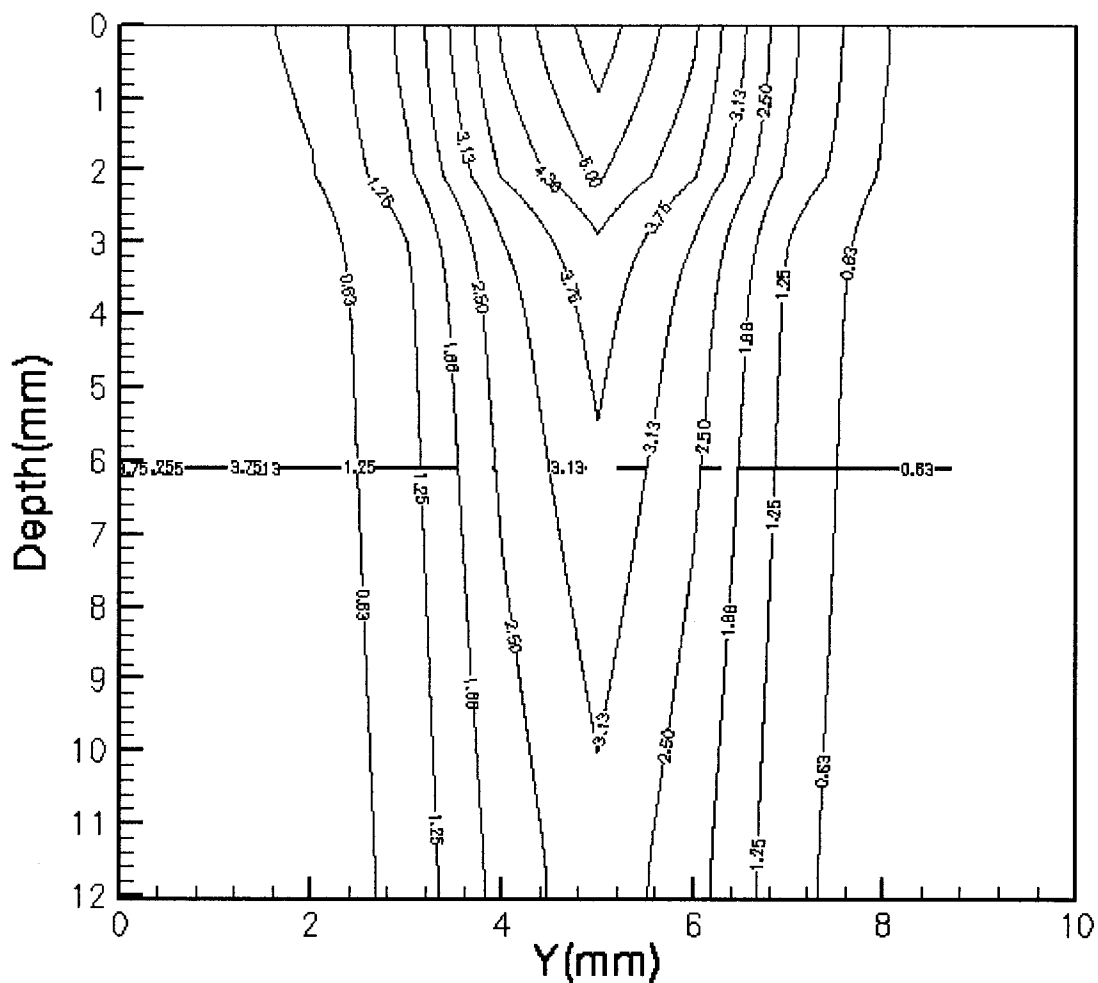
(f) $t = 10$ minutes

Figure 4.6 (continued)

As shown in Figure 4.6, the existence of the blood vessel breaks the symmetry of the temperature distribution in the skin structure. The temperature in this case is generally higher than the case without a single blood vessel, as shown in Figure 4.4. Apparently, the heat that blood brings in causes the rising of temperature in the tissue. As the blood flows through the tissue, it loses heat to its surrounding. Therefore, the temperature of the blood drops, and so does the gradient of heat flux from the blood vessel to its surrounding

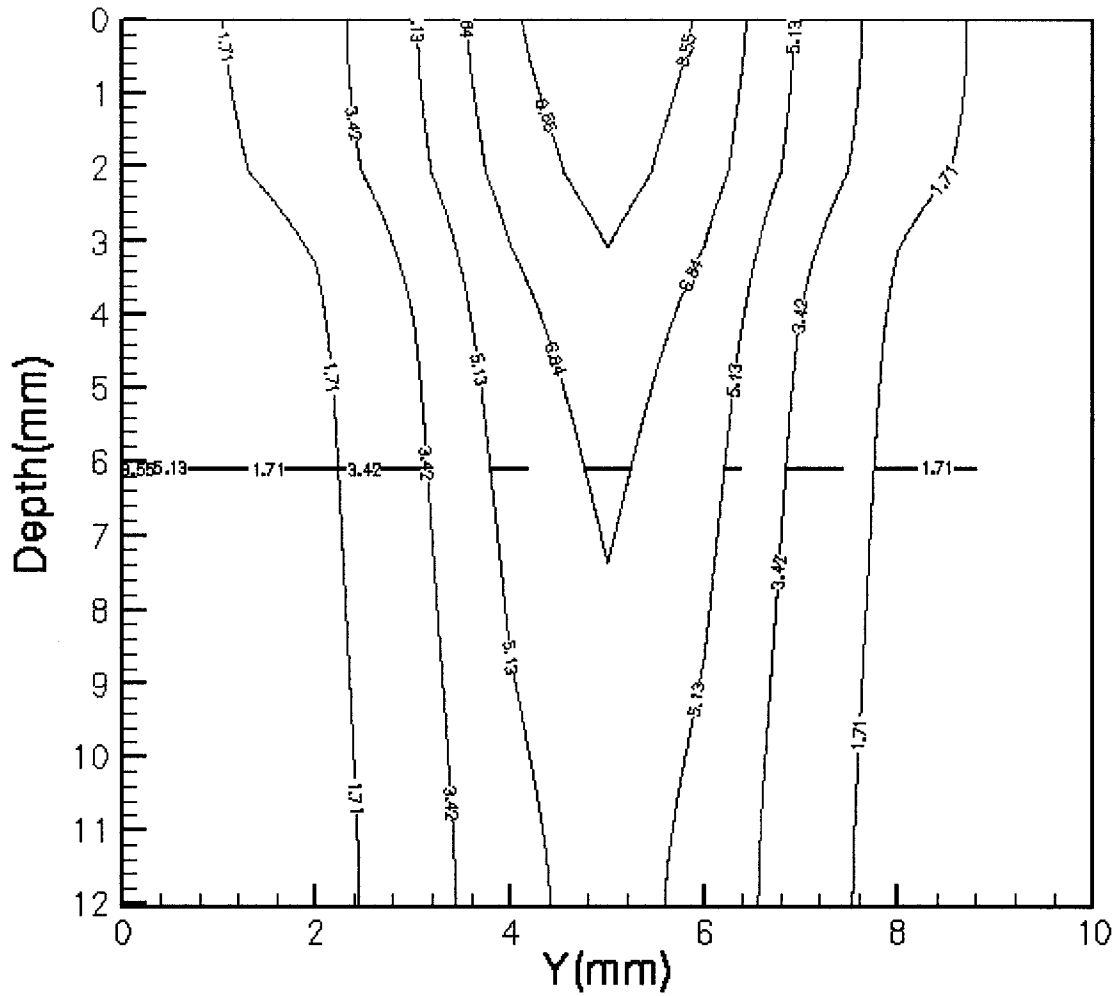
tissue. Consequently, at the same depth, the locations closer to the entry of blood vessel have the higher temperature.

Now, we show the contours of temperature distribution in the yz-cross section in three-dimensional single vessel embedded triple-layered case with insulated boundary under laser radiation in Figure 4.7.



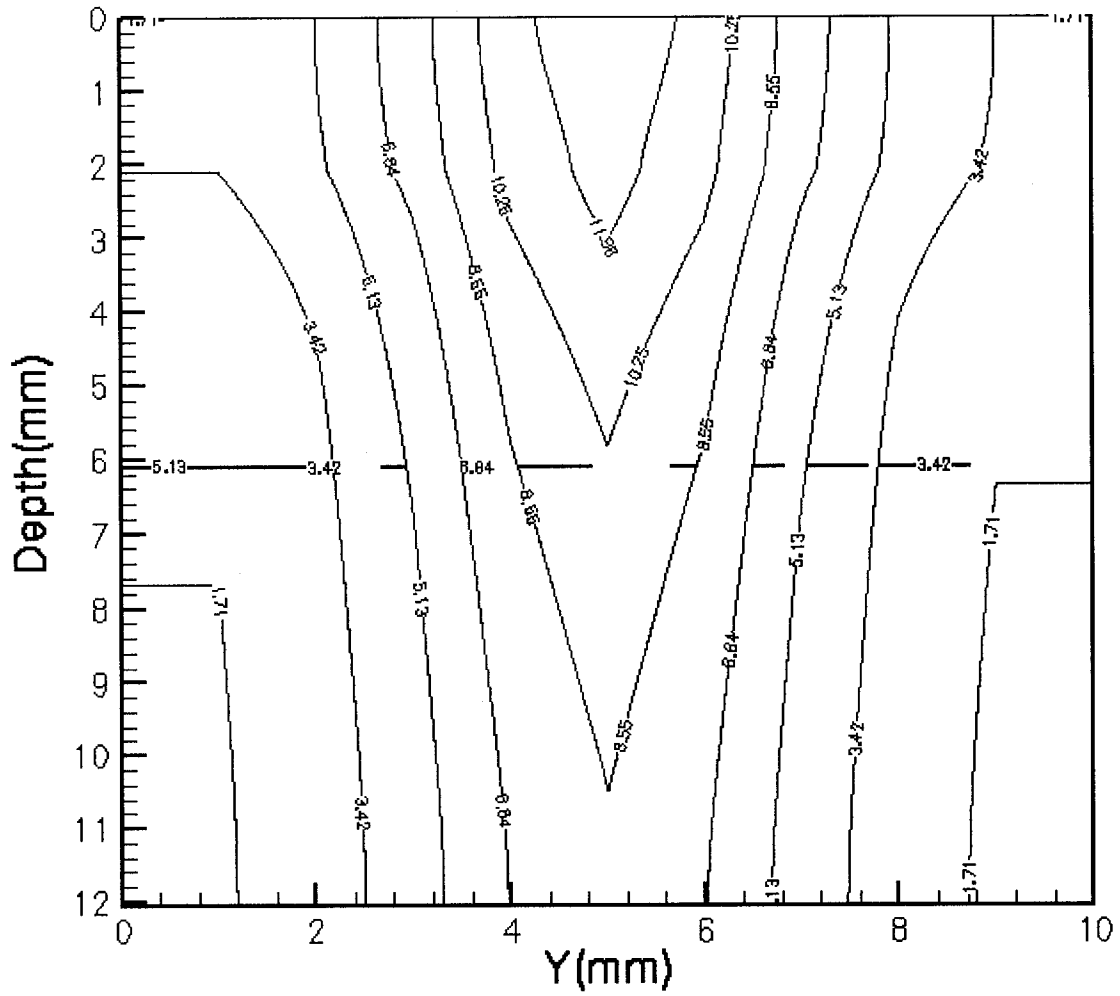
(a) $t=10s$

Figure 4.7 Contour of temperature distribution in the yz-cross section in three-dimensional single vessel embedded case with insulated boundary at various times



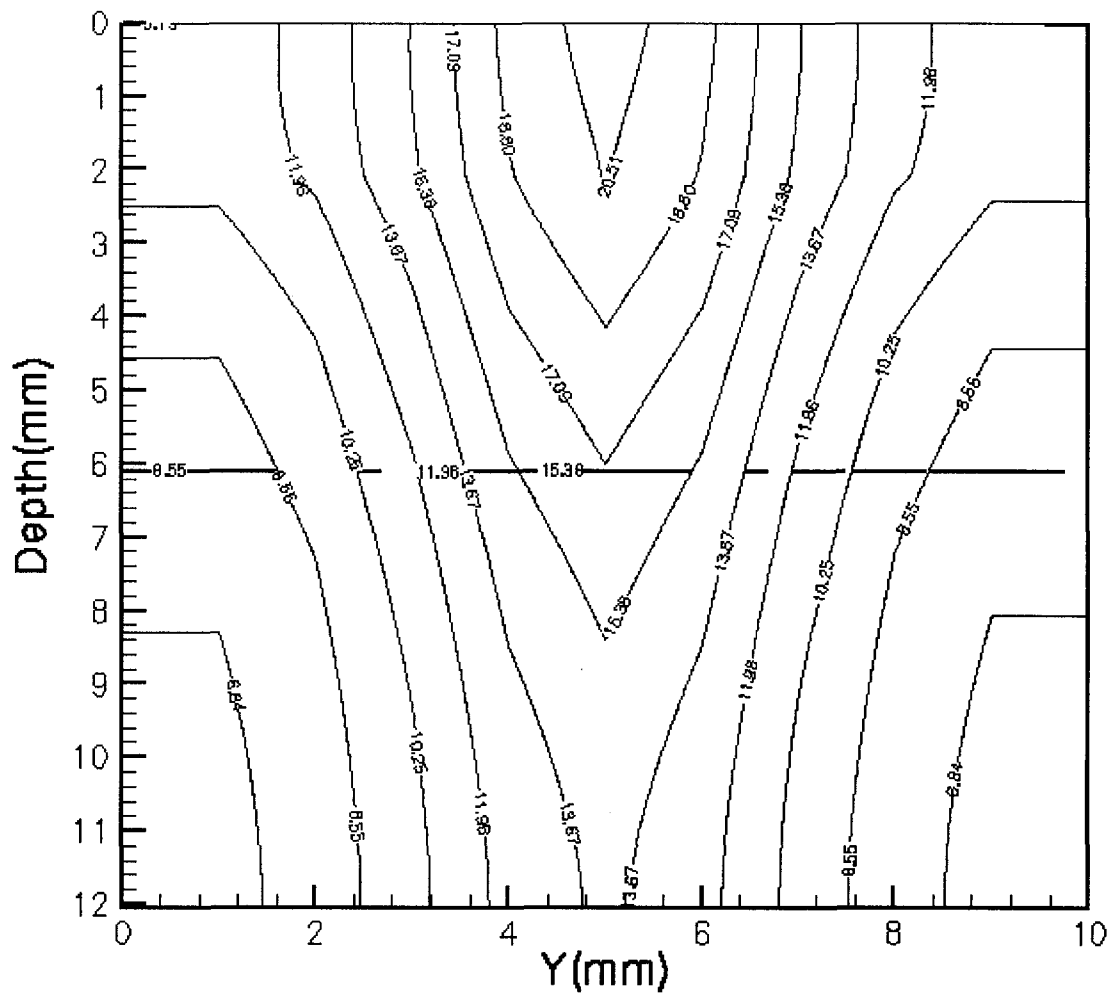
(b) $t = 30$ seconds

Figure 4.7 (continued)



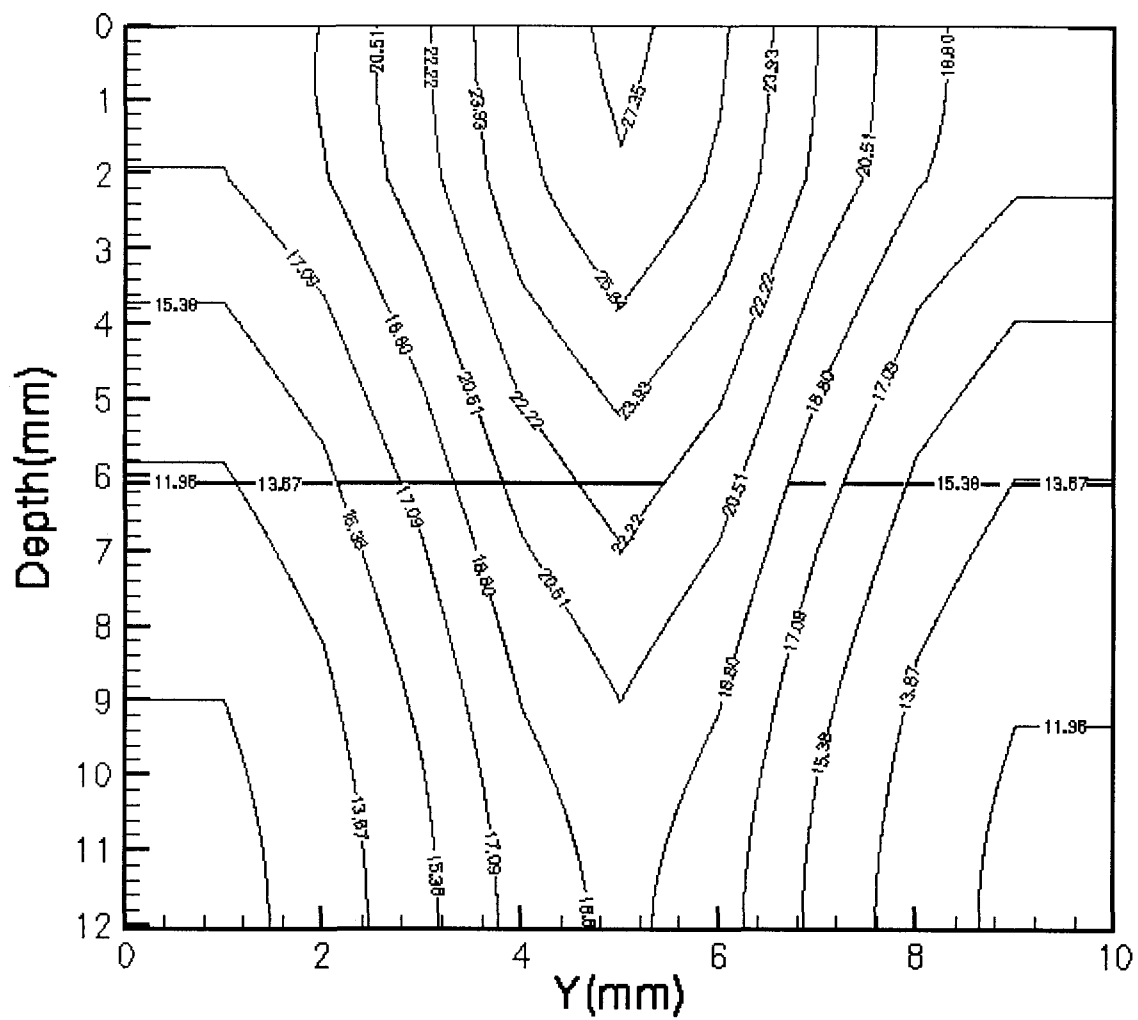
(c) $t = 60$ seconds

Figure 4.7 (continued)



(d) $t = 3$ minutes

Figure 4.7 (continued)



(e) $t = 5$ minutes

Figure 4.7 (continued)

higher than the blood later on due to laser radiation. Specifically, in Figures 4.7 (c) and 4.7 (d), when the temperature of blood vessel is higher than that in its surrounding tissue, the temperature at the locations close to the entry is higher than that far from it. Later on, in Figures 4.7 (e) and 4.7 (f), when the tissue around blood vessel is heated up by laser power to a generally higher temperature than that of the blood vessel, the temperature at the locations close to the entry becomes lower than that far from it. The changing of the temperature distribution pattern implies a “local cooling mechanism”, as discussed in many previous research [Roemer 1991] [Huang 1994][Torvi 1994] [Xuan 1997].

A contrast of the CPU time needed to solve the models in a Sun Workstation is shown in Table 4.6.

Table 4.6 Contrast of the running time for three-dimensional cases

Models	Time (s)
B.C of Constant heating three-dimensional model with blood vessel	137756.0
B.C of Constant heating three-dimensional model without blood vessel	128331.6
B.C of insulation three-dimensional model with blood vessel	150967.6
B.C of insulation three-dimensional model without blood vessel	130342.3

CHAPTER 5

CONCLUSIONS AND FUTURE WORK

Conclusions drawn from this work can be stated as follows:

A fourth-order compact finite difference scheme for solving Pennes' bioheat transfer equation has been developed. Several numerical examples were given. Numerical results show that the scheme is unconditionally stable and more accurate than the Crank-Nicholson scheme for a one-dimensional uniform-layered case.

A model simulating the interactions among human tissue, blood vessel, and external heat source (e.g., laser), has been developed. The application of the fourth-order compact finite difference scheme to the model will facilitate the prediction of the temperature distribution given a pre-specified laser radiation.

The outcomes above will provide a reliable, flexible and efficient numerical method for solving Pennes' bioheat transfer equation in skin structure.

Future studies need addressing the following issues: first, further convergence analysis of the high-order compact finite difference scheme in complicated geometries, because of the complexity of the human skin structure. High-order compact finite difference scheme will be more flexible and applicable, if preferable convergence conditions hold. Second, inverse problem of bioheat transfer [Zhen 2003][Zhang

2004][Roemer 1991][Liauh 1993][Zhou 2004]. This is important because, with knowledge of the entire temperature field in the hyperthermia treatment region, clinical personnel can potentially control the heating sources to deliver energy to the target locations. An accurate solution to inverse problems will help specify which power deposition pattern is needed to obtain an ideal tissue temperature distribution.

APPENDIX A

SOURCE CODE FOR SOLVING PENNES' BIOHEAT TRANSFER EQUATION IN A ONE-DIMENSIONAL UNIFORM-LAYERED SKIN STRUCTURE


```

c Table A.1 Program I: Source code for solving the 1D Pennes bioheat transfer equation
c in a single-layered skin structure
c Haofeng Yu
c 06/27/04
c This program is about heat transfer in the skin of a human being.
c There is a single layer in the skin.
c The governing equation used is:
c  $\rho c \frac{\partial U}{\partial t} = k \frac{\partial^2 U}{\partial z^2} - W_b C_b U$ 
  program bioheat1D
    parameter(m=99, pi=3.14159265358979323846)
c***** variable declaration *****
    integer n,t,remainder,posit
    double precision v(0:m+1),vn(0:m+1),vn1(0:m+1),vn2(0:m+1)
    double precision q2(0:m+1)
    double precision vxx(0:m+1),vxx1(0:m+1),dif
    double precision a3(0:m+1),b3(0:m+1),c3(0:m+1),d(0:m+1),d1(0:m+1)
    double precision dt,dz,er,rho,c,cb,wb,rk,zl
    double precision an, part,try,miu
    double precision p1,p2,p3,p5,p4,p6,p7,q1,q3
    REAL etime      ! Declare the type of etime()
    REAL elapsed(2) ! For receiving user and system time
    REAL total      ! For receiving total time

    er = .00001
    dz = 0.01
    dt = .0005
    rho = 0.001
    c = 4.200
    cb = 4.2
    wb = .0000005
    rk = .0002
    zl = 1.0
    alpha = rk/(rho*c)
    p4= wb*cb*zl*zl/rk
    miu=dt/(dz*dz)
c***** open the file *****
    open(unit = 1, file = 'BioHeat4th.dat', status = 'old')
c***** Exact Values *****

c // initialization!
  do i=0, m+1
    v(i) = 0.0
    q2(i) = 0.0
    a3(i) = 0.0
    c3(i) = 0.0
    b3(i) = 0.0
    d1(i) = 0.0
    d(i) = 0.0
  enddo
c // initiate the temperature
  do i=1, m
    vn(i) = 0.0
    vn1(i)=0.0

```

```

    vn2(i)=0.0
enddo
vn(0)=12.0
vn1(0)=12.0
vn2(0)=12.0

do t=1,150000
c //Calculate the exact value!
  do i=1,m
    p1=sqrt(wb*cb/rk)*(i*dz-zl)
    p2=sqrt(wb*cb/rk)
    p3 = 0.0
    do n=1,500
      p5=(2.0*n-1.0)*(2.0*n-1.0)*pi*pi/4.0
      p6=p5/(zl*zl)+wb*cb/rk
      p7=sin((n-0.5)*pi*i*dz/zl)
      an=-(2.0*n-1.0)*12.0*pi/(p4+p5)
      p3 = p3 + an*exp(-alpha*t*dt*p6)*p7
    enddo
    v(i) = 12.0*(exp(p1)+exp(-p1))/
+      (exp(p2)+exp(-p2))+p3
  enddo
c***** 4th compact scheme *****
c // initiate the coefficients in LHS of the tridiagonal,a(i),b(i),c(i)
  b3(1)=0.0
  a3(1) = 1.0
  c3(1)=0.0
  do i=2,m-1
    b3(i) = -0.1
    a3(i) = 1.0
    c3(i) = -0.1
  enddo
  b3(m) = 1.0/3.0
  a3(m) = 11.0/6.0
  c3(m)=0.0

c // initiate the coefficients in RHS of the tridiagonal,d(i)
  vxx(1) = miu*(vn(0)-2*vn(1)+vn(2))
  d(1)= miu*(vn(0)-2*vn(1)+vn(2))
  do i=2,m-1
    d(i) = (6.0*miu/5.0)*(vn(i-1)-2*vn(i)+vn(i+1))
  enddo
  d(m) = miu*(vn(m-1)-vn(m))

c // Call subroutine to solve the tridiagonal system
  call tri(m,b3,a3,c3,d,vxx)
  call equal(vn1,vn,m)

10  continue
c // Iteration!
c // Refresh the coefficients in RHS of the tridiagonal,d1(i)
  vxx1(1) = miu*(vn1(0)-2*vn1(1) + vn1(2))
  d1(1) = miu*(vn1(0)-2*vn1(1) + vn1(2))

```

```

do i=2,m-1
  d1(i) = (6.0*miu/5.0)*(vn1(i-1)-2*vn1(i) + vn1(i+1))
enddo
d1(m) = miu * (vn1(m-1)-vn1(m))
call tri(m,b3,a3,c3,d1,vxx1)

c // calculate the vnew(i) with vxx(i) and vxx1(i)
q1= wb*cb*0.5*dt
do i = 1,m
  q2(i)= rk*0.5*(vxx(i)+vxx1(i))
enddo
do i = 1,m
  vn2(i) = (q2(i)+(rho*c-q1)*vn(i))/(q1+rho*c)
enddo

c //check the error condition
do i=1,m
  if(abs(vn1(i)-vn2(i)).gt.er) then
    call equal(vn1,vn2,m)
    goto 10
  endif
enddo
call equal(vn,vn2,m)

c //output
dif = 0.0
do i=1, m
  if (dif .lt. abs(vn2(i) - v(i))) then
    dif = abs(vn2(i) - v(i))
    posi = i
  endif
enddo
remainder = mod(t,25)
if (remainder == 1) then
  write(1,*) posi,' ',dif
endif
write(*,*) 't = ',t
enddo

c // Record the CPU time
total = etime(elapsed)
write(1,*) 'End: total=', total, ' user=', elapsed(1),
+ ' system=', elapsed(2)
stop
end

```

APPENDIX B

SOURCE CODE FOR SOLVING PENNES' BIOHEAT TRANSFER EQUATION IN A ONE-DIMENSIONAL TRIPLE-LAYERED SKIN STRUCTURE

```

c      Table A.2 Program II:
c      Source code for solving the 1D Triple-layered Pennes bioheat
c      transfer equation in a Triple-layered skin structure

c      Haofeng Yu

c      07/01/04

c      This program aims to solve about heat transfer in the skin of human being.
c      There are three layers in the skin, Epiderms, Dermis and Subcutaneous.
c      The governing equation used is:
c       $\rho c \frac{\partial U}{\partial t} = k \frac{\partial^2 U}{\partial z^2} - W_b C_b U$ 
      program Bioheat1D3Layer
      parameter(nz=603,pi=3.14159265358979)
c***** variable declaration *****
      real c1,c2,c3,rk1,rk2,rk3,rho1,rho2,rho3,wb1,wb2,wb3,cb1,cb2,cb3
      integer Nt,Nx,Ny,nz1,nz2,t,counter
      integer n,remainder,posit
      double precision v(0:nz+1),vn(0:nz+1),vn1(0:nz+1),vn2(0:nz+1)
      double precision q2(0:nz+1)
      double precision vxx(0:nz+1),vxx1(0:nz+1),dif,d1(0:nz+1)
      double precision a(0:nz+1),b(0:nz+1),c(0:nz+1),d(0:nz+1)
      double precision dt,dz,er
      double precision part,try,miu
      double precision p1,p2,p3,p5,p4,p6,p7,q3
      real inta,intb,intc,intd,inte,intf
      real inta2,intb2,intc2,intd2,inte2,intf2
      REAL etime      ! Declare the type of etime()
      REAL elapsed(2) ! For receiving user and system time
      REAL total      ! For receiving total time
      er = .0001
      dz = 0.02
      dt = .001
      nz1 = 4
      nz2 = 100

      c1 = 3.6
      c2 = 3.4
      c3 = 3.06
      cb1 = 0.0
      cb2 = 4.2
      cb3 = 4.2
      rk1 = 0.00026
      rk2 = 0.00052
      rk3 = 0.00021
      rho1 = 0.0012
      rho2 = 0.0012
      rho3 = 0.001
      wb1 = 0.0
      wb2 = 0.0000005
      wb3 = 0.0000005
c //inta1,intb1,intc1,intd1,iete1 are the coefficients for the upper part to the interface.
c //inta2,intb2,intc2,intd2,iete2 are the coefficients for the upper part to the interface.

```

```

inta1=-1.0
intb1=-2.0
intc1=6.0
intd1=6.0
inte1=-6.0
inta2=1.0
intb2=2.0
intc2=6.0
intd2=-6.0
inte2=6.0
miu=dt/(dz*dz)
c***** open the files *****
open(unit = 1, file = 'new base1.dat', status = 'old')
open(unit = 2, file = 'new base4.dat', status = 'old')
open(unit = 3, file = 'new base104.dat', status = 'old')
open(unit = 4, file = 'new base604.dat', status = 'old')
open(unit = 5, file = 'new base150second.dat', status = 'old')
c***** 4th compact scheme *****
c // initialization!
do i=0, nz+1
  a(i) = 0.0
  c(i) = 0.0
  b(i) = 0.0
  d1(i) = 0.0
  d(i) = 0.0
enddo
c // initiate the temperature
do i=1, nz+1
  vn(i)=0.0
  vn1(i)=0.0
  vn2(i)=0.0
enddo
vn(0)=12.0
vn1(0)=12.0
vn2(0)=12.0
c // Start the loop by time step
c // initiate the coefficients in LHS of the tridiagonal,a(i),b(i),c(i)
b(1) = 0.0
a(1) = 1.0
c(1) = 0.0
do i=2,nz1-1
  b(i) = -0.1
  a(i) = 1.0
  c(i) = -0.1
enddo
b(nz1) = -inta1*rk1
a(nz1) = intb1*rk1-intb2*rk2*0.472222222
c(nz1) = inta2*rk2
b(nz1+1) = -0.1*0.472222222
a(nz1+1) = 1.0
c(nz1+1) = -0.1
do i=nz1+2,nz1+nz2-1
  b(i) = -0.1

```

```

    a(i) = 1.0
    c(i) = -0.1
  enddo
  b(nz1+nz2) = -inta1*rk2
  a(nz1+nz2) = (intb1*rk2-intb2*rk3*1.857142857)
  c(nz1+nz2) = inta2*rk3
  b(nz1+nz2+1) = -0.1*1.857142857
  a(nz1+nz2+1) = 1.0
  c(nz1+nz2+1) = -0.1
  do i=nz1+nz2+2,nz-1
    b(i) = -0.1
    a(i) = 1.0
    c(i) = -0.1
  enddo
  b(nz) = 1.0/3.0
  a(nz) = 11.0/6.0
  c(nz) = 0.0

do t=1,50000
c // initiate the coefficients in RHS of the tridiagonal,d(i)
  d(1)= miu*(vn(0)-2*vn(1)+vn(2))
  do i=2,nz1-1
    d(i) = (6.0*miu/5.0)*(vn(i-1)-2*vn(i) + vn(i+1))
  enddo
c *****interface 1 *****
  d(nz1)= miu*(rk1*inte1*vn(nz1-1)
&      + (rk1*intd1-rk2*intd2)*vn(nz1)-rk2*inte2*vn(nz1+1))
&      + intb2*rk2*0.00403846*vn(nz1)
c *****interface 1 *****
  do i=nz1+1,nz1+nz2-1
    d(i) = (6.0*miu/5.0)*(vn(i-1)-2*vn(i) + vn(i+1))
  enddo
  d(nz1+1) = d(nz1+1)-0.1*0.00403846*vn(nz1)
c *****interface 2 *****
  d(nz1+nz2)= miu*(rk2*inte1*vn(nz1+nz2-1)
&      +(rk2*intd1-rk3*intd2)*vn(nz1+nz2)-rk3*inte2*vn(nz1+nz2+1))
&      +intb2*rk3*0.0025*vn(nz1+nz2)
c *****interface 2 *****
  do i=nz1+nz2+1,nz-1
    d(i) = (6.0*miu/5.0)*(vn(i-1)-2*vn(i) + vn(i+1))
  enddo
  d(nz1+nz2+1)=d(nz1+nz2+1)-0.1*0.0025*vn(nz1+nz2)
  d(nz) = miu * (vn(nz-1)-vn(nz))
c // Call subroutine to solve the tridiagonal system
  call tri(nz,b,a,c,d,vxx)
  call equal(vn1,vn,nz)
10 continue
c // Iteration!
c // Refresh the coefficients in RHS of the tridiagonal,d1(i)
  vxx1(1) = miu*(vn1(0)-2*vn1(1) + vn1(2))
  d1(1) = miu*(vn1(0)-2*vn1(1) + vn1(2))
  do i=2,nz1-1
    d1(i) = (6.0*miu/5.0)*(vn1(i-1)-2*vn1(i) + vn1(i+1))

```

```

    enddo
c   *****interface 1 *****
    d1(nz1)= miu*(rk1*inte1*vn1(nz1-1)
&      + (rk1*intd1-rk2*intd2)*vn1(nz1)-rk2*inte2*vn1(nz1+1))
&      + intb2*rk2*0.00403846*vn1(nz1)
c   *****interface 1 *****
    do i=nz1+1,nz1+nz2-1
        d1(i) = (6.0*miu/5.0)*(vn1(i-1)-2*vn1(i) + vn1(i+1))
    enddo
    d1(nz1+1) = d1(nz1+1)-0.1*0.00403846*vn1(nz1)
c   *****interface 2 *****
    d1(nz1+nz2)= miu*(rk2*inte1*vn1(nz1+nz2-1)
&      +(rk2*intd1-rk3*intd2)*vn1(nz1+nz2)-rk3*inte2*vn1(nz1+nz2+1))
&      +intb2*rk3*0.0025*vn1(nz1+nz2)
c   *****interface 2 *****
    do i=nz1+nz2+1,nz-1
        d1(i) =(6.0*miu/5.0)*(vn1(i-1)-2*vn1(i) + vn1(i+1))
    enddo
    d1(nz1+nz2+1)=d1(nz1+nz2+1)-0.1*0.0025*vn1(nz1+nz2)
    d1(nz) = miu*(vn1(nz-1)-vn1(nz))
    call tri(nz,b,a,c,d1,vxx1)

c // calculate the vnew(i) with vxx(i) and vxx1(i)
    p1= wb1*cb1*0.5*dt
    do i = 1,nz1
        q2(i)= rk1*0.5*(vxx(i)+vxx1(i))
    enddo
    do i = 1,nz1
        vn2(i) = (q2(i)+(rho1*c1-p1)*vn(i))/(p1+rho1*c1)
    enddo
    p2= wb2*cb2*0.5*dt
    do i = nz1+1,nz1+nz2
        q2(i)= rk2*0.5*(vxx(i)+vxx1(i))
    enddo
    do i = nz1+1,nz1+nz2
        vn2(i) = (q2(i)+(rho2*c2-p2)*vn(i))/(p2+rho2*c2)
    enddo
    p3= wb3*cb3*0.5*dt
    do i = nz1+nz2+1,nz
        q2(i)= rk3*0.5*(vxx(i)+vxx1(i))
    enddo
    do i = nz1+nz2+1,nz
        vn2(i) = (q2(i)+(rho3*c3-p3)*vn(i))/(p3+rho3*c3)
    enddo
c //check the error condition
    do i=1,nz
        if(abs(vn1(i)-vn2(i)).gt.er) then
            call equal(vn1,vn2,nz)
            goto 10
        endif
    enddo
    call equal(vn,vn2,nz)
c //output

```



```

write(*,*) 't = ',t
enddo
c // Record the CPU time
total = etime(elapsed)
write(5,*) 'End: total=', total, ' user=', elapsed(1),
+ ' system=', elapsed(2)
stop
end

c*****
c***** subroutine equal *****
subroutine equal(wold,wnew,n)
integer n
double precision wold(0:n+1),wnew(0:n+1)
do i=1,n+1
wold(i) = wnew(i)
enddo
return
end

```

APPENDIX C

SOURCE CODE FOR SOLVING PENNES' BIOHEAT TRANSFER EQUATION IN A THREE-DIMENSIONAL TRIPLE- LAYERED SKIN STRUCTURE

```

c      Table A.3 Program III:
c      Source code for solving the 3D Triple-layered Pennes bioheat
c      transfer equation with laser power in a Triple-layered skin structure

c      Haofeng Yu

c      07/01/04

c      This program aims to solve about heat transfer in the skin of human being.
c      There are three layers in the skin, Epiderms, Dermis and Subcutaneous.
c      The skin structure is 10by10by12.08mm in geometry
c      The governing equation used is:
c       $\rho c(\partial U/\partial t) = k(\nabla^2 U) - W_b C_b U + Q$ 
c      Two boundary conditions are considered:
c      1. Dirichlet The temperature at surface is assumed to be constant, 10oC
c      2. Neumann The temperature at surface is assumed to be heat insulated

      program bioheat3D3LLaser
      parameter(nz=603,pi=3.14159265358979,nx=10,ny=10)
c***** variable declaration *****
      real c1,c2,c3,rk1,rk2,rk3,rho1,rho2,rho3,wb1,wb2,wb3,cb1,cb2,cb3
      integer x,y,z
      integer Nt,nz1,nz2,t,counter
      integer n,remainder,positi

c      -----
      double precision Q1(0:nx,0:ny,0:nz), Q2(0:nx,0:ny,0:nz)
      double precision Q3(0:nx,0:ny,0:nz)
      double precision v(0:nx,0:ny,0:nz+1),vn(0:nx,0:ny,0:nz+1)
      double precision vn1(0:nx,0:ny,0:nz+1),vn2(0:nx,0:ny,0:nz+1)
      double precision qq2(0:nz+1),dx1(0:nx),dy1(0:ny),dz1(0:nz+1)
      double precision tempx(0:nx),tempy(0:ny),tempz(0:nz+1)
      double precision vxx(0:nx,0:ny,0:nz+1),vxx1(0:nx,0:ny,0:nz+1)
      double precision vyy(0:nx,0:ny,0:nz+1),vyy1(0:nx,0:ny,0:nz+1)
      double precision vzz(0:nx,0:ny,0:nz+1),vzz1(0:nx,0:ny,0:nz+1)

      double precision ax(0:nx),bx(0:nx),cx(0:nx),dx(0:nx)
      double precision ay(0:ny),by(0:ny),cy(0:ny),dy(0:ny)
      double precision az(0:nz+1),bz(0:nz+1),cz(0:nz+1),dz(0:nz+1)
      double precision dt,er,dif
      double precision part,try,miu,miuxy
      double precision p1,p2,p3,p5,p4,p6,p7
      real inta2,intb2,intc2,intd2,inte2,intf
      real inta1,intb1,intc1,intd1,inte1,intf2
      double precision Sigma,Alpha1,Alpha2,Alpha3,Reff1,Reff2,Reff3
      double precision P0
      REAL etime      ! Declare the type of etime()
      REAL elapsed(2) ! For receiving user and system time
      REAL total     ! For receiving total time
c      // Discretization units
      er = 0.001
      deltax = 1.0
      deltay = 1.0
      deltaz = 0.02

```

```

deltaz3 = 0.02
Ration = deltaz3/deltaz
dt = .001
nz1 = 4
nz2 = 100
c // Parameters related to Laser Power
Sigma= 1.0
Alpha1=0.1
Alpha2=0.08
Alpha3=0.04
Reff1=0.93
Reff2=0.93
Reff3=0.93
P0=6.4
c // Parameters related to layers of skin
c1 = 3.6
c2 = 3.4
c3 = 3.06
cb1 = 0.0
cb2 = 4.2
cb3 = 4.2
rk1 = 0.00026
rk2 = 0.00052
rk3 = 0.00021
rho1 = 0.0012
rho2 = 0.0012
rho3 = 0.001
    wb1 = 0.0
wb2 = 0.0000005
wb3 = 0.0000005
c //inta1,intb1,intc1,intd1,iete1 are the coefficients for the upper part to the interface.
c //inta2,intb2,intc2,intd2,iete2 are the coefficients for the upper part to the interface.
inta1=-1.0
intb1=-2.0
intc1=6.0
intd1=6.0
inte1=-6.0
inta2=1.0
intb2=2.0
intc2=6.0
intd2=-6.0
inte2=6.0
miu=dt/(deltaz*deltaz)
    miu3=dt/(deltaz3*deltaz3)
miux=dt/(deltax*deltax)
    miuy=dt/(deltay*deltay)
    miuxy=dt/(deltay*deltay)
c***** file *****
open(unit = 1, file = '0603 t1000.dat', status = 'old')
open(unit = 2, file = '0603 t3000.dat', status = 'old')
open(unit = 3, file = '0603 t5000.dat', status = 'old')
open(unit = 4, file = '0603 t10000.dat', status = 'old')
open(unit = 5, file = '0603 t15000.dat', status = 'old')

```

```

open(unit = 6, file = '0603 t20000.dat', status = 'old')
open(unit = 7, file = 'time.dat', status = 'old')
c***** 4th compact scheme *****
c // Initialization!
do i=0, nx
  ax(i) = 0.0
  cx(i) = 0.0
  bx(i) = 0.0
  dx1(i) = 0.0
  dx(i) = 0.0
enddo
do j=0, ny
  Bv(j) = 0.0
  Bp(j) = 0.0
  Bv1(j) = 0.0
  ay(j) = 0.0
  cy(j) = 0.0
  by(j) = 0.0
  dy1(j) = 0.0
  dy(j) = 0.0
enddo
do k=0, nz+1
  az(k) = 0.0
  cz(k) = 0.0
  bz(k) = 0.0
  dz1(k) = 0.0
  dz(k) = 0.0
enddo
do i=0, nx
  do j=0, ny
    do k=0, nz+1
      vn(i,j,k)=0.0
      vn1(i,j,k)=0.0
      vn2(i,j,k)=0.0
    enddo
  enddo
enddo
c Calculate the laser power Q(i,j,k)
do i=0,nx
  do j=0,ny
    do z=0,nz1
      Q1(i,j,z)=Alpha1*exp(-Alpha1*z*deltaZ)/(2*pi*Sigma**2)*
$ exp(-((nx/2-i)*(nx/2-i)+(ny/2-j)*(ny/2-j))*deltax**2/
$ (2*Sigma*Sigma)) * P0*(1-Reff1 )
    enddo
    do z =nz1,nz1+nz2
      Q2(i,j,z)= Alpha2 * exp( - Alpha2 *(z-nz1) *deltaZ )*
$ exp(-Alpha1*deltaZ*nz1 )/(2*pi*Sigma**2)*
$ exp(-((nx/2-i)*(nx/2-i)+(ny/2-j)*(ny/2-j))*deltax**2/
$ (2*Sigma*Sigma)) * P0*(1-Reff2 )
    enddo
    Q1(i,j,nz1) = (Q1(i,j,nz1)+Q2(i,j,nz1))/2.0
  do z =nz1+nz2,nz

```

```

        Q3(i,j,z)= Alpha3*exp( - Alpha3 *(z-nz2-nz1) *deltaZ3 )*
$   exp(-Alpha1*deltaZ*nz1 ) *exp(-Alpha2*deltaZ*nz2 ) /
$   (2*pi*Sigma**2)*exp(-(( nx/2-i)*(nx/2-i)+(ny/2-j)*(ny/2-j))*
$   deltax**2/(2*Sigma*Sigma)) * P0*(1-Reff3 )
    enddo
        Q2(i,j,nz1+nz2) = (Q2(i,j,nz1+nz2)+Q3(i,j,nz1+nz2))/2.0
    enddo
    enddo
c   Begin the big loop by time step!!!!!!!!!!!!!!!!!!!!!!!!!!!!
do t=1,50001
c   // intialize ax,bx,cx
    bx(1)=0.0
    ax(1) = 11.0/6.0
    cx(1)=1.0/3.0
    do i=2,nx-2
        bx(i) = -0.1
        ax(i) = 1.0
        cx(i) = -0.1
    enddo
    bx(nx-1) = 1.0/3.0
    ax(nx-1) = 11.0/6.0
    cx(nx-1)=0.0
c   // intialize dx and caulculate vxx
    do j=1,ny-1
        do k=1,nz
            dx(1)= miuxy*(vn(2,j,k)-vn(1,j,k))
            do i=2,nx-2
                dx(i) = (6.0*miuxy/5.0)*(vn(i-1,j,k)-2*vn(i,j,k)
+                + vn(i+1,j,k))
            enddo
            dx(nx-1) = miuxy * (vn(nx-2,j,k)-vn(nx-1,j,k))
            call tri(nx-1,bx,ax,cx,dx,tempx)
            do i=1,nx-1
                vxx(i,j,k)=tempx(i)
            enddo
        enddo
    enddo
c   // intialize ay,by,cy
    by(1)=0.0
    ay(1) = 11.0/6.0
    cy(1)=1.0/3.0
    do i=2,ny-2
        by(i) = -0.1
        ay(i) = 1.0
        cy(i) = -0.1
    enddo
    by(ny-1) = 1.0/3.0
    ay(ny-1) = 11.0/6.0
    cy(ny-1)=0.0
c   // intialize dy and caulculate vyy
    do i=1,nx-1
        do k=1,nz
            dy(1)= miuxy*(vn(i,2,k)-vn(i,1,k))

```

```

do j=2,ny-2
    dy(j) = (6.0*miuxy/5.0)*(vn(i,j-1,k)-2*vn(i,j,k)
+
    + vn(i,j+1,k))
    enddo
dy(ny-1) = miuxy * (vn(i,ny-2,k)-vn(i,ny-1,k))
call tri(ny-1,by,ay,cy,dy,tempy)
do j=1,ny-1
    vyy(i,j,k)=tempy(j)
    enddo
    enddo
    enddo
c // intialize az,bz,cz
bz(1)=0.0
az(1) = 11.0/6.0
cz(1)=1.0/3.0
do i=2,nz1-1
    bz(i) = -0.1
    az(i) = 1.0
    cz(i) = -0.1
enddo
bz(nz1) = -inta1*rk1
az(nz1) = intb1*rk1-intb2*rk2*0.472222222
cz(nz1) = inta2*rk2
bz(nz1+1) = -0.1*0.472222222
az(nz1+1) = 1.0
cz(nz1+1) = -0.1
do i=nz1+2,nz1+nz2-1
    bz(i) = -0.1
    az(i) = 1.0
    cz(i) = -0.1
enddo
bz(nz1+nz2) = -inta1*rk2
az(nz1+nz2) = (intb1*rk2-intb2*rk3*1.857142857*ration)
cz(nz1+nz2) = inta2*rk3*ration
bz(nz1+nz2+1) = -0.1*1.857142857
az(nz1+nz2+1) = 1.0
cz(nz1+nz2+1) = -0.1
do i=nz1+nz2+2,nz-1
    bz(i) = -0.1
    az(i) = 1.0
    cz(i) = -0.1
enddo
bz(nz) = 1.0/3.0
az(nz) = 11.0/6.0
cz(nz) = 0.0
c // initiate the coefficients in RHS of the tridiagonal,d(i)
do i=1,nx-1
    do j=1,ny-1
        dz(1)= miu*(-vn(i,j,1)+vn(i,j,2))
        do k=2,nz1-1
            dz(k) = (6.0*miu/5.0)*(vn(i,j,k-1)-2*vn(i,j,k) + vn(i,j,k+1))
        enddo
    enddo
c *****interface 1 *****

```

```

dz(nz1)= miu*(rk1*inte1*vn1(i,j,nz1-1)
& + (rk1*intd1-rk2*intd2)*vn(i,j,nz1)-rk2*inte2*vn(i,j,nz1+1))
& + intb2*rk2*0.00403846*(vn(i,j,nz1)-Bv(j))
c *****interface 1 *****
do k=nz1+1,nz1+nz2-1
dz(k)=(6.0*miu/5.0)*(vn(i,j,k-1)-2*vn(i,j,k) + vn(i,j,k+1))
enddo
dz(nz1+1) = dz(nz1+1)-0.1*0.004038462*(Vn(i,j,nz1)-Bv(j))
c *****interface 2 *****
dz(nz1+nz2)= miu*rk2*inte1*vn(i,j,nz1+nz2-1)
& +(miu*rk2*intd1-miu3*rk3*ration*intd2)*vn(i,j,nz1+nz2)-
& miu3*rk3*ration*inte2*vn(i,j,nz1+nz2+1)+
& ration*intb2*rk3*0.0025*(vn(i,j,nz2+nz1)-Bv(j))
c *****interface 2 *****
do k=nz1+nz2+1,nz-1
dz(k)=(6.0*miu3/5.0)*(vn(i,j,k-1)-2*vn(i,j,k) + vn(i,j,k+1))
enddo
dz(nz1+nz2+1)=dz(nz1+nz2+1)-0.1*0.0025*(Vn(i,j,nz1+nz2)-Bv(j))
dz(nz) = miu3*(vn(i,j,nz-1)-vn(i,j,nz))
c // Call subroutine to solve the tridiagonal system
call tri(nz,bz,az,cz,dz,tempz)
do k=1,nz
vzz(i,j,k)=tempz(k)
enddo
enddo
enddo
call equal(vn1,vn,nx,ny,nz)
10 continue
c // Iteration!
c // Refresh the coefficients in RHS of the tridiagonal,d1(i)
do j=1,ny-1
do k=1,nz
dx1(1)= miuxy*(vn1(2,j,k)-vn1(1,j,k))
do i=2,nx-2
dx1(i) = (6.0*miuxy/5.0)*(vn1(i-1,j,k)-2*vn1(i,j,k)
+
+ vn1(i+1,j,k))
enddo
dx1(nx-1) = miuxy * (vn1(nx-2,j,k)-vn1(nx-1,j,k))
call tri(nx-1,bx,ax,cx,dx1,tempx)
do i=1,nx-1
vxx1(i,j,k)=tempx(i)
enddo
enddo
enddo
c //solve the vyy1()
do i=1,nx-1
do k=1,nz
dy1(1)= miuxy*(vn1(i,2,k)-vn1(i,1,k))
do j=2,ny-2
dy1(j) = (6.0*miuxy/5.0)*(vn1(i,j-1,k)-2*vn1(i,j,k)
+
+ vn1(i,j+1,k))
enddo
dy1(ny-1) = miuxy * (vn1(i,ny-2,k)-vn1(i,ny-1,k))

```



```

        call tri(ny-1,by,ay,cy,dy1,tempy)
        do j=1,ny-1
            vyy1(i,j,k)=tempy(j)
        enddo
    enddo
enddo
c //Slove the vzz1()
do i=1,nx-1
do j=1,ny-1
    dz1(1) = miu*(-vn1(i,j,1)+vn1(i,j,2))
    do k=2,nz1-1
        dz1(k)=(6.0*miu/5.0)*(vn1(i,j,k-1)-2*vn1(i,j,k)+vn1(i,j,k+1))
    enddo
c *****interface 1 *****
    dz1(nz1)= miu*(rk1*inte1*vn1(i,j,nz1-1)
& + (rk1*intd1-rk2*intd2)*vn1(i,j,nz1)-rk2*inte2*vn1(i,j,nz1+1))
& + intb2*rk2*0.00403846*(vn1(i,j,nz1)-Bv1(j))
c *****interface 1 *****
    do k=nz1+1,nz1+nz2-1
        dz1(k)=(6.0*miu/5.0)*(vn1(i,j,k-1)-2*vn1(i,j,k) + vn1(i,j,k+1))
    enddo
    dz1(nz1+1) = dz1(nz1+1)-0.1*0.004038462*(Vn1(i,j,nz1)-Bv1(j))
c *****interface 2 *****
    dz1(nz1+nz2)= miu*rk2*inte1*vn1(i,j,nz1+nz2-1)
& +(miu*rk2*intd1-miu3*ration*rk3*intd2)*vn1(i,j,nz1+nz2)-
& miu3*rk3*ration*inte2*vn1(i,j,nz1+nz2+1)+
& ration*intb2*rk3*0.0025*(vn1(i,j,nz2+nz1)-Bv1(j))
c *****interface 2 *****
    do k=nz1+nz2+1,nz-1
        dz1(k)=(6.0*miu3/5.0)*(vn1(i,j,k-1)-2*vn1(i,j,k) + vn1(i,j,k+1))
    enddo
    dz1(nz1+nz2+1)=dz1(nz1+nz2+1)-0.1*0.0025*(Vn1(i,j,nz1+nz2)-Bv1(j))
    dz1(nz) = miu3*(vn1(i,j,nz-1)-vn1(i,j,nz))
c // Call subroutine to solve the tridiagonal system
    call tri(nz,bz,az,cz,dz1,tempz)
    do k=1,nz
        vzz1(i,j,k)=tempz(k)
    enddo
enddo
enddo
c // calculate the vnew with vzz and vzz1
do i=1,nx-1
do j=1,ny-1
    p1= wb1*cb1*0.5*dt
    do k = 1,nz1
        qq2(k)= rk1*0.5*(vxx(i,j,k)+vxx1(i,j,k)+vyy(i,j,k)
+ vyy1(i,j,k)+vzz(i,j,k)+vzz1(i,j,k))
    enddo
    do k = 1,nz1
        vn2(i,j,k)=(qq2(k)+(rho1*c1-p1)*vn(i,j,k)
$ +q1(i,j,k)*dt)/(p1+rho1*c1)
    enddo

```

```

p2= wb2*cb2*0.5*dt
do k = nz1+1,nz1+nz2
  qq2(k)= rk2*0.5*(vxx(i,j,k)+vxx1(i,j,k)+vyy(i,j,k)
+      +vyy1(i,j,k)+vzz(i,j,k)+vzz1(i,j,k))
  enddo
do k = nz1+1,nz1+nz2
  vn2(i,j,k)=(qq2(k)+(rho2*c2-p2)*vn(i,j,k)
$      +q2(i,j,k)*dt)/(p2+rho2*c2)
  enddo

p3= wb3*cb3*0.5*dt
do k = nz1+nz2+1,nz
  qq2(k)= rk3*0.5*(vxx(i,j,k)+vxx1(i,j,k)+vyy(i,j,k)
+      +vyy1(i,j,k)+vzz(i,j,k)+vzz1(i,j,k))
  enddo
  do k = nz1+nz2+1,nz
    vn2(i,j,k)=(qq2(k)+(rho3*c3-p3)*vn(i,j,k)
+      +q3(i,j,k)*dt)/(p3+rho3*c3)
    enddo
    vn2(i,j,nz+1) = vn2(i,j,nz)
    vn2(i,j,0) = vn2(i,j,1)
  enddo
enddo

do j=0,ny
  do k=1,nz+1
    vn2(0,j,k) = vn2(1,j,k)
    vn2(nx,j,k) = vn2(nx-1,j,k)
  enddo
enddo
do i=0,nx
  do k=1,nz+1
    vn2(i,0,k) = vn2(i,1,k)
    vn2(i,ny,k) = vn2(i,ny-1,k)
  enddo
enddo

c //check the error condition
do i=0,nx
do j=0,ny
do k=0,nz
if(abs(vn1(i,j,k)-vn2(i,j,k)).gt.er) then
x=i
y=j
z=k
call equal(vn1,vn2,nx,ny,nz)
write(*,*) 'error too big, loop back'
goto 10
endif
enddo
enddo
enddo
call equal(vn,vn2,nx,ny,nz)

```

```

c //output
c Result at different time level
write(*,*) 't = ',t
  if (t .eq. 10000)then
    do k=1,nz
      WRITE(11,*) vn2(5,5,k)
    enddo
    WRITE(1,*) 'TITLE = "t=50"'
    WRITE(1,*) 'VARIABLES = "y", "depth", "Temp"'
    WRITE(1,*) 'zone I=604, J=11, F=POINT'
    do j=0,ny
      do k=0,nz
        WRITE(1,*) j*1.0,k*0.02,(vn2(4,j,k)+vn2(5,j,k))/2.0
      enddo
    enddo
  endif

  if (t .eq. 30000)then
    do k=1,nz
      WRITE(12,*) vn2(5,5,k)
    enddo
    WRITE(2,*) 'TITLE = "t=100"'
    WRITE(2,*) 'VARIABLES = "y", "depth", "Temp"'
    WRITE(2,*) 'zone I=604, J=11, F=POINT'
    do j=0,ny
      do k=0,nz
        WRITE(2,*) j*1.0,k*0.02,(vn2(4,j,k)+vn2(5,j,k))/2.0
      enddo
    enddo
  endif

  if (t .eq. 60000)then
    do k=1,nz
      WRITE(13,*) vn2(5,5,k)
    enddo
    WRITE(3,*) 'TITLE = "t=200"'
    WRITE(3,*) 'VARIABLES = "y", "depth", "Temp"'
    WRITE(3,*) 'zone I=604, J=11, F=POINT'
    do j=0,ny
      do k=0,nz
        WRITE(3,*) j*1.0,k*0.02,(vn2(4,j,k)+vn2(5,j,k))/2.0
      enddo
    enddo
  endif

  if (t .eq. 180000)then
    do k=1,nz
      WRITE(14,*) vn2(5,5,k)
    enddo
  endif

```

```

        enddo
        WRITE(4,*) 'TITLE = "t=300"'
        WRITE(4,*) 'VARIABLES = "y", "depth", "Temp"'
        WRITE(4,*) 'zone I=604, J=11, F=POINT'
        do j=0,ny
            do k=0,nz
                WRITE(4,*) j*1.0,k*0.02,(vn2(4,j,k)+vn2(5,j,k))/2.0

            enddo
        enddo
    endif

    if (t .eq. 300000)then
        do k=1,nz
            WRITE(15,*) vn2(5,5,k)
        enddo
        WRITE(5,*) 'TITLE = "t=400"'
        WRITE(5,*) 'VARIABLES = "y", "depth", "Temp"'
        WRITE(5,*) 'zone I=604, J=11, F=POINT'
        do j=0,ny
            do k=0,nz
                WRITE(5,*) j*1.0,k*0.02,(vn2(4,j,k)+vn2(5,j,k))/2.0

            enddo
        enddo
    endif

    if (t .eq. 600000)then
        do k=1,nz
            WRITE(16,*) vn2(5,5,k)
        enddo
        WRITE(6,*) 'TITLE = "t=500"'
        WRITE(6,*) 'VARIABLES = "y", "depth", "Temp"'
        WRITE(6,*) 'zone I=604, J=11, F=POINT'
        do j=0,ny
            do k=0,nz
                WRITE(6,*) j*1.0,k*0.02,(vn2(4,j,k)+vn2(5,j,k))/2.0

            enddo
        enddo
    endif

    enddo
c    // Record the CPU time

    total = etime(elapsed)
    write(7,*) 'End: total=', total, ' user=', elapsed(1),
+    ' system=', elapsed(2)
    stop
end

```

APPENDIX D

**SOURCE CODE FOR SOLVING PENNES' BIOHEAT TRANSFER
EQUATION IN A THREE-DIMENSIONAL SINGLE VESSEL
EMBEDDED TRIPLE-LAYERED SKIN STRUCTURE**

```

c      Table A.4 Program IV:
c      Source code for solving the 3D single vessel embedded Triple-layered Pennes bioheat
c      transfer model with laser power in a Triple-layered skin structure

c      Haofeng Yu

c      07/01/04

c      This program aims to solve about heat transfer in the skin of human being.
c      There are three layers in the skin, Epiderms, Dermis and Subcutaneous.
c      The skin structure is 10by10by12.08mm in geometry
c      The governing equation used is:
c       $\rho c (\partial U / \partial t) = k (\nabla^2 U) - W_b C_b U + W_b C_b U_b + Q$ 
c      Two boundary conditions are considered:
c      1. Dirichlet The temperature at surface is assumed to be constant, 10oC
c      2. Neumann The temperature at surface is assumed to be heat insulated

program bioheat3D3LVesselLaser
parameter(nz=603,pi=3.14159265358979,nx=10,ny=10)
c***** variable declaration *****
real c1,c2,c3,rk1,rk2,rk3,rho1,rho2,rho3,wb1,wb2,wb3,cb1,cb2,cb3
integer x,y,z
integer Nt,nz1,nz2,t,counter
integer n,remainder,positi

c
double precision Bp(0:ny),Bdiv(0:ny),Bv(0:ny),Bv1(0:ny)
double precision Br,Bu,BPF,BAlpha,BL,Bk,BCb,Bratio
double precision Q1(0:nx,0:ny,0:nz), Q2(0:nx,0:ny,0:nz)
double precision Q3(0:nx,0:ny,0:nz)

double precision v(0:nx,0:ny,0:nz+1),vn(0:nx,0:ny,0:nz+1)
double precision vn1(0:nx,0:ny,0:nz+1),vn2(0:nx,0:ny,0:nz+1)
double precision qq2(0:nz+1),dx1(0:nx),dy1(0:ny),dz1(0:nz+1)
double precision tempx(0:nx),tempy(0:ny),tempz(0:nz+1)
double precision vxx(0:nx,0:ny,0:nz+1),vxx1(0:nx,0:ny,0:nz+1)
double precision vyy(0:nx,0:ny,0:nz+1),vyy1(0:nx,0:ny,0:nz+1)
double precision vzz(0:nx,0:ny,0:nz+1),vzz1(0:nx,0:ny,0:nz+1)
double precision ax(0:nx),bx(0:nx),cx(0:nx),dx(0:nx)
double precision ay(0:ny),by(0:ny),cy(0:ny),dy(0:ny)
double precision az(0:nz+1),bz(0:nz+1),cz(0:nz+1),dz(0:nz+1)
double precision dt,er,dif
double precision part,try,miu,miuxy
double precision p1,p2,p3,p5,p4,p6,p7
real inta2,intb2,intc2,intd2,inte2,intf
real inta1,intb1,intc1,intd1,inte1,intf2
double precision Sigma,Alpha1,Alpha2,Alpha3,Reff1,Reff2,Reff3
double precision P0
REAL etime ! Declare the type of etime()
REAL elapsed(2) ! For receiving user and system time
REAL total ! For receiving total time
c // Discretization units
er = 0.001
deltax = 1.0

```

```

deltay = 1.0
deltaz = 0.02
    deltaz3 = 0.02
    Ration = deltaz3/deltaz
dt = .001
nz1 = 4
nz2 = 100
c    //      Parameters related to blood vessel
    Br=0.01
    Bu=80
    BPF=200
    BAlpha=0.002
    BL=20
    Bk=0.0005
    BCb=0.004134
    Bratio = Balpha*BPF/(Bcb*Bu)
c    //      Parameters related to Laser Power
    Sigma= 1.0
    Alpha1=0.1
    Alpha2=0.08
    Alpha3=0.04
    Reff1=0.93
    Reff2=0.93
    Reff3=0.93
    P0=6.4
c    //      Parameters related to layers of skin
c1 = 3.6
c2 = 3.4
c3 = 3.06
cb1 = 0.0
cb2 = 4.2
cb3 = 4.2
rk1 = 0.00026
rk2 = 0.00052
rk3 = 0.00021
rho1 = 0.0012
rho2 = 0.0012
rho3 = 0.001
    wb1 = 0.0
wb2 = 0.0000005
wb3 = 0.0000005
c //inta1,intb1,intc1,intd1,iete1 are the coefficients for the upper part to the interface.
c //inta2,intb2,intc2,intd2,iete2 are the coefficients for the upper part to the interface.
inta1=-1.0
intb1=-2.0
intc1=6.0
intd1=6.0
inte1=-6.0
inta2=1.0
intb2=2.0
intc2=6.0
intd2=-6.0
inte2=6.0

```

```

miu=dt/(deltaz*deltaz)
miu3=dt/(deltaz3*deltaz3)
miux=dt/(deltax*deltax)
miuy=dt/(deltay*deltay)
miuxy=dt/(deltay*deltay)
c***** file *****
open(unit = 1, file = '0603 t1000.dat', status = 'old')
open(unit = 2, file = '0603 t3000.dat', status = 'old')
open(unit = 3, file = '0603 t5000.dat', status = 'old')
open(unit = 4, file = '0603 t10000.dat', status = 'old')
open(unit = 5, file = '0603 t15000.dat', status = 'old')
open(unit = 6, file = '0603 t20000.dat', status = 'old')
open(unit = 7, file = 'time.dat', status = 'old')
c***** 4th compact scheme *****
c // Initialization!
do i=0, nx
  ax(i) = 0.0
  cx(i) = 0.0
  bx(i) = 0.0
  dx1(i) = 0.0
  dx(i) = 0.0
enddo
do j=0, ny
  Bv(j) = 0.0
  Bp(j) = 0.0
  Bv1(j) = 0.0
  ay(j) = 0.0
  cy(j) = 0.0
  by(j) = 0.0
  dy1(j) = 0.0
  dy(j) = 0.0
enddo
do k=0, nz+1
  az(k) = 0.0
  cz(k) = 0.0
  bz(k) = 0.0
  dz1(k) = 0.0
  dz(k) = 0.0
enddo
do i=0, nx
  do j=0, ny
    do k=0, nz+1
      vn(i,j,k)=0.0
      vn1(i,j,k)=0.0
      vn2(i,j,k)=0.0
    enddo
  enddo
enddo

c Blood temperature at entry of vessel
Bv1(0) = 10.0
Bv(0) = 10.0
c Calculate the laser power Q(i,j,k)

```



```

do i=0,nx
do j=0,ny
do z=0,nz1
Q1(i,j,z)=Alpha1*exp(-Alpha1*z*deltaZ)/(2*pi*Sigma**2)*
$ exp(-((nx/2-i)*(nx/2-i)+(ny/2-j)*(ny/2-j))*deltax**2/
$ (2*Sigma*Sigma)) * P0*(1-Reff1 )
enddo
do z =nz1,nz1+nz2
Q2(i,j,z)= Alpha2 * exp( - Alpha2 *(z-nz1) *deltaZ )*
$ exp(-Alpha1*deltaZ*nz1 )/(2*pi*Sigma**2)*
$ exp(-((nx/2-i)*(nx/2-i)+(ny/2-j)*(ny/2-j))*deltax**2/
$ (2*Sigma*Sigma)) * P0*(1-Reff2 )
enddo
Q1(i,j,nz1) = (Q1(i,j,nz1)+Q2(i,j,nz1))/2.0
do z =nz1+nz2,nz
Q3(i,j,z)= Alpha3*exp( - Alpha3 *(z-nz2-nz1) *deltaZ3 )*
$ exp(-Alpha1*deltaZ*nz1 ) *exp(-Alpha2*deltaZ*nz2 ) /
$ (2*pi*Sigma**2)*exp(-(( nx/2-i)*(nx/2-i)+(ny/2-j)*(ny/2-j))*
$ deltax**2/(2*Sigma*Sigma)) * P0*(1-Reff3 )
enddo
Q2(i,j,nz1+nz2) = (Q2(i,j,nz1+nz2)+Q3(i,j,nz1+nz2))/2.0
enddo
enddo

c Begin the big loop by time step!!!!!!!!!!!!!!!!!!!!!!
do t=1,50001
c // intialize ax,bx,cx
bx(1)=0.0
ax(1) = 11.0/6.0
cx(1)=1.0/3.0
do i=2,nx-2
bx(i) = -0.1
ax(i) = 1.0
cx(i) = -0.1
enddo
bx(nx-1) = 1.0/3.0
ax(nx-1) = 11.0/6.0
cx(nx-1)=0.0
c // intialize dx and calculate vxx
do j=1,ny-1
do k=1,nz
dx(1)= miuxy*(vn(2,j,k)-vn(1,j,k))
do i=2,nx-2
dx(i) = (6.0*miuxy/5.0)*(vn(i-1,j,k)-2*vn(i,j,k)
+
+ vn(i+1,j,k))
enddo
dx(nx-1) = miuxy * (vn(nx-2,j,k)-vn(nx-1,j,k))
call tri(nx-1,bx,ax,cx,dx,tempx)
do i=1,nx-1
vxx(i,j,k)=tempx(i)
enddo
enddo
enddo
enddo

```

```

c      // intialize ay,by,cy
      by(1)=0.0
      ay(1) = 11.0/6.0
      cy(1)=1.0/3.0
      do i=2,ny-2
        by(i) = -0.1
        ay(i) = 1.0
        cy(i) = -0.1
      enddo
      by(ny-1) = 1.0/3.0
      ay(ny-1) = 11.0/6.0
      cy(ny-1)=0.0
c      // intialize dy and caulculate vyy
      do i=1,nx-1
        do k=1,nz
          dy(1)= miuxy*(vn(i,2,k)-vn(i,1,k))
          do j=2,ny-2
            dy(j) = (6.0*miuxy/5.0)*(vn(i,j-1,k)-2*vn(i,j,k)
+          + vn(i,j+1,k))
            enddo
            dy(ny-1) = miuxy * (vn(i,ny-2,k)-vn(i,ny-1,k))
            call tri(ny-1,by,ay,cy,dy,tempy)
            do j=1,ny-1
              vyy(i,j,k)=tempy(j)
            enddo
          enddo
        enddo
      enddo
c      // intialize az,bz,cz
      bz(1)=0.0
      az(1) = 11.0/6.0
      cz(1)=1.0/3.0
      do i=2,nz1-1
        bz(i) = -0.1
        az(i) = 1.0
        cz(i) = -0.1
      enddo
      bz(nz1) = -inta1*rk1
      az(nz1) = intb1*rk1-intb2*rk2*0.472222222
      cz(nz1) = inta2*rk2
      bz(nz1+1) = -0.1*0.472222222
      az(nz1+1) = 1.0
      cz(nz1+1) = -0.1
      do i=nz1+2,nz1+nz2-1
        bz(i) = -0.1
        az(i) = 1.0
        cz(i) = -0.1
      enddo
      bz(nz1+nz2) = -inta1*rk2
      az(nz1+nz2) = (intb1*rk2-intb2*rk3*1.857142857*ration)
      cz(nz1+nz2) = inta2*rk3*ration
      bz(nz1+nz2+1) = -0.1*1.857142857
      az(nz1+nz2+1) = 1.0
      cz(nz1+nz2+1) = -0.1

```

```

do i=nz1+nz2+2,nz-1
  bz(i) = -0.1
  az(i) = 1.0
  cz(i) = -0.1
enddo
bz(nz) = 1.0/3.0
az(nz) = 11.0/6.0
cz(nz) = 0.0
c // initiate the coefficients in RHS of the tridiagonal,d(i)
  do i=1,nx-1
    do j=1,ny-1
      dz(1)= miu*(-vn(i,j,1)+vn(i,j,2))
      do k=2,nz1-1
        dz(k) = (6.0*miu/5.0)*(vn(i,j,k-1)-2*vn(i,j,k) + vn(i,j,k+1))
      enddo
c *****interface 1 *****
      dz(nz1)= miu*(rk1*inte1*vn1(i,j,nz1-1)
& + (rk1*intd1-rk2*intd2)*vn(i,j,nz1)-rk2*inte2*vn(i,j,nz1+1))
& + intb2*rk2*0.00403846*(vn(i,j,nz1)-Bv(j))
c *****interface 1 *****
      do k=nz1+1,nz1+nz2-1
        dz(k)=(6.0*miu/5.0)*(vn(i,j,k-1)-2*vn(i,j,k) + vn(i,j,k+1))
      enddo
      dz(nz1+1) = dz(nz1+1)-0.1*0.004038462*(Vn(i,j,nz1)-Bv(j))
c *****interface 2 *****
      dz(nz1+nz2)= miu*rk2*inte1*vn(i,j,nz1+nz2-1)
& +(miu*rk2*intd1-miu3*rk3*ration*intd2)*vn(i,j,nz1+nz2)-
& miu3*rk3*ration*inte2*vn(i,j,nz1+nz2+1)+
& ration*intb2*rk3*0.0025*(vn(i,j,nz2+nz1)-Bv(j))
c *****interface 2 *****
      do k=nz1+nz2+1,nz-1
        dz(k)=(6.0*miu3/5.0)*(vn(i,j,k-1)-2*vn(i,j,k) + vn(i,j,k+1))
      enddo
      dz(nz1+nz2+1)=dz(nz1+nz2+1)-0.1*0.0025*(Vn(i,j,nz1+nz2)-Bv(j))
      dz(nz) = miu3*(vn(i,j,nz-1)-vn(i,j,nz))
c // Call subroutine to solve the tridiagonal system
      call tri(nz,bz,az,cz,dz,tempz)
      do k=1,nz
        vzz(i,j,k)=tempz(k)
      enddo
    enddo
  enddo
  call equal(vn1,vn,nx,ny,nz)
10 continue
c // Iteration!
c // Refresh the coefficients in RHS of the tridiagonal,d1(i)
  do j=1,ny-1
    do k=1,nz
      dx1(1)= miuxy*(vn1(2,j,k)-vn1(1,j,k))
      do i=2,nx-2
        dx1(i) = (6.0*miuxy/5.0)*(vn1(i-1,j,k)-2*vn1(i,j,k)
+
+ vn1(i+1,j,k))
      enddo

```

```

dx1(nx-1) = miuxy * (vn1(nx-2,j,k)-vn1(nx-1,j,k))
call tri(nx-1,bx,ax,cx,dx1,tempx)
do i=1,nx-1
    vxx1(i,j,k)=tempx(i)
enddo
    enddo
enddo
c //solve the vyy1()
do i=1,nx-1
    do k=1,nz
        dy1(1)= miuxy*(vn1(i,2,k)-vn1(i,1,k))
        do j=2,ny-2
            dy1(j) = (6.0*miuxy/5.0)*(vn1(i,j-1,k)-2*vn1(i,j,k)
+
            + vn1(i,j+1,k))
        enddo
        dy1(ny-1) = miuxy * (vn1(i,ny-2,k)-vn1(i,ny-1,k))
        call tri(ny-1,by,ay,cy,dyl,tempy)
        do j=1,ny-1
            vyy1(i,j,k)=tempy(j)
        enddo
    enddo
enddo
c //Slove the vzz1()
do i=1,nx-1
    do j=1,ny-1
        dz1(1) = miu*(-vn1(i,j,1)+vn1(i,j,2))
        do k=2,nz1-1
            dz1(k)=(6.0*miu/5.0)*(vn1(i,j,k-1)-2*vn1(i,j,k)+vn1(i,j,k+1))
        enddo
c *****interface 1 *****
        dz1(nz1)= miu*(rk1*inte1*vn1(i,j,nz1-1)
& + (rk1*intd1-rk2*intd2)*vn1(i,j,nz1)-rk2*inte2*vn1(i,j,nz1+1))
& + intb2*rk2*0.00403846*(vn1(i,j,nz1)-Bv1(j))
c *****interface 1 *****
        do k=nz1+1,nz1+nz2-1
            dz1(k)=(6.0*miu/5.0)*(vn1(i,j,k-1)-2*vn1(i,j,k) + vn1(i,j,k+1))
        enddo
        dz1(nz1+1) = dz1(nz1+1)-0.1*0.004038462*(Vn1(i,j,nz1)-Bv1(j))
c *****interface 2 *****
        dz1(nz1+nz2)= miu*rk2*inte1*vn1(i,j,nz1+nz2-1)
& +(miu*rk2*intd1-miu3*ration*rk3*intd2)*vn1(i,j,nz1+nz2)-
& miu3*rk3*ration*inte2*vn1(i,j,nz1+nz2+1)+
& ration*intb2*rk3*0.0025*(vn1(i,j,nz2+nz1)-Bv1(j))
c *****interface 2 *****
        do k=nz1+nz2+1,nz-1
            dz1(k)=(6.0*miu3/5.0)*(vn1(i,j,k-1)-2*vn1(i,j,k) + vn1(i,j,k+1))
        enddo
        dz1(nz1+nz2+1)=dz1(nz1+nz2+1)-0.1*0.0025*(Vn1(i,j,nz1+nz2)-Bv1(j))
        dz1(nz) = miu3*(vn1(i,j,nz-1)-vn1(i,j,nz))
c // Call subroutine to solve the tridiagonal system
        call tri(nz,bz,az,cz,dz1,tempz)
        do k=1,nz
            vzz1(i,j,k)=tempz(k)

```

```

        enddo
    enddo
    enddo
c   Calculate temperature in the periphery
    do j=0,ny
        Bp(j)=(vn2(4,j,304)+vn2(4,j,305)+vn2(5,j,304)+vn2(5,j,305))/4.0
    enddo
c   calculate Bv1(j)the influence from blood with Bp(j),Bv(j)
    do j=1,ny
        Bdiv(j-1) = -1.0*Bratio*(Bv1(j-1) - Bp(j-1))
        Bv1(j) = Bv1(j-1) + 0.5*deltay*(Bdiv(j-1)-Bratio*(Bv1(j-1)
@  + deltax*Bdiv(j-1) - Bp(j)))
    enddo
c // calculate the vnew with vzz and vzz1
    do i=1,nx-1
        do j=1,ny-1
            p1= wb1*cb1*0.5*dt
            do k = 1,nz1
                qq2(k)= rk1*0.5*(vxx(i,j,k)+vxx1(i,j,k)+vyy(i,j,k)
+                +vyy1(i,j,k)+vzz(i,j,k)+vzz1(i,j,k))
            enddo
            do k = 1,nz1
                vn2(i,j,k)=(2*p1*Bv1(j)+qq2(k)+(rho1*c1-p1)*vn(i,j,k)
$                +q1(i,j,k)*dt)/(p1+rho1*c1)
            enddo
            p2= wb2*cb2*0.5*dt
            do k = nz1+1,nz1+nz2
                qq2(k)= rk2*0.5*(vxx(i,j,k)+vxx1(i,j,k)+vyy(i,j,k)
+                +vyy1(i,j,k)+vzz(i,j,k)+vzz1(i,j,k))
            enddo
            do k = nz1+1,nz1+nz2
                vn2(i,j,k)=(2*p2*Bv1(j)+qq2(k)+(rho2*c2-p2)*vn(i,j,k)
$                +q2(i,j,k)*dt)/(p2+rho2*c2)
            enddo
            p3= wb3*cb3*0.5*dt
            do k = nz1+nz2+1,nz
                qq2(k)= rk3*0.5*(vxx(i,j,k)+vxx1(i,j,k)+vyy(i,j,k)
+                +vyy1(i,j,k)+vzz(i,j,k)+vzz1(i,j,k))
            enddo
            do k = nz1+nz2+1,nz
                vn2(i,j,k)=(2*p3*Bv1(j)+qq2(k)+(rho3*c3-p3)*vn(i,j,k)
+                +q3(i,j,k)*dt)/(p3+rho3*c3)
            enddo
                vn2(i,j,nz+1) = vn2(i,j,nz)
                vn2(i,j,0) = vn2(i,j,1)
        enddo
    enddo
    do j=0,ny
        do k=1,nz+1
            vn2(0,j,k) = vn2(1,j,k)
            vn2(nx,j,k) = vn2(nx-1,j,k)
        enddo
    enddo

```

```

do i=0,nx
  do k=1,nz+1
    vn2(i,0,k) = vn2(i,1,k)
    vn2(i,ny,k) = vn2(i,ny-1,k)
  enddo
enddo
do j=0,ny
  Bp(j)=(vn2(4,j,304)+vn2(4,j,305)+vn2(5,j,304)+vn2(5,j,305))/4.0
enddo
c //check the error condition
do i=0,nx
do j=0,ny
  do k=0,nz
if(abs(vn1(i,j,k)-vn2(i,j,k)).gt.er) then
  x=i
  y=j
  z=k
call equal(vn1,vn2,nx,ny,nz)
  write(*,*) 'error too big, loop back'
  goto 10
endif
enddo
enddo
enddo
do j=0,ny
  Bv(j) = Bv1(j)
enddo
write(*,*) 'loop fished*****'
call equal(vn,vn2,nx,ny,nz)
c //output
c Result at different time level
if (t .eq. 10000)then
  do k=1,nz
    WRITE(11,*) vn2(5,5,k)
  enddo
  WRITE(1,*) 'TITLE = "t=50"'
  WRITE(1,*) 'VARIABLES = "y", "depth", "Temp"'
  WRITE(1,*) 'zone I=607, J=11, F=POINT'
  do j=0,ny
    do k=0,nz
      WRITE(1,*) j*1.0,k*0.02,(vn2(4,j,k)+vn2(5,j,k))/2.0
      if (k .eq.304) then
        WRITE(1,*) j*1.0,6.081,Bv1(j)
        WRITE(1,*) j*1.0,6.090,Bv1(j)
        WRITE(1,*) j*1.0,6.099,Bv1(j)
      endif
    enddo
  enddo
enddo
enddo
if (t .eq. 30000)then
  do k=1,nz
    WRITE(12,*) vn2(5,5,k)
  enddo
enddo

```

```

        enddo
        WRITE(2,*) 'TITLE = "t=100"'
        WRITE(2,*) 'VARIABLES = "y", "depth", "Temp"'
        WRITE(2,*) 'zone I=607, J=11, F=POINT'
        do j=0,ny
            do k=0,nz
                WRITE(2,*) j*1.0,k*0.02,(vn2(4,j,k)+vn2(5,j,k))/2.0
                if (k .eq.304) then
                    WRITE(2,*) j*1.0,6.081,Bv1(j)
                    WRITE(2,*) j*1.0,6.090,Bv1(j)
                    WRITE(2,*) j*1.0,6.099,Bv1(j)
                endif
            enddo
        enddo
    endif

if (t .eq. 60000)then
    do k=1,nz
        WRITE(13,*) vn2(5,5,k)
    enddo
    WRITE(3,*) 'TITLE = "t=200"'
    WRITE(3,*) 'VARIABLES = "y", "depth", "Temp"'
    WRITE(3,*) 'zone I=607, J=11, F=POINT'
    do j=0,ny
        do k=0,nz
            WRITE(3,*) j*1.0,k*0.02,(vn2(4,j,k)+vn2(5,j,k))/2.0
            if (k .eq.304) then
                WRITE(3,*) j*1.0,6.081,Bv1(j)
                WRITE(3,*) j*1.0,6.090,Bv1(j)
                WRITE(3,*) j*1.0,6.099,Bv1(j)
            endif
        enddo
    enddo
endif

if (t .eq. 180000)then
    do k=1,nz
        WRITE(14,*) vn2(5,5,k)
    enddo
    WRITE(4,*) 'TITLE = "t=300"'
    WRITE(4,*) 'VARIABLES = "y", "depth", "Temp"'
    WRITE(4,*) 'zone I=607, J=11, F=POINT'
    do j=0,ny
        do k=0,nz
            WRITE(4,*) j*1.0,k*0.02,(vn2(4,j,k)+vn2(5,j,k))/2.0
            if (k .eq.304) then
                WRITE(4,*) j*1.0,6.081,Bv1(j)
                WRITE(4,*) j*1.0,6.090,Bv1(j)
                WRITE(4,*) j*1.0,6.099,Bv1(j)
            endif
        enddo
    enddo
endif
enddo

```

```

endif

if (t .eq. 300000)then

    do k=1,nz
        WRITE(15,*) vn2(5,5,k)
    enddo
    WRITE(5,*) 'TITLE = "t=400"'
    WRITE(5,*) 'VARIABLES = "y", "depth", "Temp"'
    WRITE(5,*) 'zone I=607, J=11, F=POINT'
    do j=0,ny
        do k=0,nz
            WRITE(5,*) j*1.0,k*0.02,(vn2(4,j,k)+vn2(5,j,k))/2.0
            if (k .eq.304) then
                WRITE(5,*) j*1.0,6.081,Bv1(j)
                WRITE(5,*) j*1.0,6.090,Bv1(j)
                WRITE(5,*) j*1.0,6.099,Bv1(j)
            endif
        enddo
    enddo
endif

if (t .eq. 600000)then
    do k=1,nz
        WRITE(16,*) vn2(5,5,k)
    enddo
    WRITE(6,*) 'TITLE = "t=500"'
    WRITE(6,*) 'VARIABLES = "y", "depth", "Temp"'
    WRITE(6,*) 'zone I=607, J=11, F=POINT'
    do j=0,ny
        do k=0,nz
            WRITE(6,*) j*1.0,k*0.02,(vn2(4,j,k)+vn2(5,j,k))/2.0
            if (k .eq.304) then
                WRITE(6,*) j*1.0,6.081,Bv1(j)
                WRITE(6,*) j*1.0,6.090,Bv1(j)
                WRITE(6,*) j*1.0,6.099,Bv1(j)
            endif
        enddo
    enddo
endif

c // Record the CPU time
total = etime(elapsed)
write(7,*) 'End: total=', total, ' user=', elapsed(1),
+ ' system=', elapsed(2)
stop
end

```


APPENDIX E

SOURCE CODE OF A SUBROUTINE FOR EVALUATING TWO ARRAYS

c Table A.5 Subroutine 1: Source code for equalizing two 3D arrays

```
c***** subroutine equal *****
  subroutine equal(wold,wnew,xn,yn,zn)
  integer xn,yn,zn
  double precision wold(0:xn,0:yn,0:zn+1),wnew(0:xn,0:yn,0:zn+1)
  do i=0,xn
    do j=0,yn
      do k=0,zn+1
        wold(i,j,k) = wnew(i,j,k)
      enddo
    enddo
  enddo
  return
end
```

APPENDIX F

SOURCE CODE OF A SUBROUTINE FOR SOLVING A TRIDIAGONAL LINEAR SYSTEM

c Table A.6 Subroutine 2: Source code for solving the tri-diagonal system by Thomas Algorithm

```

c***** subroutine tri*****
  subroutine tri(n,b,a,c,d,vvv)
    integer n
    double precision a(0:n+1),b(0:n+1),c(0:n+1),d(0:n+1)
    double precision alpha(0:n+1),beta(0:n+1),vvv(0:n+1)
    alpha(n+1)=0
    beta(n+1)=0
    do i=n,1,-1
      alpha(i)=(d(i)+c(i)*alpha(i+1))/(a(i)-c(i)*beta(i+1))
      beta(i)=b(i)/(a(i)-c(i)*beta(i+1))
    enddo
    do i=1,n
      vvv(i)= alpha(i)+beta(i)*vvv(i-1)
    enddo
    return
  end

```

REFERENCES

- [Baish 1990] J. W. Baish, "Heat transport by countercurrent blood vessels in the presence of an arbitrary temperature gradient," *ASME Journal of Biomechanical Engineering*, Vol. 112, pp. 207-211, 1990.
- [Barun 2003] V. V. Barun and A. P. Ivanov, "Thermal action of a short light pulse on biological tissues," *International Journal of Heat and Mass Transfer*, Vol. 46, pp. 3243-3254, 2003.
- [Bechnke 1984] W. P. Bechnke, "Predicting flash fire protection of clothing from laboratory tests using second-degree burn to rate performance," *Fire Mat.*, Vol. 8, pp. 57-63, 1984.
- [Buell 1989] J. C. Buell, "A hybrid numerical method for three-dimensional spatially-developing free-shear flows," *Journal of Computational Physics*. Vol. 95, pp. 313-338, 1989.
- [Burden 2001] R. L. Burden and J. D. Faires, *Numerical analysis (Seventh edition)*, Higher Education Press, Beijing, 2001.
- [Cai 1995] R. Cai, "Analytical solution of unsteady one-dimensional bioheat transfer equation," *Chinese Science Bulletin*, Vol. 40, No. 19, pp.1663-1665, 1995.
- [Cai 1998] R. Cai and N. Zhang, "Unsteady one-dimensional analytical solutions for bioheat transfer equations," *Process in Natural Science*, Vol. 8, No. 6, pp. 733-739, 1998.
- [Cattaneo 1958] C. Cattaneo, "A form of heat conduction equation which eliminates the paradox of instantaneous propagation," *Compte Rendus*, Vol. 247, pp. 431-433, 1958.
- [Chato 1989] J. C. Chato, J. J. Eckburg and E. Hurlburt, "Comparison of three bioheat transfer models using finite difference technique," *American Society of Mechanical Engineers, Heat Transfer Division*, HTD-Vol. 126, pp. 17-21, 1989.
- [Chan 1992] C. L. Chan, "Boundary element method analysis for the bioheat transfer equation", *Journal of Biomechanical Engineering*, Vol. 114, pp. 358-365, 1990.
- [Charney 1988] C. K. Charney and R. C. Levin, "Heat transfer normal to paired arterioles and venules embedded in perfused tissue during hyperthermia," *ASME Journal of Biomechanical Engineering*, Vol. 110, No. 4, pp. 277-282, 1988.

- [Charney 1989] C. K. Charney and R. C. Levin, "Bioheat transfer in a branching countercurrent network during hyperthermia," *ASME Journal of Biomechanical Engineering*, Vol. 111, pp. 263-270, 1989.
- [Charney 1990] C. K. Charney, S. Weinbaum and R. L. Levin, "An evaluation of the Weinbaum-Jiji bioheat equation for normal and hyperthermic Conditions," *Journal of Biomechanical Engineering*, Vol. 112, pp. 80-87, 1990.
- [Chatterjee 1994] I. Chatterjee and R. E. Adams, "Finite element thermal modeling of the human body under hyperthermia treatment for cancer," *International Journal of Computer Applications in Technology*, Vol. 7, No. 3-6, pp. 151-159, 1994.
- [Chen 1980] M. M. Chen and K. R. Holmes, "Micro-vascular contributions in tissue heat Transfer," *Annals of the New York Academy of Sciences*, Vol. 335, pp. 137-150, 1980.
- [Chen 1993] Y. Chen and J. Shi, Eds., *Pathology of Burns (in Chinese)*. pp. 287-340. 1993.
- [Clegg 1989] S. T. Clegg and R. B. Roemer, "Predictions of three dimensional temperature distributions during hyperthermia experiments," *Proceedings of ASME Winter Annual Meeting*, pp.10-15, 1989.
- [Crezee 1990] J. Crezee, Lagendijk and J. J. W., "Experimental verification of bioheat transfer theories: measurement of temperature profiles around large artificial vessels in perfused tissue," *Physics Medicine and Biology*, Vol. 35, pp. 905-923, 1990.
- [Dai 2003a] W. Dai and H. Yu, "A fourth-order compact finite difference scheme for solving a 1-D Pennes' bioheat transfer equation in a uniform tissue", *the Proceeding of International Conference on Mathematics and Engineering Techniques in Medicine and Biological Sciences*, Las Vegas, NV, Jun. 2003.
- [Dai 2003b] W. Dai, G. Li, R. Nassar R. and T. Zhu, "A domain decomposition method for solving the Pennes' bioheat transfer in 3D triple-layered skin structure," *Second MIT Conference on Computational Fluid and Solid Mechanics*, pp.1650-1654, 2003.
- [Dai 2004] W. Dai and H. Yu, "A fourth-order compact finite difference scheme for solving a 1-D Pennes' bioheat transfer equation in uniform and triple-layer tissue," *Journal of Numerical Heat Transfer*, to be published.
- [Deng 2001] Z. S. Deng, J. Liu, "Blood perfusion-based model for characterizing the temperature fluctuation in living tissues," *Physica*, Vol. 300, pp. 521-530, 2001.
- [Dewhirst 1984] M. W. Dewhirst, et al., "Importance of minimum tumor temperature in determining early and long-term responses of canine and feline tumors to heat," *Cancer Research*, Vol. 44, No. 1, pp. 43-50, 1984.

[Gautherie 1969] M. Gautherie, "Etude par thermometrie infrarouge des proprietes thermiques de tissus humains 'in vivo' influence de la temperature et de la vascularisation," *Reev. Franc. Etud. Clin. Biol.*, Vol. 14, pp. 885-901, 1969.

[Gottlieb 1977] D. Gottlieb and S. A. Orszag, *Numerical Analysis of Spectral Methods SIAM*, Philadelphia, U.S., 1977.

[Guiot 1998] C. Guiot, E. Madon, D. Allegro, P.O. Pianta, B. Baiotto and P. Gabriele, "Perfusion and thermal field during hyperthermia. Experimental measurements and modeling in recurrent breast cancer," *Phys. Med. Biol.*, Vol. 43, pp. 2831-2843, 1998.

[Habash 1999] R. Habash, "Simulation of heating transfer in living biomass under microwave hyperthermia," *IEEE 1999 International Symposium on Electromagnetic Compatibility*, pp. 919-923, 1999.

[Han 1994] J. Han. and F. J. Klavs, "Combined Experimental and Modeling Studies of Laser-assisted Chemical Vapor Depositio of Copper from Copper(I)-Hexafluoroacetylacetonate Trimethylvinylsilane," *J. Appl. Phys.*, Vol. 75, No.4, pp. 2240-2250, 1994.

[Huang 1994] H. W. Huang, C. L. Chan and R. B. Roemer, "Analytical solutions of Pennes bio-heat transfer equation with a blood vessel," *Journal of Biomechanical Engineering, Transactions of the ASME*, Vol. 116, pp. 208-212, 1994.

[Iskander 1982] M. Iskander, P. Turner, J. Dubow and J. Kao, "Two-dimensional technique to calculate the EM power deposition pattern in the human body," *Journal of Microwave Power*, Vol. 17, No. 3, pp. 175-185, 1982.

[Kaminski 1990] W. Kaminski, "Hyperbolic heat conduction equation for material with a nonhomogeneous inner structure," *ASME J. Heat Transfer*, Vol. 112, pp. 555-560, 1990.

[Khaled 2003] A.R.A. and K. Vafai, "The role of porous media in modeling flow and heat transfer in biological tissues Source," *International Journal of Heat and Mass Transfer*, Vol. 46, No. 26, pp. 4989-5003, 2003.

[Killer 1991] K. R. Killer and L. J. Hayes, "Analysis of tissue injury by burning: Comparison of in situ and skin flap models," *Int. J. Heat Mass Transfer*, Vol. 34, pp. 1393-1406, 1991.

[Kim 1987] J. Kim, P. Moin and R. D. Moser, "Turbulence statistics in fully developed channel flow at low Reynolds number," *J. Fluid Mech*, Vol. 177, pp. 133-166, 1987.

[Kolios 1995] M. C. Kolios, M. D. Sherar and J. W. Hunt, "Thermal model predictions of ultrasonic lesion formation," *Advances in Heat and Mass Transfer in Biotechnology ASME*, HTD-Vol.332, pp.139-144, 1995.

- [Kolios 1998] M. C. Kolios, A. E. Worthington, M. D. Sherar and J. Hunt, "Experimental evaluation of two simple thermal models using transient temperature analysis," *Physics in medicine and biology*, Vol. 43, pp. 3325-3340, 1998.
- [Kreiss 1972] H. O. Kreiss and J. Olgcr, "Comparison of accurate methods for the integration of hyperbolic equations," *Tellus*, Vol. 3, pp. 99, 1972.
- [Lagendijk 1982] Lagendijk and J. J. W., "The influence of blood flow in large vessels on the temperature distribution hyperthermia," *Physics Medicine and biology*, Vol. 27, pp. 17-23, 1982.
- [Larkin 1977] J. M. Larkin, et al., "Systemic thermography: Description of a method and physiologic tolerance in clinical subjects," *Cancer Research*, Vol. 40, No. 6, pp. 3155-3159, 1977.
- [Lecarpentier 1993] G. L. Lecarpentier, M. Motamedi, L. P. Mcmath and S. Rastegar, "Welch A.J. Continuous wave laser ablation of tissue: analysis of thermal and mechanical events," *IEEE Trans. Biomed. Eng.*, Vol. 40, pp. 188-200, 1993.
- [Lele 1989] S. K. Lele, "Direct Numerical simulation of compressible free shear flows," *AIAA paper*, AIAA-89-0374, Reno, 1989.
- [Lele 1992] S. K. Lele, "Compact finite difference schemes with spectral-like resolution," *J. Comput. Phys.*, Vol. 103, pp. 16-42, 1992.
- [Li 1989] J. Li and H. Liang, *The laser medicine and its biomedical applications (in Chinese)*. Beijing China: Science Press, 1989.
- [Liauh 1993] C. T. Liauh and R. B. Roemer, "A semilinear state and parameter estimation algorithm for inverse hyperthermia problems," *Journal of Biomechanical Engineering*, Vol. 115, pp. 257-263, 1993.
- [Liu 1995] J. Liu, Z. Ren and C. Wang, "Interpretation of living tissue's temperature oscillations by thermal wave theory," *Chinese Sci. Bull.*, Vol. 40, pp. 1493-1495, 1995.
- [Liu 1997] J. Liu and W. Lu, "Dual reciprocity boundary element method for solving thermal wave model of bioheat transfer," *Space Medical Engineering*, Vol. 10, No. 6, pp. 2-6, 1997.
- [Liu 1999] J. Liu, X. Chen and L.X. Xu, "New thermal wave aspects on burn evaluation of skin subjected to instantaneous heating," *IEEE Transactions on Biomedical Engineering*, Vol. 46, pp. 420-428, 1999.

- [Liu 2000a] J. Liu, "Preliminary survey on the mechanisms of the wave-like behaviors of heat transfer in living tissues," *Forschung Im Ingenieurwesen Springer-Verlag*, Vol. 66, pp. 1-10, 2000.
- [Liu 2000b] J. Liu and L. X. Xu, "Boundary information based diagnostics on the thermal states of biological bodies," *International Journal of Heat and Mass Transfer*, Vol. 43, pp. 2827-2839, 2000.
- [Lu 1998] W. Lu, J. Liu and Y. Zeng, "Simulation of the thermal wave propagation in biological tissues by the dual reciprocity boundary element method," *Engineering Analysis with Boundary Elements*, Vol. 22, pp. 67-174, 1998.
- [Majchrzak 1999] E. Majchrzak and B. Mochnachi, "Numerical model of heat transfer between blood vessel and biological tissue," *Computer Assisted Mechanics and Engineering Sciences*, Vol. 6, pp. 439-447, 1999.
- [Mandal 1989] S. Mandal, T. Sundararajan and P.S. Ghoshdastidar, "Coupled analysis of thermal and electromagnetic phenomena during hyperthermia in biological tissues," *American Society of Mechanical Engineers, Heat Transfer Division*, HTD-Vol. 126, pp. 59-66, 1989.
- [Mans 2003] F. Mans, D. Borja and J. M. Parel, "Semianalytical thermal model for subablative laser heating of homogeneous nonperfused biological tissue: application to laser thermokeratolasty," *Journal of Biomedical Optics*, Vol. 8, No. 2, pp. 288-297, 2003.
- [Martin 1989] G. T. Martin and H. F. Bowman, "The temperature distribution in laser irradiated tissue with blood perfusion," *American Society of Mechanical Engineers, Heat Transfer Division*, HTD-Vol. 126, pp. 97-102, 1989.
- [Mooibroek 1985] J. Mooibroek, Lagendijk and J. J. W., "The influence of artery-vein vessel pairs on the heat transport in vascularized tissue," *Strahlentherapie*, Vol. 161, pp. 45, 1985.
- [Moritz 1947] A. R. Moritz and F. C. Henriques, "Studies of thermal injuries II: The relative importance of time and surface temperature in the causation of cutaneous burns," *America J. Pathol.*, Vol. 23, pp. 695-700, 1947.
- [Mukherjee 1982] S. Mukherjee and M. Morjaria, "On the efficiency and accuracy of the boundary element method and finite element method," *International Journal for Numerical Methods in Engineering*, Vol. 20, pp. 515-522, 1982.
- [Niu 2001] J. H. Niu, H. Z Wang, et. al., "Cellular neural network analysis for two-dimensional bioheat transfer equation," *Medical & Biological Engineering & Computing*, Vol. 39, pp. 601-604, 2001.

- [Pennes 1948] H. H. Pennes, "Analysis of tissue and arterial blood temperature in the resting human forearm," *J. Appl. Physiol.*, Vol. 1, pp. 93-122, 1948.
- [Pettigrew 1974] R. T. Pettigrew, et al., "Circulatory and biochemical effects of whole-body hypothermia," *British Journal of Surgery*, Vol. 61, No. 9, pp. 727, 1974.
- [Poinsot 1989] T. Poinsot and S. K. Lele, "Boundary conditions for direct simulations of compressible viscous flows," *Journal of Computational Physics*, Vol. 101, No. 1, pp. 104-129, 1992.
- [Rai 1989] M. Rai and P. Moin, "Comprehensive comparison with spectral methods," *AIAA paper*, AIAA-89-0369, Reno, 1989.
- [Rawnsley 1994] R. Rawnsley, R. B. Roemer and A. Dutton, "The simulation of large vessel effects in experimental hyperthermia," *ASME Journal of BioMechanical Engineering*, Vol. 116, No. 3, pp. 256-262, 1994.
- [Roemer 1989] R. B. Roemer, E. G. Moros and K. Hynynen, "A comparison of bioheat transfer and effective conductivity equation predictions to experimental hyperthermia data," *Proceedings of ASME Winter Annual Meeting*, pp. 11-15, 1989.
- [Roemer 1990] R. B. Roemer, "Thermal dosimetry," *Thermal Dosimetry and Treatment Planning*, M. Gautherie ed., Springer-Verlag, Berlin, 1990.
- [Roemer 1991] R. B. Roemer, "Optimal power deposition in hyperthermia. I. The treatment goal: the ideal temperature distribution: the role of large blood vessel", *International Journal of Hyperthermia*, Vol. 7, No. 2, pp. 317-341, 1991.
- [Rogallo 1984] R. Rogallo, "Numerical Experiments in Homogeneous Turbulence," NASATM-81315, 1981.
- [Sandham 1989] N. D. Sandham and W. C. Reynolds, *Thermal Sciences Division, Mech. Engrg.*, Stanford University, Report No. TF-45. 1989; AIAA paper, AIAA-89-0371, Reno, 1989.
- [Song 1987] J. Song, L. X. Xu, D. E. Lemons and S. Weinbaum, "Enhancements in the effective thermal conductivity in rat spinotrapezius due to vasoregulations," *J. Biomech. Eng. Trans. ASME*, Vol. 119, pp. 461-468, 1987.
- [Strohbehn 1984] J. W. Strohbehn and R. B. Roemer, "A survey of computer simulations of hyperthermia treatments," *IEEE Transactions on Biomedical Engineering*, Vol. 31, No. 1, pp. 136-149, 1984.
- [Stoll 1959] A. M. Stoll and L. C. Greene, "Relationship between pain and tissue damage due to thermal radiation," *J. Appl. Physiol.*, Vol. 14, pp. 373-382, 1959.

[Torvi 1994] D. A. Torvi and D. J. Dale, "A finite element model of skin subjected to a flash fire," *ASME J. Biomech. Eng.*, Vol. 116, pp. 250-255, 1994.

[Van der Zee 1986] J. Van der Zee, et al., "Retrospective analysis of the response of tumors in patients treated with a combination of radiotherapy and hyperthermia", *Int. J. Hyperthermia*, Vol. 2, No. 4, pp. 337-349, 1986.

[Vanderby 1988] R. Vanderby, B.R. Paliwal, R. T. Wakai, et. al., "A parametric study of temperature distribution in ferromagnetic hyperthermia," *American Society of Mechanical Engineers, Bioengineering Division (Publication) BED*, Vol. 9, pp. 291-299, 1988.

[Vernotte 1958] P. Vernotte, "Les paradoxes de la theorie continue de l'equation de la chaleur," *Compte Rendus*, Vol. 246, pp. 3154-3155, 1958.

[Weinbaum 1984] S. Weinbaum, L. M. Jiji and D. E. Lemona, "Theory and experiment for the effect of vascular temperature on surface tissue heat transfer - Part I: anatomical foundation and model conceptualization," *ASME Journal of Biomechanical Engineering*, Vol. 106, pp. 321-330, 1984.

[Weinbaum 1985] S. Weinbaum and L. M. Jiji, "New simplified bioheat equation for the effect of blood flow on local average tissue temperature," *Journal of Biomechanical Engineering, Transactions of the ASME*, Vol. 107, No. 2, pp. 131-139, 1985.

[Williams 1990] W. Williams, "A structural model of heat transfer due to blood vessels in living tissue," Ph.D. thesis, University of Arizona, Tucson. 1990.

[Xu 1991] L. X. Xu and M. M Chen, et al, "The theoretical evaluation of the Pennes, the Chen-Holmes and the Weinbaum-Jiji bioheat transfer models in the pig renal cortex," *Advances in Biological Heat and Mass Transfer, ASME, HTD-Vol. 189*, pp. 15-21, 1991.

[Xu 1993] L. X. Xu, E. Rudle and K. R. Holmes, "Transurethral thermal therapy (T3) for the treatment of benign prostatic hyperplasia in the canine: analysis using Pennes bioheat equation," *Advances in Bioheat and Mass Transfer: Microscale Analysis of Thermal Injury Processes, Instrumentation, Modelling and Clinical Applications, ASME. HTD-Vol. 268*, pp. 31-35, 1993.

[Xuan 1997] Y. Xuan and W. Roetzel, "Bioheat equation of the human thermal system," *Chem. Eng. Technol.* Vol. 20, pp. 268-276, 1997.

[Young 1993] L. A. Young and R. F. Boehm, "A finite difference heat transfer analysis of a percutaneous transluminal microwave angioplasty system," *Journal of Biomechanical Engineering*, Vol. 115, pp. 441-446, 1993.

[Zhang 2004] L. Zhang and W. Dai, "A numerical method for solving an inverse 3D Pennes' bioheat transfer in a triple-layered skin structure," Submitted to *Numeical Heat Transfer*, 2004.

[Zhen 2003] P. Zhen, "Modeling of the inverse heat-conduction problem with application to laser chemical vapor deposition and bioheat transfer," PHD dissertation, Louisiana Tech University, 2003.

[Zhou 2004] J. Zhou and J. Liu, "Numerical study on 3D light and heat transport in biological tissues embedded with large blood vessels during laser-induced thermotherapy," *Numerical Heat Transfer, Part A*, Vol. 45, pp. 415-449, 2004.

[Zhu 2001] L. Zhu and C. Diao, "Theoretical simulation of temperature distribution in the brain during mild hypothermia treatment for brain injury," *Med. Biol. Eng. Comput.*, Vol. 39, pp. 681-687, 2001.